AN ABSTRACT OF THE THESIS OF

James D. Newell for the degree of Master of Science in Civil Engineering presented on April 22, 2003.
Title: Steel Confined Yielding Damper for Earthquake Resistant Design

Abstract Approved:
Redacted for Privacy

Christopher C. Higgins

An experimental study of a passive energy dissipation tension-compression yielding brace or buckling restrained brace has been conducted. The Confined Yielding Damper (CYD) consists of a steel yielding core confined within a tube filled with non-cohesive media. The external tube and confined non-cohesive media provide lateral stability to the core enabling the device to yield in compression as well as tension. This device is similar to the Unbonded Brace developed by Nippon Steel of Japan. Fourteen full-scale CYDs were tested to determine the effect of varied confining media, perforation blocking configuration, and a random displacement history. Based on the Confined Yielding Dampers tested relatively stable and symmetric hysteretic damping can be achieved with the CYD device.

Steel Confined Yielding Damper for Earthquake Resistant Design

by
James D. Newell

A THESIS

submitted to

Oregon State University

in partial fulfillment of
the requirements for the
degree of

Master of Science

Presented April 22, 2003
Commencement June 2003

Master of Science thesis of James D. Newell presented on April 22, 2003.

APPROVED:

Redacted for Privacy

Major Professor, representing Civil Engineering

Redacted for Privacy

Head of the Department of Civil, Construction, and Environmental Engineering

Redacted for Privacy

Dean of the Graduate School

I understand that my thesis will become part of the permanent collection of Oregon State University libraries. My signature below authorizes release of my thesis to any reader upon request.

Redacted for Privacy

James D. Newell, Author

ACKNOWLEDGEMENTS

The author would like to express sincere appreciation to Major Professor Dr. Christopher Higgins. Without his guidance, support, and hard work this thesis would not have been possible. Additionally the author would like to thank committee members Dr. Thomas Miller, Dr. David Rosowsky, and Dr. David Gobeli.

This research was funded by the National Science Foundation (NSF) under Grant No. CMS-0099701 as part of the US-Japan Cooperative Research in Urban Earthquake Disaster Mitigation Program. Professor K. Kasai of the Tokyo Institute of Technology was the Japanese counterpart and Dr. Peter Chang was the program manager. Additional funding from the 2002 AISC/Klingelhofer Fellowship supported this research. Their support is gratefully acknowledged. The opinions, findings, and conclusions are those of the author and do not necessarily reflect the views of NSF, AISC, or the individuals acknowledged above.

TABLE OF CONTENTS

LIST OF FIGURES

LIST OF FIGURES (Continued)

LIST OF TABLES

LIST OF APPENDIX FIGURES

LIST OF APPENDIX FIGURES (Continued)

LIST OF APPENDIX FIGURES (Continued)

LIST OF APPENDIX FIGURES (Continued)

LIST OF APPENDIX FIGURES (Continued)

Steel Confined Yielding Damper for Earthquake Resistant Design

INTRODUCTION and BACKGROUND

In the United States there is a shift toward performance based design of structures and an increased demand for higher performance levels for structures during earthquakes. Building owners are increasingly interested in immediate occupancy following large earthquakes and want to mitigate economic losses due to structural damage during a seismic event. One method for protecting structures and achieving higher performance levels is the application of passive energy dissipaters. Viscous, viscoelastic, and metallic dampers are types of passive dampers currently being used to increase the performance level of structures during seismic events. While viscous and viscoelastic dampers are becoming more common, application of metallic dampers has recently begun to increase in the U.S.

Metallic dampers rely on the hysteretic damping capacity of the metal component of the device and the post-yield properties of the metallic elements to provide the design level of ductility and energy dissipation. The 1997 Uniform Building Code (UBC) permits inelastic deformation of structural members during the design level earthquake. If this were not allowed member sizes required to ensure elastic performance during the

design earthquake would be much larger and prohibitively costly. The metallic damper system utilizes the inelastic deformation allowance of the UBC by providing elements designed to dissipate the input seismic energy through controlled cyclic inelastic deformations.

One such metallic damper, a tension-compression yielding brace or buckling-restrained brace (BRB) termed the Unbonded Brace™ (UBB) has been developed by Nippon Steel of Japan (Aiken, et al. 2000; Black, et al. 2002; Wantanabe, 1992; Wantanabe, et al. 1998). The damper relies upon a structural tube filled with mortar that confines a steel yielding core. This steel core is similar to diagonal bracing in a typical braced frame. A debonding agent is applied between the concrete and steel allowing space for Poisson's effect and reduces shear stress transfer between the steel yielding core, mortar, and confining tube. The thickness of this debonding agent is critical to the performance of the damper system and must be carefully designed and fabricated. The mortar provides buckling resistance that allows the steel core to yield in compression as well as the typical yielding in tension, thereby permitting stable and symmetric hysteretic energy dissipation capacity under fully reversed cyclic loading. To ensure that the damper does not buckle in the first mode as an ordinary brace would, the UBB must satisfy the following condition:

$$\frac{\pi^2 EI}{L^2} \geq \alpha P \tag{1}$$

where: E = Young's Modulus; I = moment of inertia of the outer confining tube; L = brace length, taken as work point to work point; α = global buckling factor of safety; P = design axial load including the effects of strain hardening (Wantanabe, 1992). Any contribution of the mortar to the moment of inertia is neglected due to the assumption that the mortar is cracked during cyclic loading (Wantanabe, 1992; Wantanabe, et al. 1988). When the conditions of this equation are met, the external structural tube will provide the necessary global buckling resistance and enable the steel core to yield in compression instead of global brace buckling in first mode. Tests conducted both in Japan and the United States to assess the performance of UBBs indicated the device provides stable, reasonably symmetric hysteretic energy dissipation of the input cyclic loading (Aiken, et al. 2000; Black, et al. 2002; Wantanabe, 1992; Wantanabe, et al. 1998).

Buckling-restrained braced frames (BRBF) with UBBs have seen over 200 Japanese applications since 1987 (Black, et al. 2002) and are gaining increased acceptance as a seismic force resisting system (SFRS) by the U.S. structural engineering community. BRBFs have been used in 13 U.S. projects to date, including both new and retrofit construction (Black, et al. 2002). All applications have used imported Nippon Steel UBBs from Japan. Currently no adopted U.S. code provisions exist for BRBF design. A draft document is under development by a joint American Institute of Steel Construction / Structural Engineers Association of

California (AISC/SEOC) committee and it is anticipated this work will be incorporated into the *2007 AISC Seismic Provisions for Structural Steel Buildings.*

This paper addresses an alternative form of BRB in which the mortar used to fill the confining tube of the UBB is replaced with confined non-cohesive media. This non-cohesive media is placed under a normal confining force to provide buckling resistance of the core enabling the device to yield in compression. Confined Yielding Dampers (CYDs) provide benefits including economical use of standard materials, for example, A36 steel bar stock for the yielding core and A53A steel pipe for the confining tube. Further, this new device offers simplified connection design and detailing, opens the market for U.S. fabrication of CYDs using no patented technologies, reduces costs associated with importing BRBs from Japan (most current U.S. projects use UBBs imported though Nippon Steel), applicability to a wider range of building structures as the brace yield force levels under investigation are lower than are currently available, post event inspection, and simplified design of the damper device because the debonding layer required in UBBs is not necessary.

EXPERIMENTAL PROGRAM

Test Specimens

Small scale experimental CYD tests were carried out at Clarkson University (Higgins and Newell, 2001; Higgins and Newell, 2002). Test results indicated relatively stable and symmetric hysteretic damping with a reduced scale device. The current testing program was therefore undertaken to characterize full-scale CYD performance and establish design guidelines for future application of CYDs as a SFRS in structures.

Four yielding core configurations were investigated: 125 kip (556 kN) yield force in a dog bone configuration, 125 kip (556 kN) yield force in a perforated configuration, 50 kip (222 kN) yield force in a dog bone configuration, and 50 kip (222 kN) yield force in a perforated configuration. The CYD configurations, illustrated in Fig. 1, consist of a steel yielding core element within a steel pipe filled with a confined non-cohesive media. The non-cohesive media takes the place of the mortar used in the UBB in providing lateral stability to the yielding core, enabling yielding of the core in compression cycles. A constant confining media volume was maintained with steel end caps and 1/2 in. (12.70 mm) diameter A193 B-7 high strength threaded rod. Specimen cross-sections are shown in Fig. 2.

To develop a realistic sized brace for testing, a prototype structure was used. A full-scale specimen yielding core length of 16 ft. (4.88 m) was

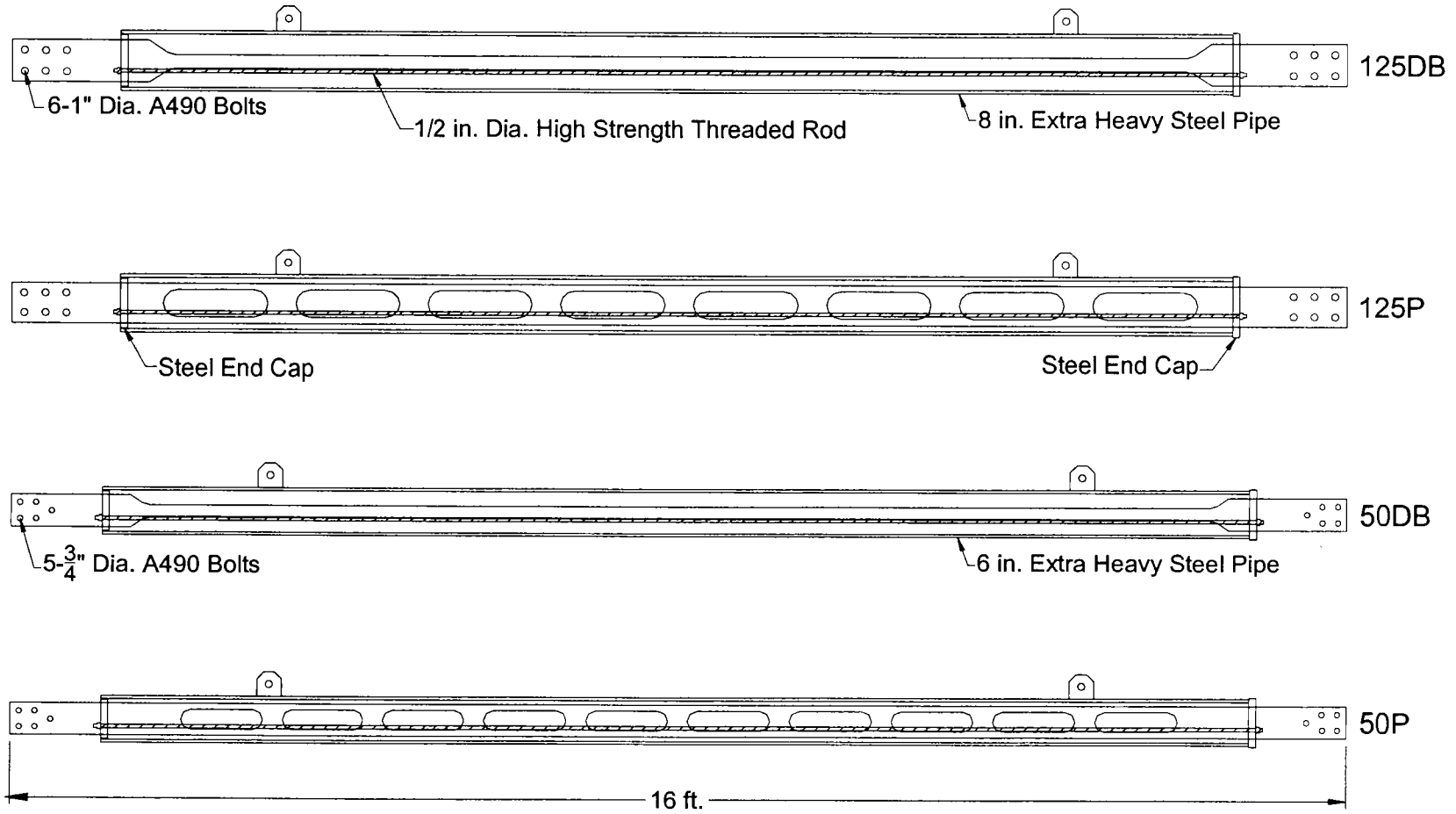

Figure 1: CYD configurations.

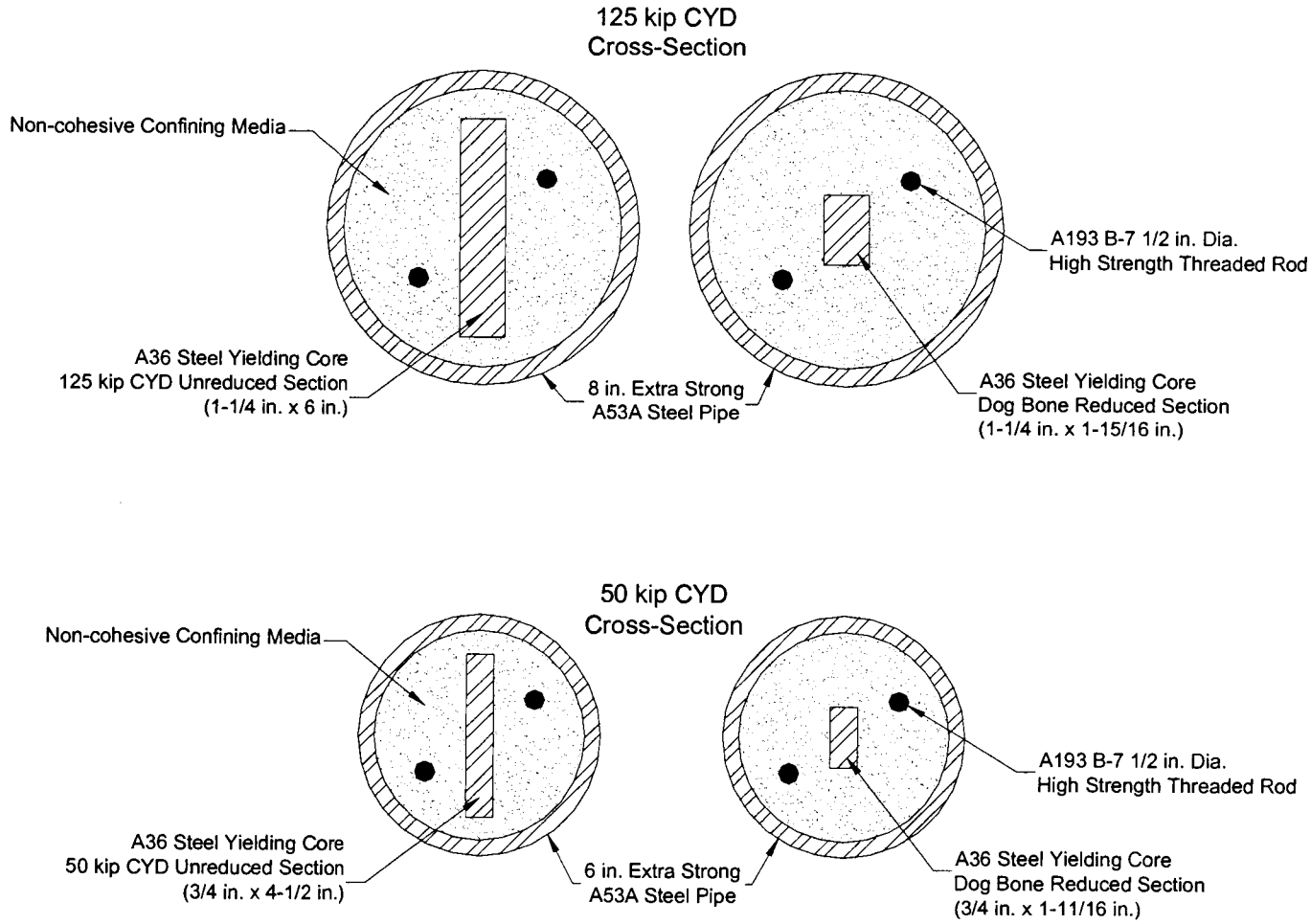

Figure 2: CYD cross-sections.

selected for a single diagonal brace in a typical bay with column-to-column centerline spacing of 15 ft. (4.57 m), beam-to-beam centerline spacing of 13 ft. (3.96 m) and considering the gusset plate beam to column to brace connection, as illustrated in Fig. 3.

In this research two different yield force levels were investigated: 125 kip (556 kN) and a 50 kip (222 kN) yield force levels. A dog bone and perforated yielding core configuration were tested at each force level. The yielding core reduced cross-sectional area was calculated based on the desired yield force and material properties determined from tension coupon testing. The dog bone configuration is typical of current BRBs. The perforated configuration has the potential for greater variation in the yield force and stiffness of the device by varying geometric properties and was therefore investigated. The legs of different perforations could be fabricated to different lengths, cross-sectional areas or tapered allowing for tailoring of device performance.

Specimens were named by yield force level, yielding core configuration, and specimen identification number. 125DB-1 was a 125 kip (556 kN) yield force, dog bone configuration, and specimen identification number 1. 50P-2 was a 50 kip (222 kN) yield force, perforated configuration, and specimen identification number 2.

The 125 kip yield force dampers consisted of 1-1/4 in. (31.75 mm) by 6 in. (152.40 mm) A36 steel bar stock with a yield stress of 51.8 ksi

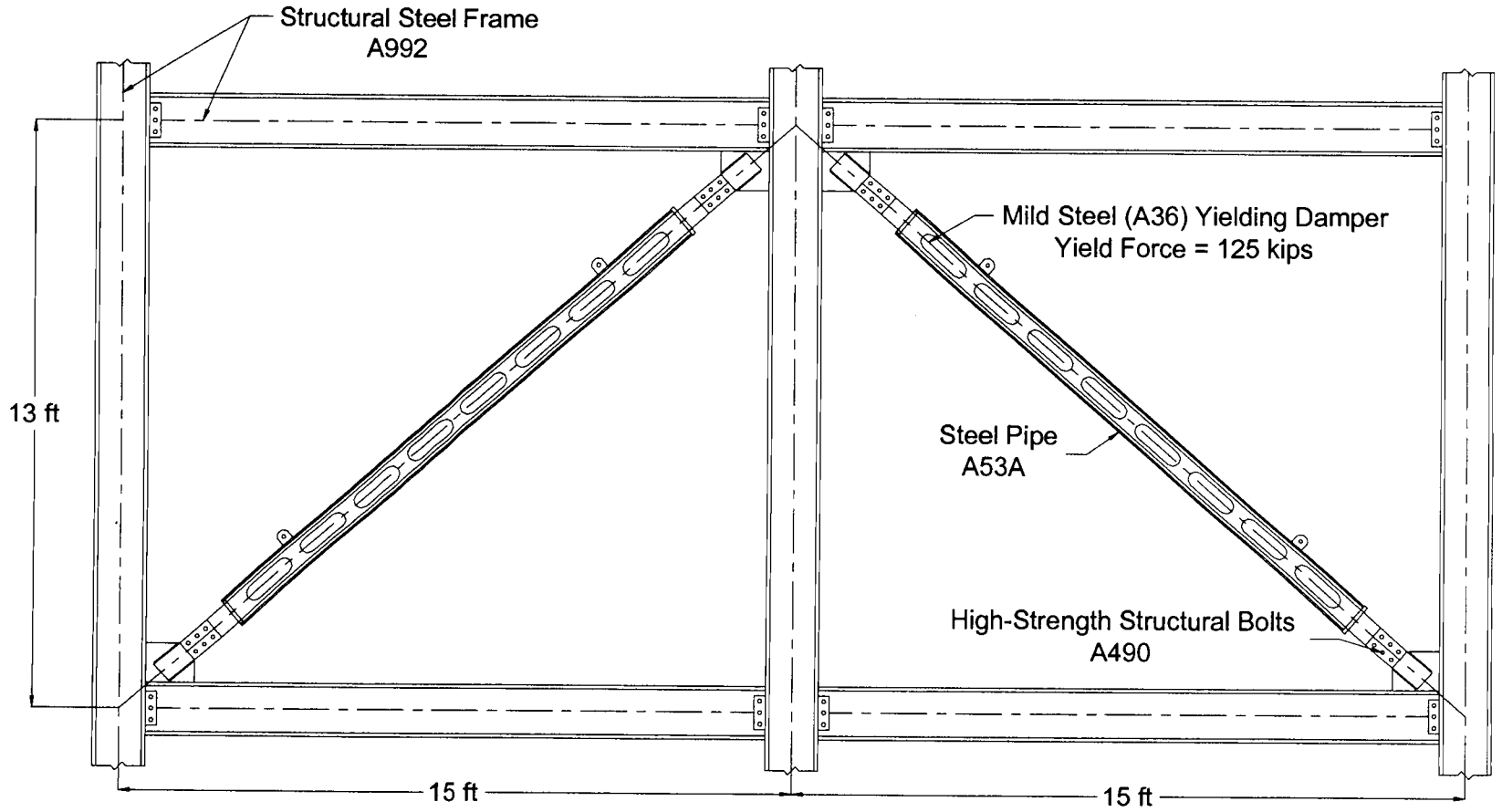

Figure 3: Prototype frame with CYDs.

(357.2 MPa) and an ultimate stress of 72.1 ksi (497.1 MPa), based on tension coupon testing. The reduced cross-sectional area of the 125DB specimen was 2.422 in^2 (1562.6 mm^2) and the reduced cross-sectional area of each leg of the 125P specimen was 1.211 in^2 (781.3 mm^2) resulting in an area for both legs equivalent to that of the dog bone specimen. Length of individual perforation legs was 11 in. (279.40 mm) with a 2.3 factor of safety against buckling assuming pinned ends. Yielding core geometry for all specimens is shown in Fig. 4. Elastic stiffness and yield displacement of the 125DB specimens were 451 kip/in (79.0 kN/mm) and 0.278 in. (7.06 mm), respectively, and for the 125P specimens were 581 kip/in (101.7 kN/mm) and 0.216 in. (5.49 mm). These stiffness and yield displacement values are summarized in Table 1 and take into account the unreduced sections of the yielding core that remain elastic after the reduced sections have yielded up to the first line of bolts. Connections for both 125 kip (556 kN) yield force configurations were detailed as slip-critical bolted connections with class A slip surfaces and six (6) fully tensioned 1 in. (25.40 mm) diameter A490 high strength structural bolts at each end of the brace designed per *1993 Load and Resistance Factor Design Specification for Structural Steel Buildings* (AISC, 1993). Slip – critical connections were designed for the ultimate strength of the steel yielding core taking into account the compressive overstrength factor of 1.1 typical of previously tested BRBs (Aiken, et al. 2000). A490 high strength

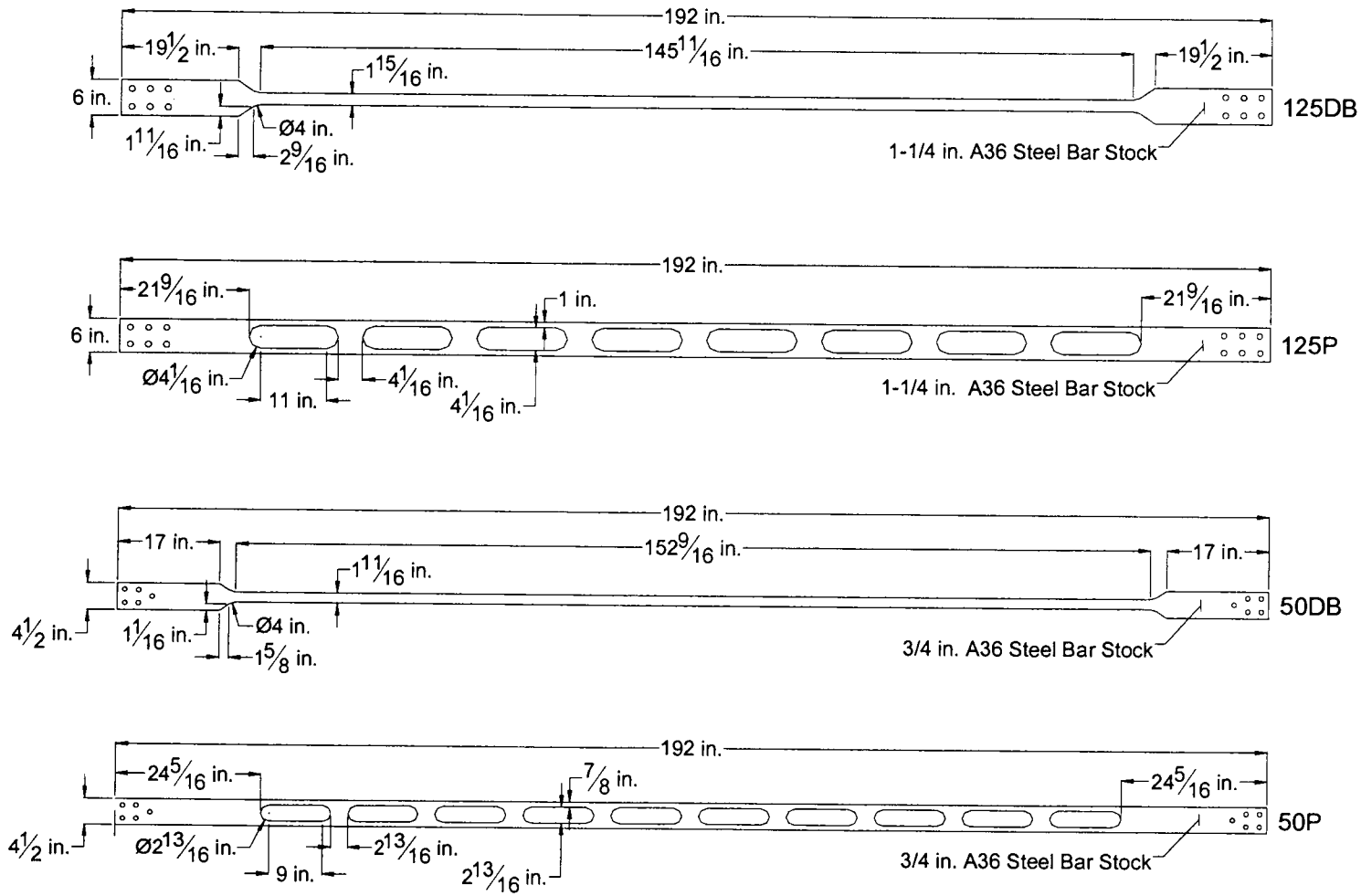

Figure 4: Yielding core geometries.

Table 1: Yielding Core Properties

Specimen	Yield Stress F_y		Area of Reduced Cross-Section		Yield Force P_y		Yield Displacement Δ_{by}		Local Brace Stiffness K	
	(ksi)	(MPa)	(in^2)	(mm^2)	(kip)	(kN)	(in)	(mm)	(kip/in)	(kN/mm)
(1)	(2)		(3)		(4)		(5)		(6)	
125DB	51.8	357.2	2.422	1562.6	125	556	0.278	7.06	451	79.0
125P	51.8	357.2	2.422	1562.6	125	556	0.216	5.49	581	101.7
50DB	39.5	272.4	1.266	816.8	50	222	0.222	5.64	225	39.4
50P	39.5	272.4	1.266	816.8	50	222	0.174	4.42	287	50.3

structural bolts were used because there fully tensioned slip-critical capacity is greater than A325 high strength structural bolts and thus connection geometry could be shortened. The calculated 202.8 kip (902.1 kN) slip capacity of the bolted connection was 1.06 times greater than the 192.1 kip (854.5 kN) ultimate compressive strength of the yielding core. Connection net section was designed to remain elastic at a load equal to yielding core ultimate tensile strength. Yielding core stress on the net section at the first line of bolts was calculated to be 37.3 ksi (257.2 MPa) for this case. Washers were used under both the head of the bolt and nut per *RCSC Specification for Structural Joints* (RCSC, 1994) for steel with a nominal yield stress less than 40 ksi (275.8 MPa). The two splice plates per connection used to join yielding core and reaction system were 3/4 in. (25.4 mm) by 6 in. (152.40 mm) A36 steel bar stock. The confining tube for the 125 kip (556 kN) yield force specimens was an 8 in. (203.20 mm) extra heavy steel pipe (A53A) with a factor of safety against global buckling of 2.7 assuming pin ended connections, work point to work point on the brace length, and considering the ultimate compressive strength of the yielding core.

The 50 kip (222 kN) yield force dampers consisted of 3/4 in. (19.05 mm) by 4-1/2 in. (114.30 mm) A36 steel bar stock with a yield stress of 39.5 ksi (272.4 MPa) and an ultimate stress of 63.6 ksi (438.5 MPa) based on tension coupon testing. The reduced cross-sectional area of the 50DB

specimen was 1.266 in^2 (816.7 mm^2) and the reduced cross-sectional area of each leg of the 50P specimen was 0.633 in^2 (408.4 mm^2) providing an area of both legs equivalent to that of the dog bone specimen. Length of individual perforation legs was 9 in. with a 2.4 factor of safety against buckling assuming pinned ends. Yielding core geometry is shown in Fig. 4. Elastic stiffness and yield displacement of the 50DB specimens were 225 kip/in (39.4 kN/mm) and 0.222 in. (5.64 mm), respectively, and for the 50P specimens were 287 kip/in (50.3 kN/mm) and 0.174 in. (4.42 mm). These values are summarized in Table 1 and take into account the unreduced sections of the yielding core that remain elastic after the reduced sections have yielded up to the first line of bolts. Connections for both of these 50 kip (222 kN) yield force configurations were detailed as slip-critical bolted connections with class A slip surfaces and five (5) fully tensioned 3/4 in. diameter A490 high strength structural bolts at each end of the brace designed per *1993 Load and Resistance Factor Design Specification for Structural Steel Buildings* (AISC, 1993). Slip-critical connections were designed for the ultimate strength of the steel yielding core taking into account the compressive overstrength factor of 1.1 typical of previously tested BRBs (Aiken, et al. 2000). The calculated 92.4 kip (411.0 kN) slip capacity of the bolted connection was 1.04 times greater than the 88.5 kip (393.6 kN) ultimate compressive strength of the yielding core. Connection net section was designed to remain elastic at a load equal to yielding core

ultimate tensile strength. Yielding core stress on the net section at the first single bolt was calculated to be 29.6 ksi (204.1 MPa) and at the first line of two bolts the stress was 31.2 ksi (215.1 kN) for this case. Washers were used under both the head of the bolt and nut per *RCSC Specification for Structural Joints* (RCSC, 1994) for steel with a nominal yield stress less than 40 ksi (275.8 MPa). The two splice plates per connection used to join yielding core and reaction system were 1 in. (25.4 mm) by 6 in. (152.40 mm) A36 steel bar stock. The confining tube for the 50 kip (222 kN) yield force specimens was a 6 in. (152.40 mm) extra heavy steel pipe (A53A) with a factor of safety against buckling of 2.3 assuming pin ended connections, work point to work point brace length, and considering the ultimate compressive strength of the yielding core.

Structural Testing Matrix

Fourteen full-scale CYDs were tested to characterize device performance and investigate the influence of various parameters on behavior as shown in the testing matrix, Table 2. The effects of different confining media were investigated using the 125 DB specimens. Four different readily available aggregates were used as confining media: sand, pea gravel (1/4 in. (6.35 mm) minus gravel), 3/4 in. (19.05 mm) to #4 gravel, and 3/4 in. (19.05 mm) minus gravel (which consisted of equal parts of the above). Pea gravel was used as the confining media for all other

Table 2: Test Matrix

Specimen (1)	Parameter (2)
125DB-1	Pea Gravel
125DB-2	Pea Gravel (Pencil Vibrator)
125DB-3	Sand
125DB-4	3/4" - #4 Gravel
125DB-5	3/4" - minus Gravel
125P-1	All perforations spray foamed
125P-2	First perforation @ each end completely blocked, remaining perforations with spray foamed radius
125P-3	First 2 perforations @ each end completely blocked, remaining perforations with spray foamed radius
125P-4	First 2 perforations @ each end completely blocked, remaining perforations blocked with knockout minus 2 in. length (with cut in middle of knockout)
125P-5	First 2 perforations @ each end completely blocked, remaining perforations blocked with plate minus 2 in. length, minus 1/2 in. width
50DB-1	Increasing amplitude displacement protocol
50DB-2	Reverse displacement protocol from 2.0 Δ_{bm}
50P-1	Increasing amplitude displacement protocol
50P-2	Random displacement history

DB Dog bone configuration
P Perforated configuration

specimens. Different configurations of perforation blocking (Fig. 5) were tested with the 125P specimens to optimize performance and minimize first mode buckling of individual legs. A decreasing amplitude displacement history was compared to the typical increasing amplitude displacement protocol with the 50DB specimens. CYD performance when subjected to a random displacement history was evaluated with the 50P specimens with perforation blocking as shown in Fig. 6.

Specimen Fabrication

The dog bone and perforated configuration yielding cores were fabricated using abrasive water jet cutting techniques. A 50,000 psi (344.75 MPa) water and garnet abrasive cutting stream was CNC controlled to cut the required configurations. Testing of both water jet and traditionally machined tension coupons did not indicate a change in the stress-strain behavior from the water jet cutting process of the 1-1/4 in. (31.75 mm) A36 steel bar stock used for the 125 kip (556 kN) yielding cores.

The weight of confining media placed in the tube was calculated to achieve approximate 95% relative density. Actual confining media volumes, weights, and densities are given in Table 3. The tube was filled with confining media in a vertical orientation with the yielding core maintained in proper alignment. Confining media was placed in approximately 30 lb (0.13 kN) lifts and compacted internally with a pencil

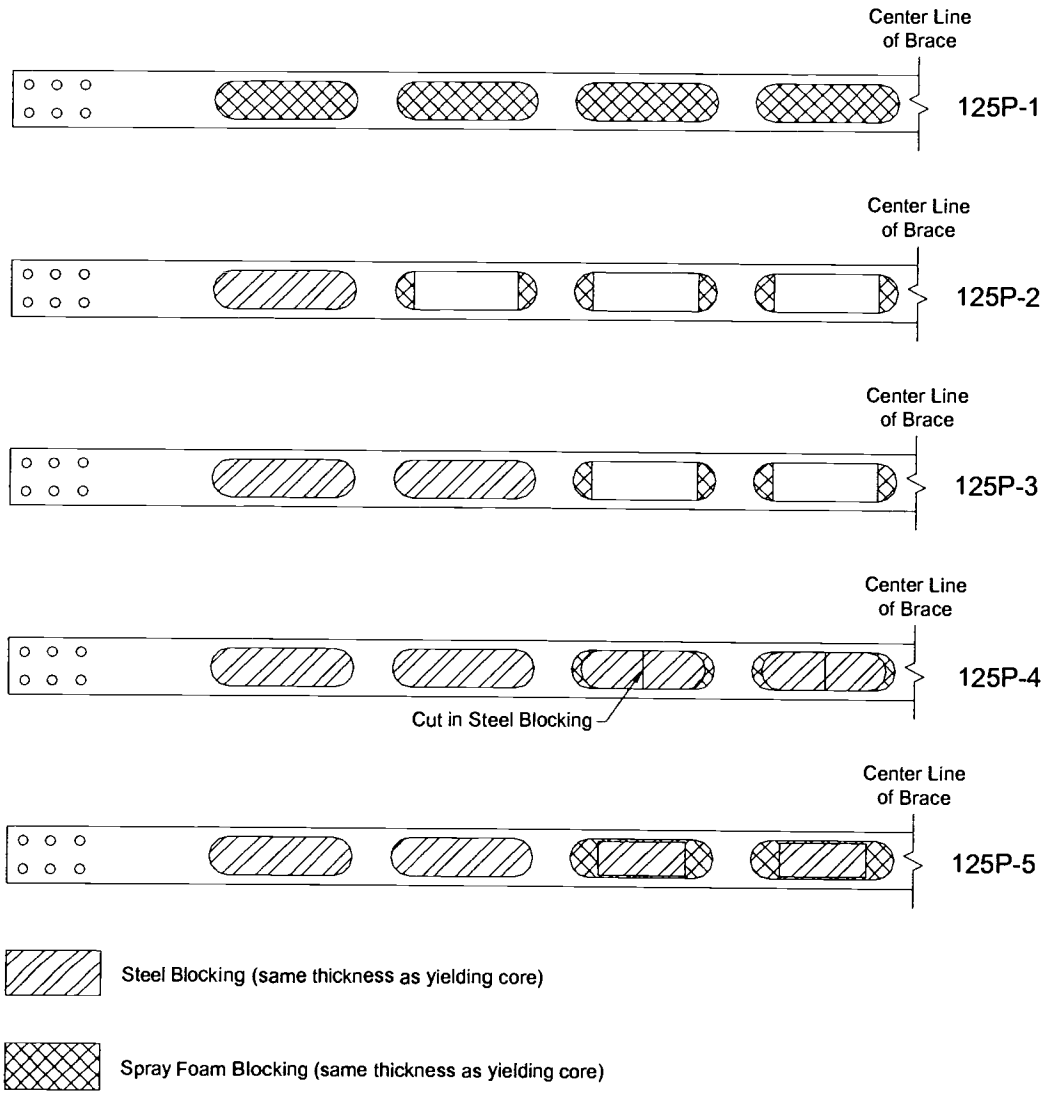

Figure 5: CYD blocking configurations used with 125 kip perforated specimens.

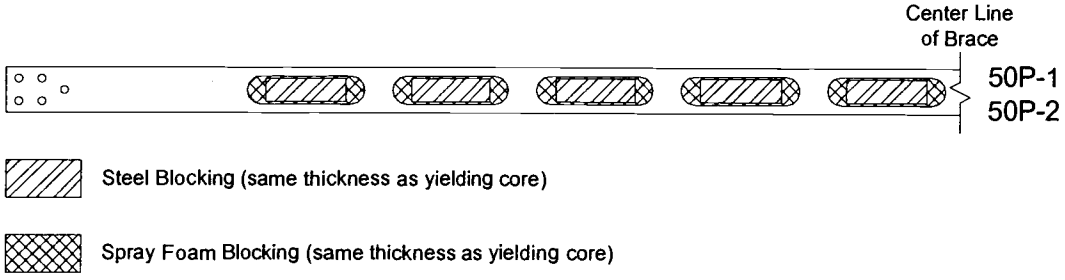

Figure 6: CYD blocking configuration used with 50 kip perforated specimens.

Table 3: Confining Media Properties

Specimen	Confining Media	Compaction Method	Weight of Confining Media		Volume of Voids		Confining Media Density	
			(lb)	(kN)	(ft^3)	(m^3)	(lb/ft^3)	(kN/m^3)
(1)	(2)	(3)	(4)		(5)		(6)	
125DB-1	Pea Gravel	DBH	412.00	1.83	3.88	0.1099	106.19	16.68
125DB-2	Pea Gravel	DBH/PV	438.50	1.95	3.85	0.1090	113.90	17.89
125DB-3	Sand	DBH	382.50	1.70	3.86	0.1093	99.09	15.56
125DB-4	3/4" - #4 Gravel	DBH	400.00	1.78	3.88	0.1099	103.09	16.19
125DB-5	3/4" - minus Gravel	DBH	466.75	2.08	3.88	0.1099	120.30	18.89
125P-1	Pea Gravel	DBH	361.75	1.61	3.46	0.0980	104.55	16.42
125P-2	Pea Gravel	DBH	390.25	1.74	3.66	0.1037	106.63	16.75
125P-3	Pea Gravel	DBH	375.75	1.67	3.59	0.1017	104.67	16.44
125P-4	Pea Gravel	DBH	356.00	1.58	3.46	0.0980	102.89	16.16
125P-5	Pea Gravel	DBH/PV	387.50	1.72	3.44	0.0974	112.65	17.69
50DB-1	Pea Gravel	DBH/PV	265.75	1.18	2.28	0.0646	116.56	18.31
50DB-2	Pea Gravel	DBH/PV	268.25	1.19	2.28	0.0646	117.65	18.48
50P-1	Pea Gravel	DBH/PV	236.00	1.05	2.10	0.0595	112.38	17.65
50P-2	Pea Gravel	DBH/PV	231.25	1.03	2.10	0.0595	110.12	17.30

DB Dog bone configuration
P Perforated configuration

DBH Dead blow hammer
PV Pencil vibrator

vibrator and/or externally with a 5 lb (0.02 kN) dead blow hammer on the outside of the confining tube. Method of compaction is included in Table 3. The confining media volume was maintained with steel end caps and 1/2 in. (12.70 mm) diameter A193 B-7 high strength threaded rod. The threaded rod was encased in concrete prestressing strand sheathing to reduce interaction between the threaded rod and confining media. Six 700 lb (3.11 kN) Bellville Washers stacked in series were used at one end of the threaded rod to maintain approximately 2 kip (8.90 kN) of confining force per threaded rod. Sheet metal and spray foam crush-zones 6 in. (152.40 mm) in length were added to the dog bone yielding cores in the transition zone from reduced to unreduced cross section to minimize the effects (compressive stiffening) of the shoulders of the dog bone yielding core bearing on the confining media. Perforated specimens were encased in sheet metal to maintain alignment of blocking material within individual perforations.

Structural Testing Setup

Specimens were tested in a horizontal configuration, Fig. 7, with a structural steel reaction system at each end attached to the strong floor. Roller supports were provided at approximate third points of the confining tube to protect the test setup from any overall damper instability. The rollers provided negligible resistance to tube movement in the brace axial

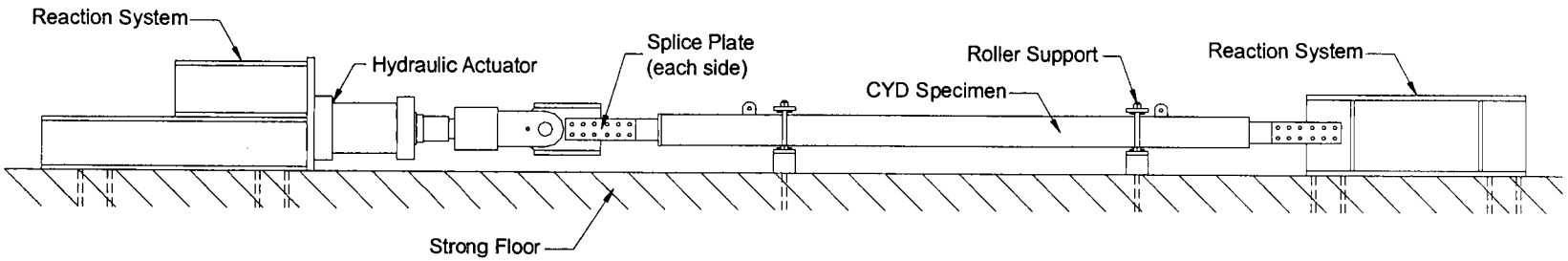

Figure 7: Experimental setup.

direction but prevented any excessive deformation in the transverse directions. Load was applied at a rate of 1.33 in/min (33.78 mm/min) with a 500 kip (2224 kN) capacity servo-controlled hydraulic actuator. Specimen yielding core axial deformation was used as the feedback sensor for the servo-control system. Instrumentation consisted of strain gages, force washer load cells, displacement transducers and an in-line load cell. Strain gages on the steel yielding cores were placed to measure axial strain and determine if the yielding core was bending within the elastic range of the gages used. Strain gages were bonded to the middle of each face of the steel yielding core as shown in Fig. 8 for the 125 kip (556 kN) specimens and Fig. 9 for the 50 kip (222 kN) specimens. Strain gages on the confining tube were placed to measure axial strain and determine if the confining tube was bending. Strain gages were bonded at 90° orientations from each other around the circumference of the pipe at the middle and north quarter point (Fig. 10). Force washer load cells were used to measure the force in the 1/2 in. (12.70 mm) diameter A193 B-7 high strength threaded rod used to maintain confining media volume and their orientation is shown in Fig. 11. Two displacement sensors (string potentiometers) (Fig. 11) were used to measure overall yielding core deformation. Displacement values from these two sensors were averaged to remove any bending component due to brace end rotation outside of the confining tube. Two other displacement sensors measured relative deformation of the yielding core into and out of

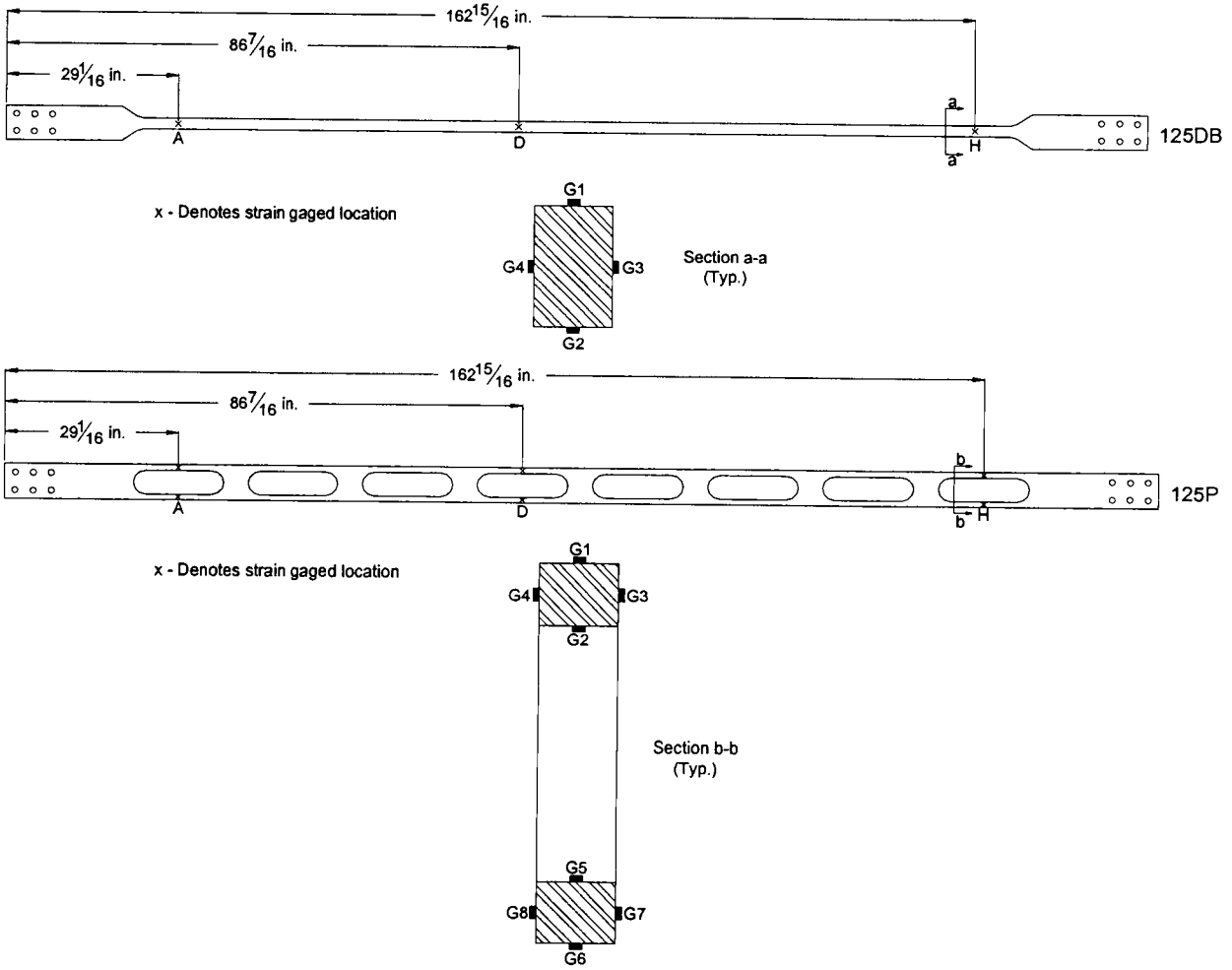

Figure 8: Yielding core strain gage configuration used on 125 kip specimens.

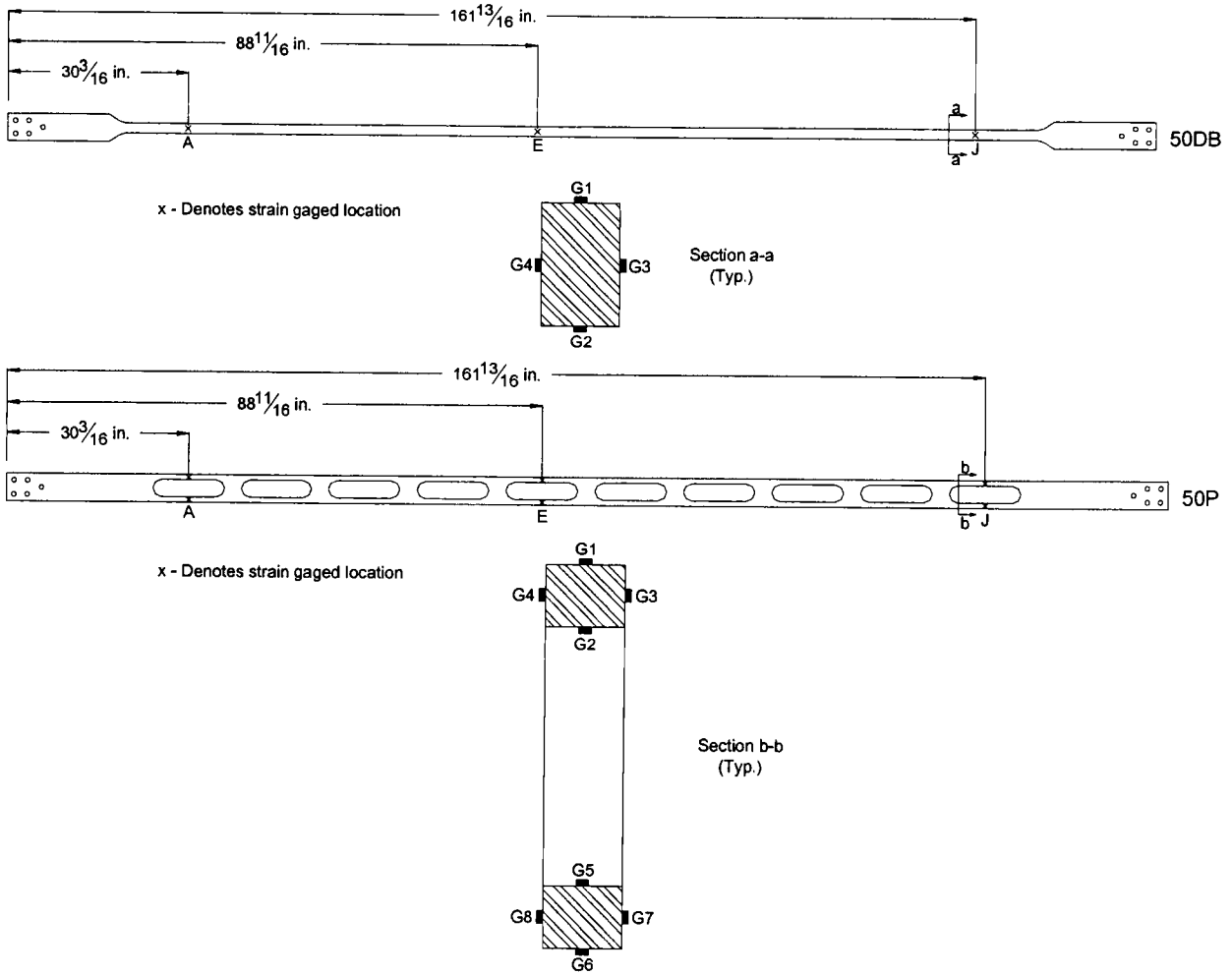

Figure 9: Yielding core strain gage configuration used on 50 kip specimens.

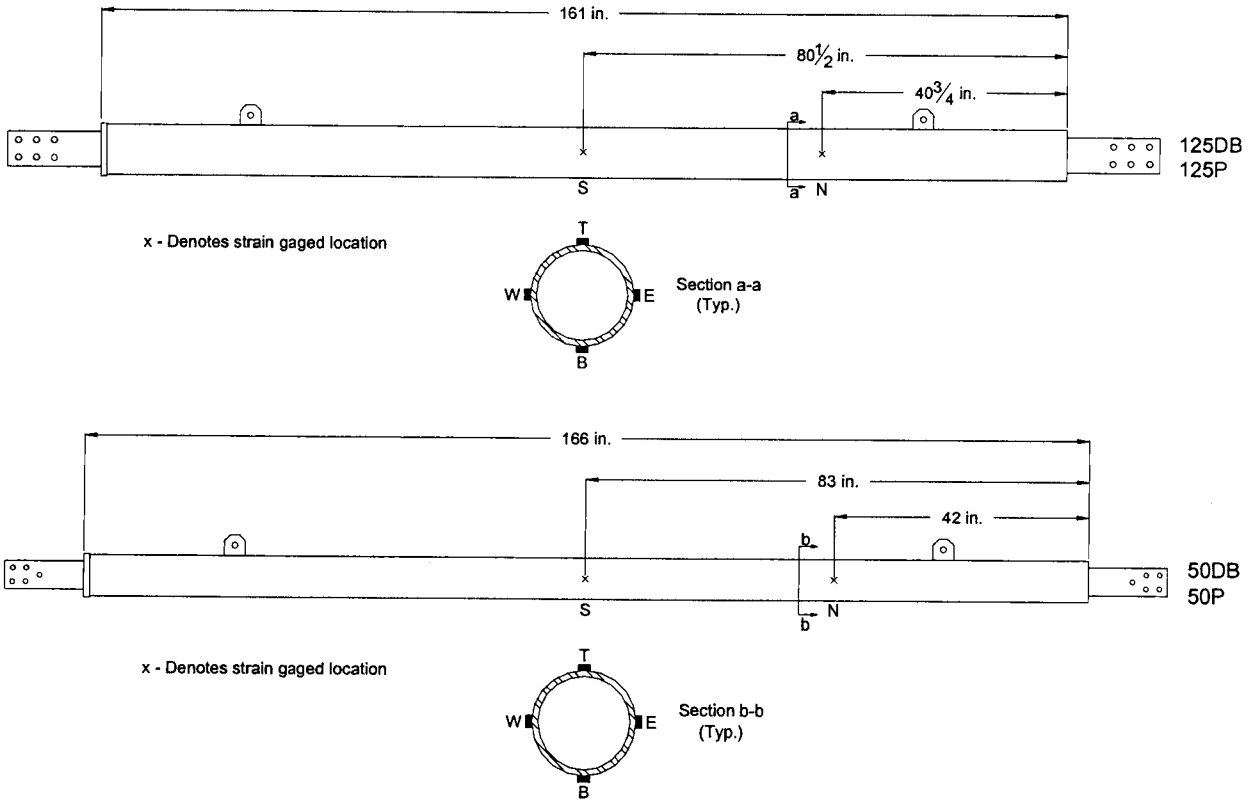

Figure 10: Confining tube strain gage configurations.

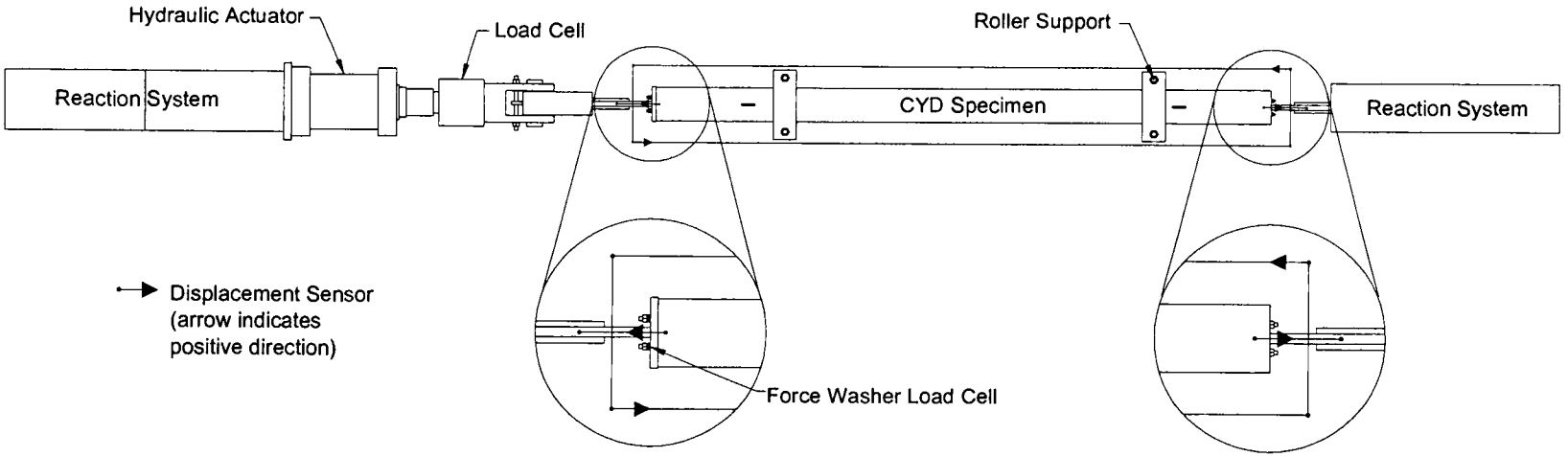

Figure 11: Instrumentation plan.

the confining tube at each end, shown in Fig. 11. A PC-based data acquisition system was used to acquire data at a continuous rate of 5 Hz during testing.

Increasing Amplitude Displacement Protocol

The displacement protocol (Fig. 12) was based on the guidelines of ATC 24 (ATC, 1992) and the draft *AISC/SEAOC Recommended Buckling-Restrained Brace Frame Provisions* (AISC/SEAOC, 2001). Increasing amplitude fully reversed cyclic axial displacement was applied until failure. Two cycles each were applied at 0.25 Δ_{by}, 0.50 Δ_{by}, and 0.75 Δ_{by}, where Δ_{by} is equal to the yield displacement of the steel core. Six cycles at Δ_{by} were then applied. The remaining protocol was based on the design story drift of 1% on the prototype structure shown in Fig. 3. For one (1) 16 ft. (4.88 m) brace in a 13 ft. (3.96 m) by 15 ft. (4.57 m) bay or two (2) 16 ft. (4.88 m) braces in a 13 ft. (3.96 m) by 30 ft. (9.14 m) bay, 1% story drift corresponds to a local brace displacement of 1.19 in. (30.23 mm) (Δ_{bm}). Four cycles each were applied at deformation levels corresponding to 0.5 Δ_{bm}, 1.0 Δ_{bm}, and 1.5 Δ_{bm}. Two cycles were applied at 2.0 Δ_{bm} and higher deformation levels incremented by 0.5 Δ_{bm} to failure.

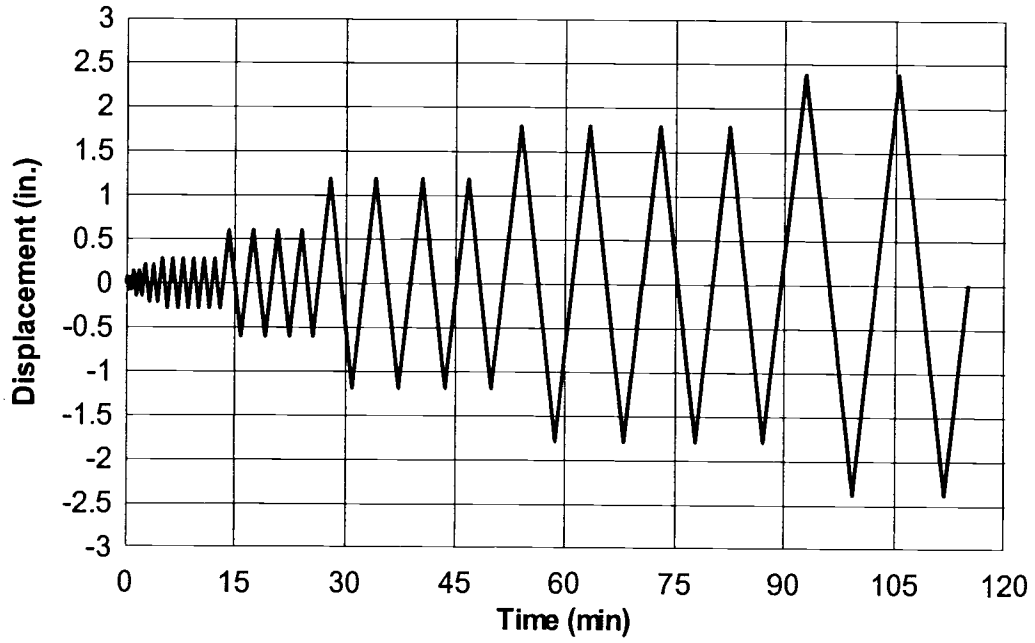

Figure 12: Increasing amplitude displacement protocol imposed on most test specimens.

Random Displacement History Development

Specimen 50P-2 was subjected to multiple iterations of a random displacement history derived from nonlinear dynamic time history analysis of a three-story BRBF building.

The building modeled in this analysis is based on the work of Sabelli (2000) and the SAC model building design criteria. The building plan dimensions as shown in Fig. 13 are 124 ft. by 184 ft. with 30 ft. by 30 ft. bays and a 2 ft. perimeter wall offset. Story heights are a typical 13 ft. The SFRS consisted of eight BRBFs with four in each orthogonal direction. The building was designed for a site in metropolitan Los Angeles according to the *1997 NEHRP Recommended Provisions for Seismic Regulation of New Buildings and Other Structures* (FEMA, 1997) and the *1997 Uniform Building Code* (ICBO, 1997).

For analysis, one BRBF was modeled with an additional single column representing the secondary P-Δ load affect attributed to the BRBF. The horizontal stiffness contribution of this equivalent gravity framing column was neglected as is standard design practice. The modeled frame along with member properties is shown in Fig. 14 and Table 4. Three-dimensional analysis was not considered given the regular building layout.

Story masses applied to the modeled frame were calculated based on the total story mass divided by the number of braced frames in a given

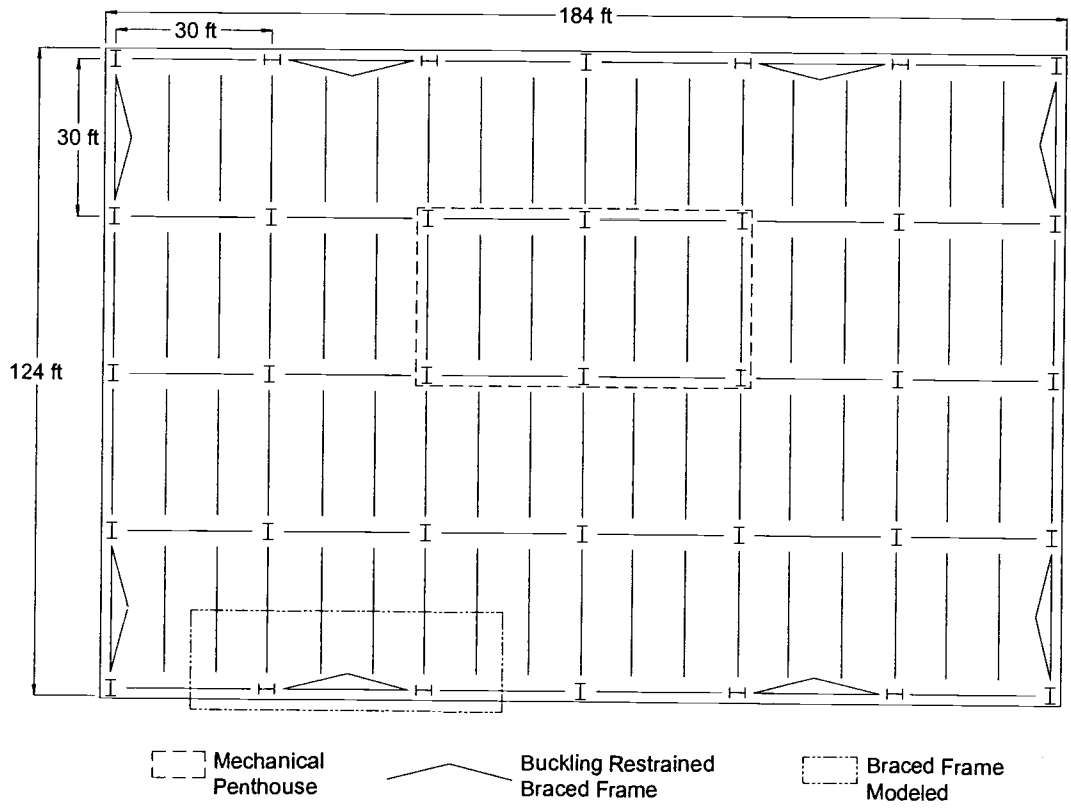

Figure 13: Three-story building plan (Sabelli, 2000) used for time history analysis.

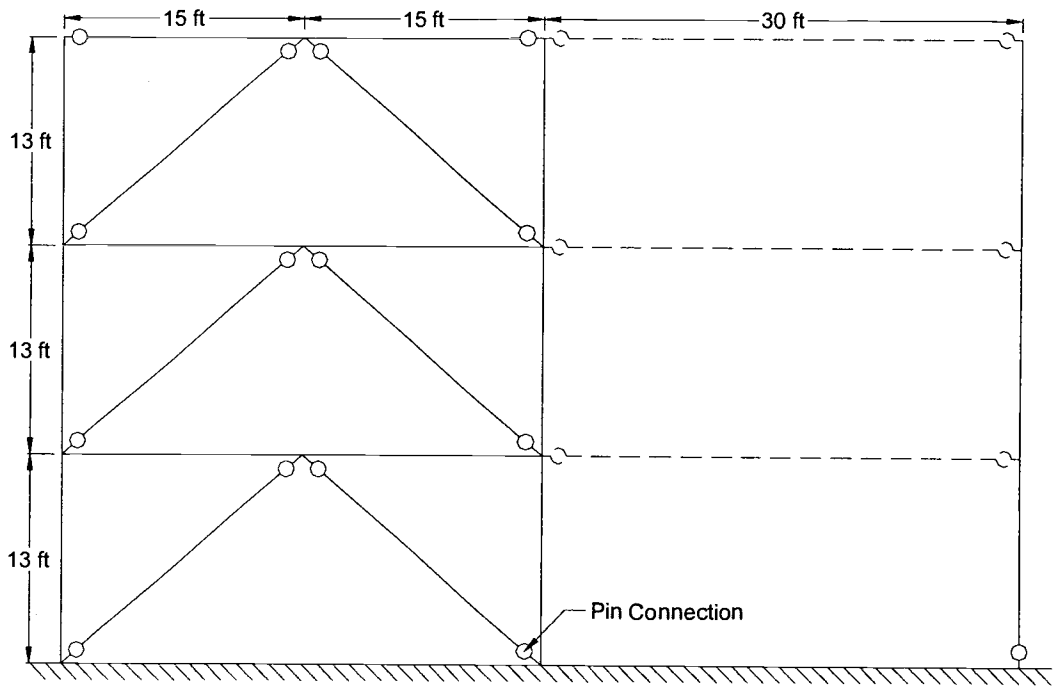

Figure 14: Three-story BRBF model.

Table 4: Three-Story BRBF Model Member Properties

Story	Brace Yield Force P_y		Horiz. Brace Stiffness K_h		BF Column	BF Beam	Non-BF Columns (Minor Axis)					
							Side	Interior	Mech.	Perp. BF	ΣI_y	ΣZ_y
	(kip)	(kN)	(kip/in)	(kN/mm)							(in^4) (mm^4)	(in^3) (mm^4)
(1)	(2)		(3)		(4)	(5)	(6)	(7)	(8)	(9)	(10)	(11)
3	117	520	588	103								
2	196	872	943	165	W12x96	W14x48	W14x48	W14x61	W14x74	W12x96	1033 429967063	290 4752249
1	243	1081	1088	191								

orthogonal direction. Design loads used in these calculations are shown in Table 5. At the roof level one half of the ceiling/flooring and mechanical/electrical loads were applied. Seismic masses for each story are shown in Table 6. Lumped masses were used given that only horizontal ground motions were considered. Braced frame beam and column loads were calculated using the load combination 1.2D + 0.5L + 1.0E. The earthquake term was applied in the form of dynamic ground motion records. P-Δ column loads were calculated using the same load combination and considering 60% live load reduction. Table 6 summarizes the calculated nodal loads. Braced frame dead and live loads were applied at third points of the beams where subframing (not explicitly modeled) was connected to the beams.

Nonlinear dynamic time history analysis was conducted using the nonlinear structural analysis computer program PC-ANSR (Maison, 1992). Frame members were modeled using element type 4, a nonlinear beam-column element. Beams were considered inextensible. Nodal displacements within a story were set to be equivalent. This was consistent with the assumption of rigid diaphragms. Therefore the non-braced frame beams were not modeled in this analysis. Horizontal stiffness of the P-Δ columns was neglected. Connections with gusset plates for brace attachment were modeled as fixed. The roof beam/column connections where no braces framed in were considered pinned (simple shear tab). All

Table 5: Three-Story Building Design Loads

Load (1)	Unit Weight (2)		
Dead Loads			
Steel Framing	As Designed		
Floor and Roof	50 psf	2.3941 kPa	
	(3 in. Metal Deck with 2 ½ in. Normal Weight Concrete)		
Roofing	7 psf	0.3352 kPa	
Ceiling/Flooring	3 psf	0.1436 kPa	
Mechanical/Electrical	7 psf	0.3352 kPa	
	47 psf	2.2505 kPa	(At Penthouse)
Partitions	20 psf	0.9576 kPa	(Gravity Design)
	10 psf	0.4788 kPa	(Seismic Design and Analysis)
Exterior Wall	25 psf	1.1970 kPa	
Live Load	50 psf	2.3941 kPa	

Table 6: Three-Story BRBF Model Loads

Story	Seismic Mass		BF Column Load		BF Beam Load		P-Δ Column Load	
	(kip-sec^2/in)	(kN-sec^2/mm)	(kip)	(kN)	(kip)	(kN)	(kip)	(kN)
(1)	(2)		(3)		(4)		(5)	
3	1.0700	0.1874	30.3	134.8	12.2	54.4	410.3	1825.0
2	1.1915	0.2087	50.1	222.8	19.2	85.4	466.4	2074.5
1	1.1915	0.2087	50.1	222.8	19.2	85.4	466.4	2074.5

framing members were ASTM A992 steel, with a strain hardening modulus 5% that of Young's Modulus. Braces were modeled as nonlinear truss elements (element type 2). ASTM A36 steel was assumed for the braces. The compressive yield stress was modeled as 110% of the tensile yield stress based on typical buckling restrained brace test results (Aiken, et al. 2000). Brace cross-sectional area was calculated from the brace yield force given by Sabelli (2000) and a nominal yield stress of 36 ksi. An equivalent Young's Modulus was then calculated from this area and the horizontal brace stiffness. A post-yield slope of 7.5% of the elastic stiffness was used as calculated from previous UBB testing (Aiken, et al. 2000). Inherent viscous damping of 5% was assumed per standard practice in the seismic design of steel structures and was applied as mass and initial stiffness proportional damping factors.

Ground motions considered (LA01-LA20) were developed for the SAC steel project (Woodward-Clyde Federal Services, 1997). The 20 earthquake records used are for a site in Los Angeles with a 10% probability of exceedence in 50 years (design basis earthquakes, 475 year return period). Nonlinear dynamic time history analysis was completed for the LA series earthquakes and the results analyzed to determine the event that produced the greatest BRB demand. Of the 20 synthetic earthquake records, LA20 generated the highest BRB demand in terms of maximum brace displacement and cumulative ductility. First story compression

dominated brace axial displacement time history response for LA20 is shown in Fig. 15. This displacement history was simplified and scaled to develop a random displacement history (Fig. 16). In the simplification, large displacement peak-to-peak displacements were retained and smaller elastic cycles were neglected. Displacement values were scaled such that the maximum compressive displacement corresponds to 1% story drift (1.19 in. (30.23mm) local brace displacement, Δ_{bm}). The random displacement history was applied at the same 1.33 in/min (33.78 mm/min) displacement rate as the increasing amplitude displacement history. Multiple iterations of this random displacement history were applied to specimen 50P-2. After each iteration both load and displacement were returned to zero with an additional small inelastic displacement and elastic unloading.

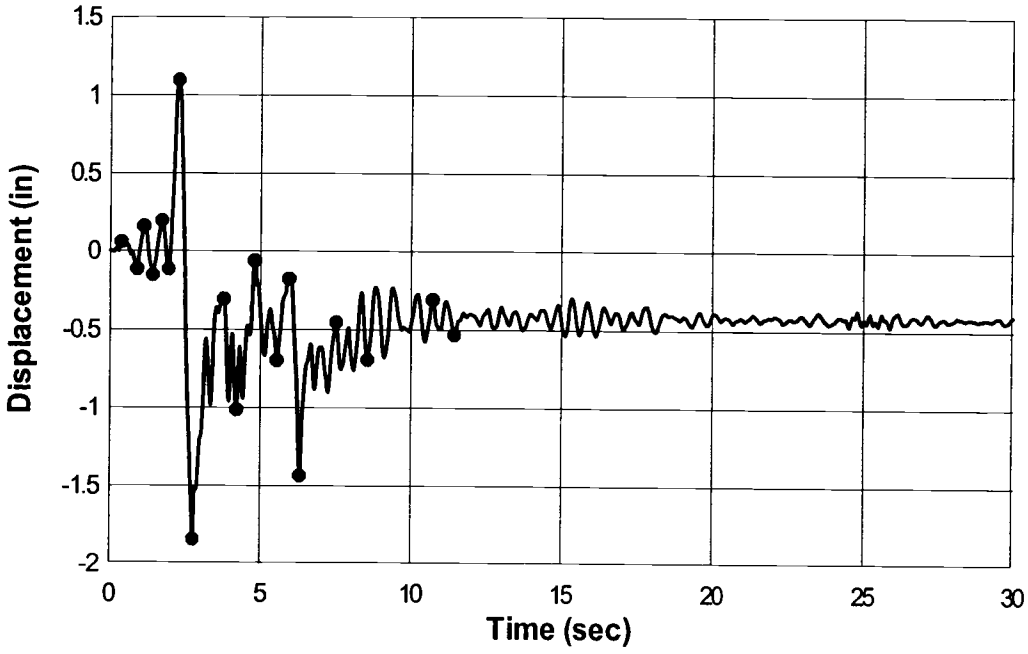

Figure 15: First story BRB axial displacement time history for LA20.

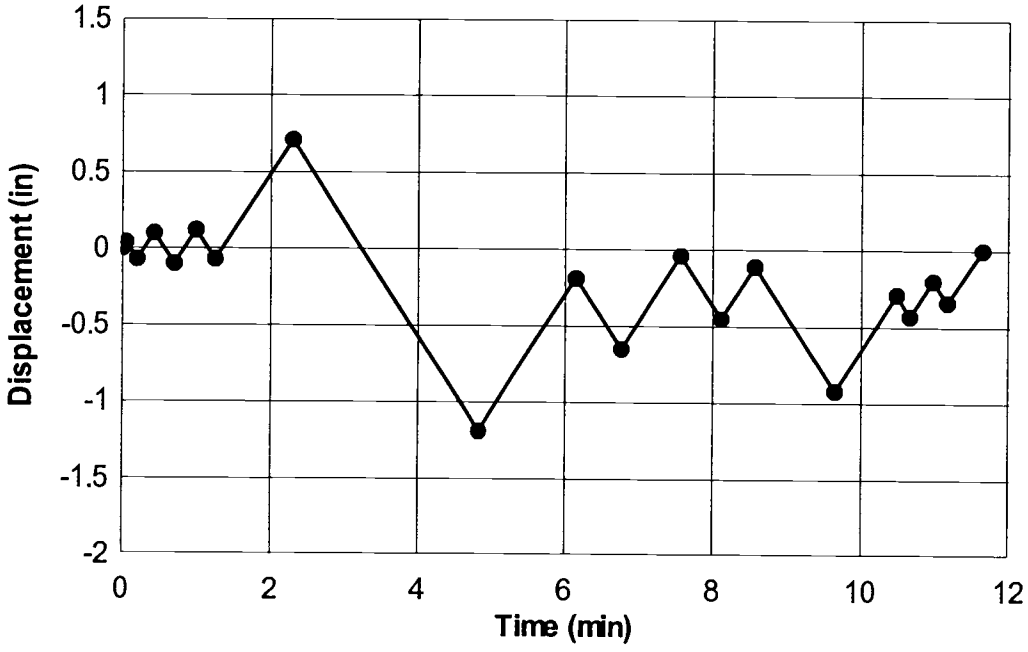

Figure 16: Simplified random displacement history imposed on specimen 50 DB-2.

EXPERIMENTAL RESULTS

Parameters Used for Comparison

AISC/SEAOC Recommended Buckling-Restrained Brace Frame Provisions (AISC/SEAOC, 2001) specify that the ratio of maximum compressive force to maximum tensile force (C/T) shall not exceed 1.3. This criterion serves to limit potential unbalanced forces and ensures reasonably symmetric hysteretic behavior. BRB demand from the increasing amplitude displacement protocol defined in the *AISC/SEAOC Provisions* is based on nonlinear dynamic time history analysis of BRBF buildings (Sabelli, 2000). BRBs are required to achieve displacements corresponding to 1.5 Δ_{bm} (mean of Sabelli analysis) and cumulative ductilities of 140 Δ_{by} (mean plus one standard deviation of Sabelli analysis). These are believed to be conservative values and may be revised as more data becomes available (AISC/SEAOC, 2001).

Test Observations

Results for all specimens are summarized in Table 7 and shown in the appendix. Post-test yielding core pictures, load-displacement plot, displacement plot, string pot displacement plot, yielding core/confining tube relative displacement plot, and an additional plot illustrating performance are shown for each specimen. Displacements reported in hystersis and

Table 7: CYD Performance Summary

Specimen	Max. Tensile Force T		Max. Compressive Force C		C/T	Max. Tensile Displacement		Max. Compressive Displacement		Total Energy Dissipated		Cumulative Ductility	Fracture On Cycle	1st Compressive Degradation On Cycle
	(kip)	(kN)	(kip)	(kN)		(in)	(mm)	(in)	(mm)	(kip-in)	(kN-mm)	(Δ_{by})		
(1)	(2)		(3)		(4)	(5)		(6)		(7)		(8)	(9)	(10)
125DB-1	151.6	674.3	154.7	688.1	1.02	2.404	61.06	2.452	62.28	5230	590881	176	1 @ 2.0 Δ_{bm}	2 @ 1.5 Δ_{bm}
125DB-2	155.8	693.0	163.5	727.2	1.05	2.394	60.81	2.074	52.68	6165	696517	183	2 @ 2.0 Δ_{bm}	2 @ 1.5 Δ_{bm}
125DB-3	145.8	648.5	95.5	424.8	0.66	4.177	106.10	1.705	43.31	2051	231720	125 #	**	1 @ 0.5 Δ_{bm}
125DB-4	143.6	638.7	137.0	609.4	0.95	2.969	75.41	2.803	71.20	5852	661154	272	1 @ 3.0 Δ_{bm}	3 @ 0.5 Δ_{bm}
125DB-5	167.2	743.7	143.9	640.1	0.86	2.391	60.73	2.057	52.25	5785	653585	216	2 @ 2.0 Δ_{bm}	2 @ 1.5 Δ_{bm}
125P-1	131.9	586.7	131.1	583.1	0.99	1.269	32.23	1.038	26.37	1525	172293	83 #	4 @ 1.0 Δ_{bm}	1 @ 0.5 Δ_{bm}
125P-2	158.6	705.5	169.6	754.4	1.07	2.204	55.98	1.689	42.90	4955	559812	220	1 @ 2.0 Δ_{bm}	3 @ 1.0 Δ_{bm}
125P-3	159.9	711.2	182.4	811.3	1.14	2.364	60.05	2.342	59.49	5858	661832	261	1 @ 2.0 Δ_{bm}	2 @ 1.5 Δ_{bm}
125P-4	166.2	739.3	257.6	1145.8	1.55 #	2.408	61.16	2.278	57.86	7637	862822	280	**	##
125P-5	167.1	743.3	252.9	1124.9	1.51 #	2.410	61.21	2.095	53.21	6792	767355	236	**	##
50DB-1	64.6	287.3	68.8	306.0	1.07	1.816	46.13	1.660	42.16	1957	221100	182	3 @ 1.5 Δ_{bm}	4 @ 1.0 Δ_{bm}
50DB-2	68.0	302.5	78.2	347.8	1.15	2.356	59.84	2.344	59.54	1230	138964	101 #	**	2 @ 1.5 Δ_{bm}
50P-1	67.0	298.0	73.3	326.0	1.09	1.804	45.82	1.715	43.56	1639	185173	195	2 @ 1.5 Δ_{bm}	2 @ 1.0 Δ_{bm}
50P-2	57.9	257.5	72.1	320.7	*	0.718	18.24	1.223	31.06	1475	166660	180	**	Iteration 3

DB Dog bone configuration
P Perforated configuration

* Unequal tensile and compressive displacements
** Limit state other than fracture
# Does not meet AISC / SEAOC Provisions
Compressive Degradation not observed

displacement figures are the CYD yielding core axial displacement based on weighted average of the east and west yielding core displacement sensors. The string pot displacements show the east and west yielding core string pot displacements. A differential displacement of these sensors provides an indication of out of plane bending of the yielding core outside the confining tube. The yielding core/confining tube relative displacement plot shows the relative movement of the yielding core into and out of the confining tube at each end. Typically the majority of yielding core displacement took place at the south (actuator) end of the specimen.

Bolt slip was not observed indicating adequate slip critical connection design. Detailing of class A slip surface eliminated the expense of sand blasted faying surfaces and did not decrease CYD performance.

Yielding was distributed along the entire reduced section yielding core length for both the dog bone and perforated configurations as evidenced by uniform flaking of mill scale. Strain gages on the yielding core did not indicate bending (with the exception of 125DB-3) and showed equivalent strain at the three instrumented locations up to the 3000 microstrain range limitation of the gages.

The typical failure mechanism observed was fracture of the steel yielding core induced by increased tensile strains due to local high amplitude buckling at the actuator end of the specimen. Increasing the length of unreduced cross-section within the confining tube would provide

increased buckling resistance for this portion of the device. This would provide a larger unreduced yielding core surface area to be in contact with the confining media thereby limiting buckling and the associated bending strains.

Confining Media Effects

CYD performance was determined to be highly dependent on confining media particle size. 125DB specimens were tested using pea gravel, sand, 3/4 in. (19.05 mm) to #4 gravel, and 3/4 in. (19.05 mm) minus gravel.

Specimen 125DB-2 tested with pea gravel confining media provided reasonably stable and symmetric hysteretic response. The load-displacement curve for this specimen is shown in Fig. 17. The C/T value of 1.05 is well within the suggested 1.3 limit and in line with a compressive overstrength of 1.1 typical of UBBs. A total of 6165 kip-in (696517 kN-mm) of energy was dissipated by the device. The cumulative ductility of 183 Δ_{by} exceeded the 140 Δ_{by} requirement of the *AISC/SEAOC Provisions*.

Pea gravel confining media was also used for specimen 50DB-1. Fig. 18 shows reasonably stable and symmetric dissipation of 1957 kip-in (221100 kN-mm) of energy. The C/T value was 1.07 and a cumulative ductility of 182 Δ_{by} was achieved. The smaller yield force device dissipated

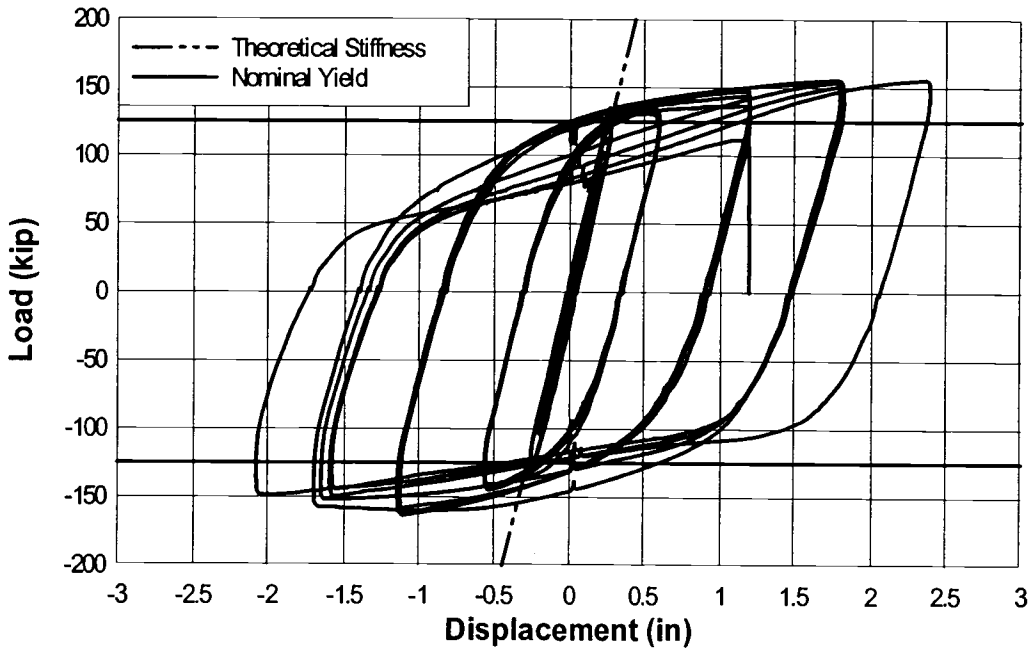

Figure 17: Specimen 125DB-2 hysteresis.

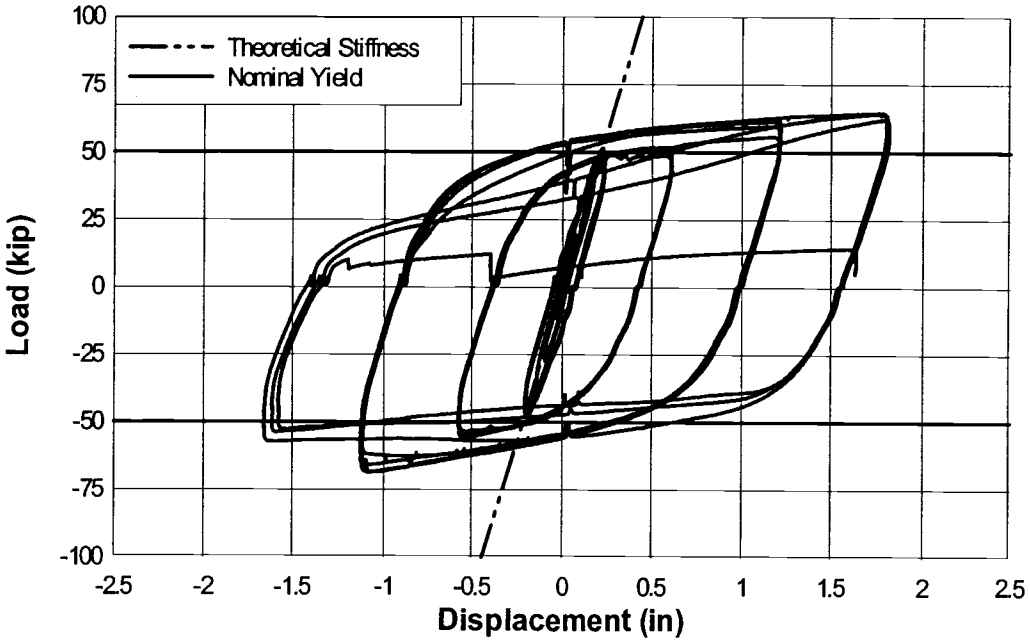

Figure 18: Specimen 50DB-1 hysteresis.

proportionally less energy but still achieved approximately the same cumulative ductility as 125DB-2.

Sand confining media did not adequately prevent the yielding core (125DB-3) from translating through the confining media. As a result the core buckled in approximately the fourth mode in the weak direction and second mode in the strong direction. The load-displacement curve (Fig. 19) shows this buckling with significant pinching of the hysteresis loops. After the second cycle at 1.5 Δ_{bm} a large tension excursion was applied to a displacement of 4.2 in. (106.7 mm) without yielding core fracture. This indicates the dog bone yielding core is capable of undergoing significant inelastic deformation and that the buckling did not produce large strain concentrations at one particular location along the yielding core. Sand confining media for this specimen geometry does not provide sufficient confinement to enable stable and symmetric hysteretic damping.

Larger sized aggregates alone did not significantly enhance performance. Significant crushing of the 3/4 in. (19.05 mm) to #4 gravel and the associated confining media volume loss led to considerable localized buckling at the ends of the reduced section of specimen 125DB-4. Compressive degradation was observed significantly earlier than with pea gravel or 3/4 in. (19.05 mm) minus gravel confining media (cycle 3 @ 0.5 Δ_{bm} vs. cycle 2 @ 1.5 Δ_{bm}). 3/4 in. (19.05 mm) to #4 gravel is not an optimal confining media for this specimen geometry.

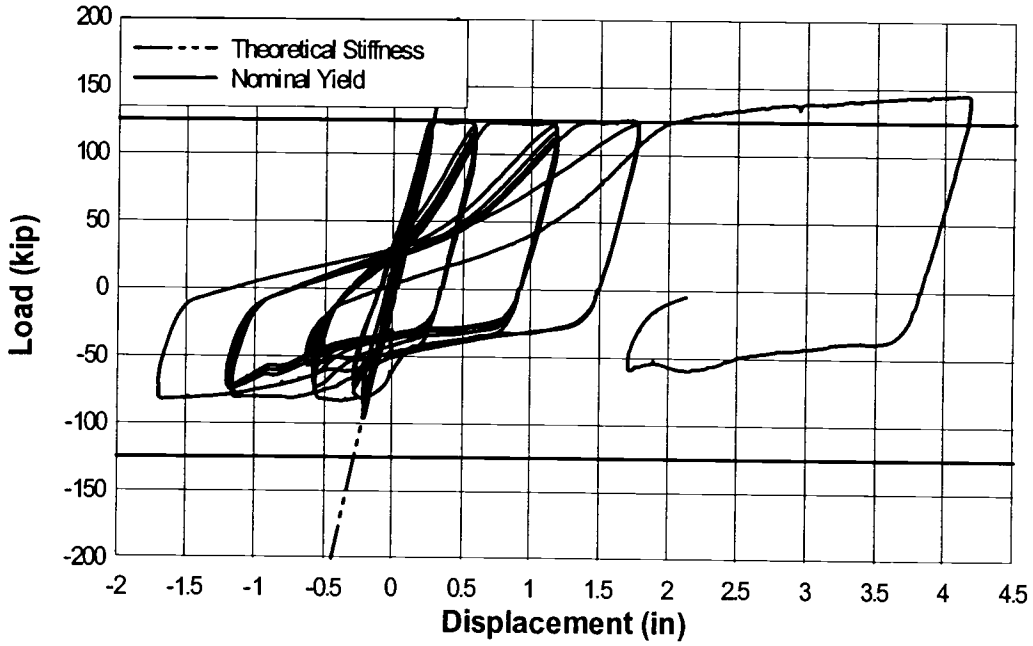

Figure 19: Specimen 125DB-3 hysteresis.

Specimen 125DB-5 tested with 3/4 in. (19.05 mm) minus gravel confining media performed similar to specimen 125DB-2 confined with pea gravel. The larger aggregate locks together preventing translation with fines filling voids. No significant benefit was observed by using the 3/4 in. (19.05 mm) minus gravel. Pea gravel was used as the confining media for remaining testing and the cost associated with producing the 3/4 in. (19.05 mm) minus gravel blend were avoided.

For all specimens the threaded rods were initially tensioned to approximately 5 kip (22.2 kN) each to maintain the confining media volume. This force diminished during testing due to crushing of gravel confining media and associated volume change. Typically 1 kip (4.4 kN) of tension force remained in each threaded rod after testing when the dead blow hammer was used for compaction. When the pencil vibrator and dead blow hammer were both used for compaction typically 2 kip (8.9 kN) of tension force remained in each threaded rod when testing was complete. This higher retention of rod force can be attributed to increased confining material relative density when compacted using both methods. With more confining material contained within the same volume, particle translation is reduced and localized crushing does not create significant confining media volume change.

Testing of different confining media indicated that particle size and shape must be such that localized crushing of the confining media does not

create a significant volume loss, and that there is adequate particle interlock so that the yielding core cannot translate through the confining media. It is hypothesized that a rectangular confining tube may help to prevent confining media translation. The rolled corners of a rectangle section might better lock-in the confining media than the circular shape of a pipe.

Perforation Blocking Effects

Specimen 125P-1 was tested with perforations filled with spray foam to prevent the yielding core perforation ends from bearing on the pea gravel confining media. Desirable structural performance was not achieved. Fig. 20 shows a lack of stable hysteresis due to the legs of the first perforation at the actuator end buckling in towards each other. Abrupt stiffening occurred when the buckled legs came into contact with each other.

Following the poor performance of specimen 125P-1, different configurations of perforation blocking were investigated to prevent buckling of perforation legs. Combinations in which the complete width of the first two perforations on each end and partial width (perforation width minus 1/2 in.) of the remaining perforations were blocked with steel plate provided the

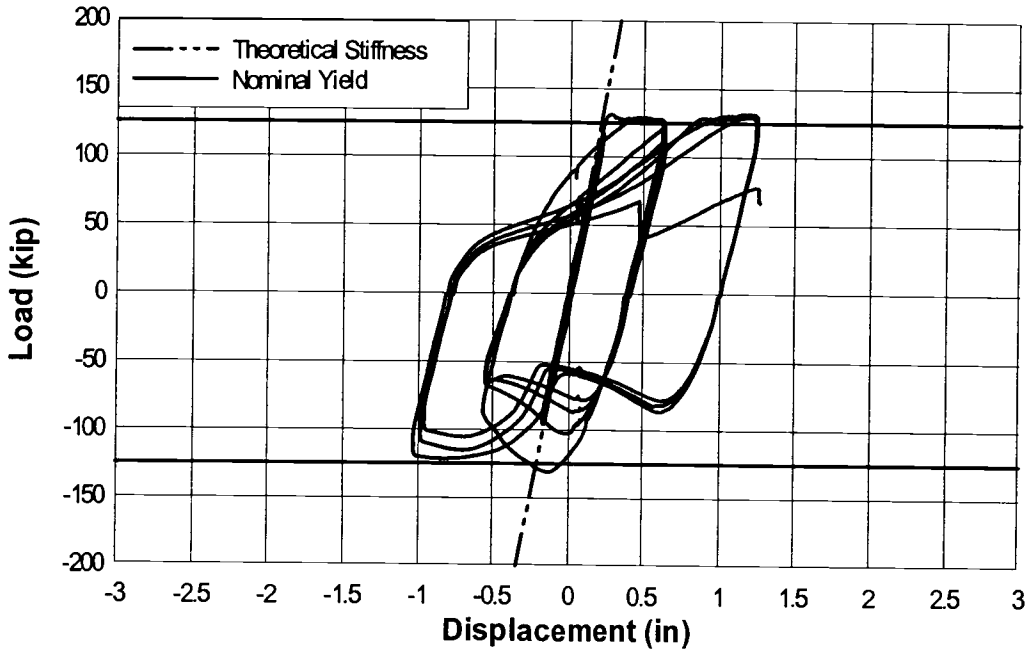

Figure 20: Specimen 125P-1 hysteresis.

best results. It is possible that perforation blocking could be completely avoided by using shorter perforation leg lengths, while still achieving required ductility.

Reasonably stable and symmetric hysteretic behavior is shown in Fig. 21, for specimen 125P-5. The first two perforations at each end were completely blocked with their original knockout from water jet cutting. Remaining perforations were blocked with a plate 2 in. (50.8 mm) shorter and 1/2 in. (12.7 mm) narrower than the perforation dimensions. The elastic compressive stiffness for this blocked configuration was 845 kip/in (148 kN/mm), which was 1.45 times greater than the compression stiffness with no perforation blocking. This accounts for the compressive stiffening observed in the hysteresis curve. Perforation blocking did not affect tensile stiffness. The C/T value of 1.51 is above the AISC/SEAOC 1.3 limit. Future detailing of shorter legs would eliminate the need for perforation blocking and the associated compressive stiffening (high C/T value). A total of 6792 kip-in (696517 kN-mm) of energy was dissipated by the device. A cumulative ductility of 236 Δ_{by} was achieved before testing was suspended to limit damage to the reaction system from the high compressive forces.

Specimen 50P-1 was tested with the first two perforations at each end blocked with a steel plate 1 in. (25.4 mm) shorter and equal in width to the peroration dimension. Remaining perforations were blocked with a plate 1 in. (25.4 mm) shorter and 1/2 in. (12.7 mm) narrower than the

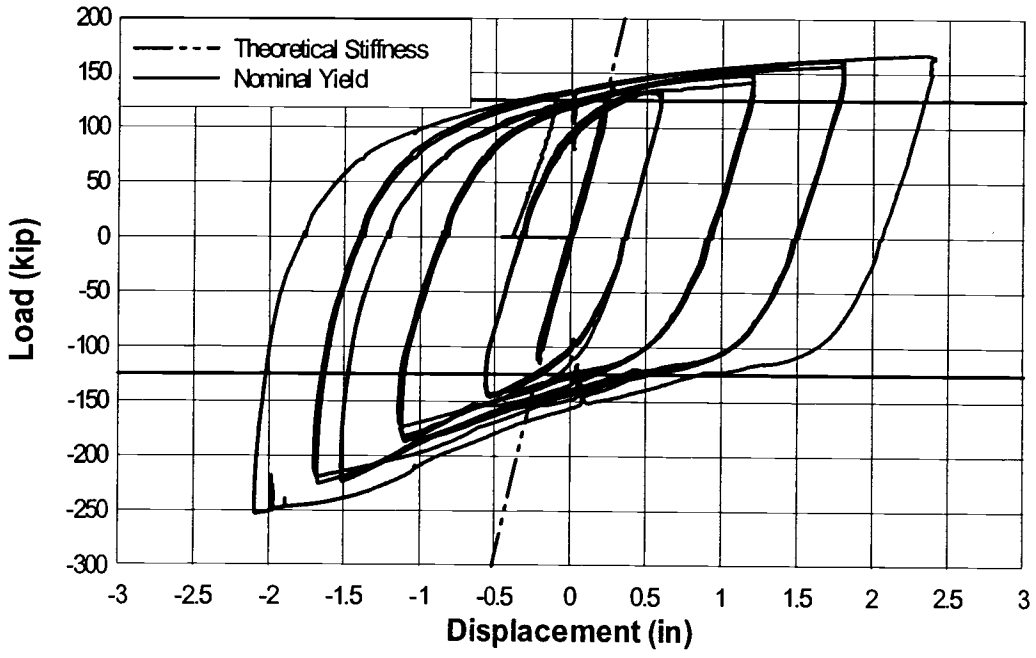

Figure 21: Specimen 125P-5 hysteresis.

perforation dimensions. The hysteresis curve (Fig. 22) indicates reasonably stable and symmetric hysteretic damping. Compressive stiffening observed in specimen 125P-5 was eliminated by not blocking the full length of the two perforations at each end. The weak direction of each perforation leg was in the out of plane direction. Buckling observed was in the out of plane direction and thus not restrained by perforation blocking. 1639 kip-in (185173 kN-mm) of energy was dissipated by the device. The C/T value was 1.09 and a cumulative ductility of 195 Δ_{by} was achieved. The smaller yield force device dissipated proportionally less energy but still achieved approximately the same cumulative ductility as 125P-5.

Decreasing Amplitude Displacement History

A decreasing amplitude displacement history was applied to specimen 50DB-2. One cycle at 2.0 Δ_{bm} was followed by two cycles at 1.5 Δ_{bm}. Yielding core fracture was observed on the subsequent cycle at 1.0 Δ_{bm}. The energy dissipated and cumulative ductility were 1230 kip-in (138964 kN-mm) and 101 Δ_{by}, respectively. These values are less than those of specimen 50DB-1 subjected to the increasing amplitude displacement protocol. However the largest single excursion displacement was 0.5 Δ_{bm} larger for specimen 50DB-2. This provides an indication that device performance is dependent on applied displacement history and devices can sustain very large cycles.

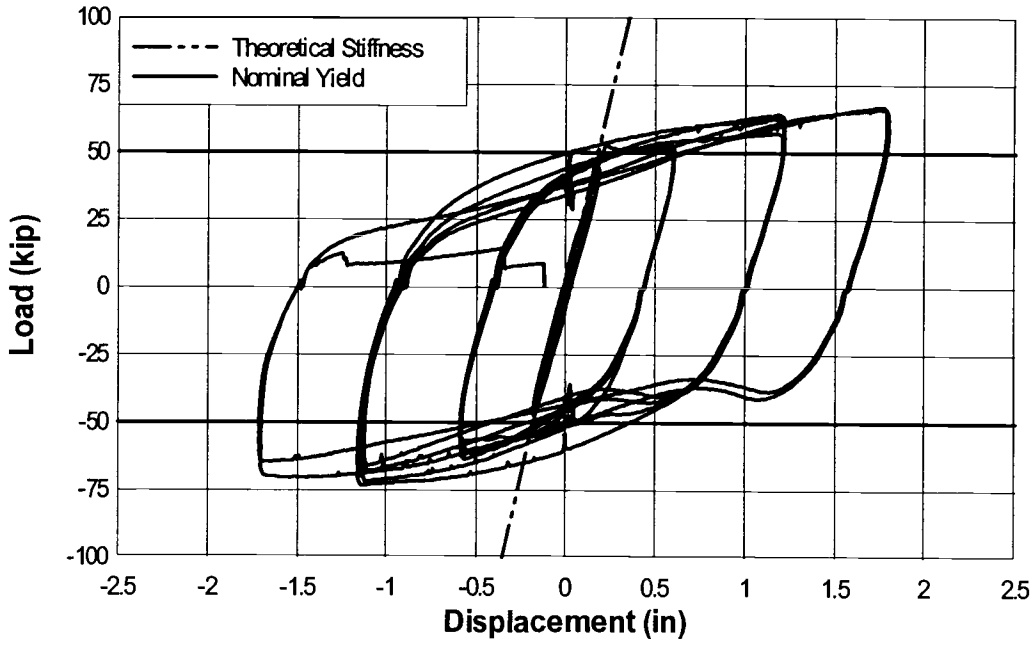

Figure 22: Specimen 50P-1 hysteresis.

Random Displacement History

Specimen 50P-2 was subjected to a random displacement history as defined above. Seven complete iterations of the random displacement and an eighth iteration up to the point of maximum compressive displacement were applied. Loading was suspended at maximum compressive displacement to examine the yielding core in that state. Confining media and the yielding core were removed from the confining tube. The yielding core was inspected for damage resulting from the applied random displacement history. A new yielding core and confining media could have been placed back into the confining tube and the device reinstalled for subsequent testing. Buckling and compressive stiffening was observed in the hysteresis curve (Fig. 23). Local buckling of the yielding core against the side of the confining tube resulted in this post-buckling compressive stiffening. Fig. 24 presents each individual iteration of random displacement history and shows progressive degradation in CYD performance. There was a gradual decrease in the energy dissipated per iteration (Table 8) due to pinching of the hysteresis loops. Cumulative ductility values per iteration however do not illustrate this performance degradation because the same displacements were reached but at lower brace axial forces. Therefore cumulative ductility performance specifications should be combined with other measures to ensure reasonably stable and symmetric hysteretic response, such as efficiency of

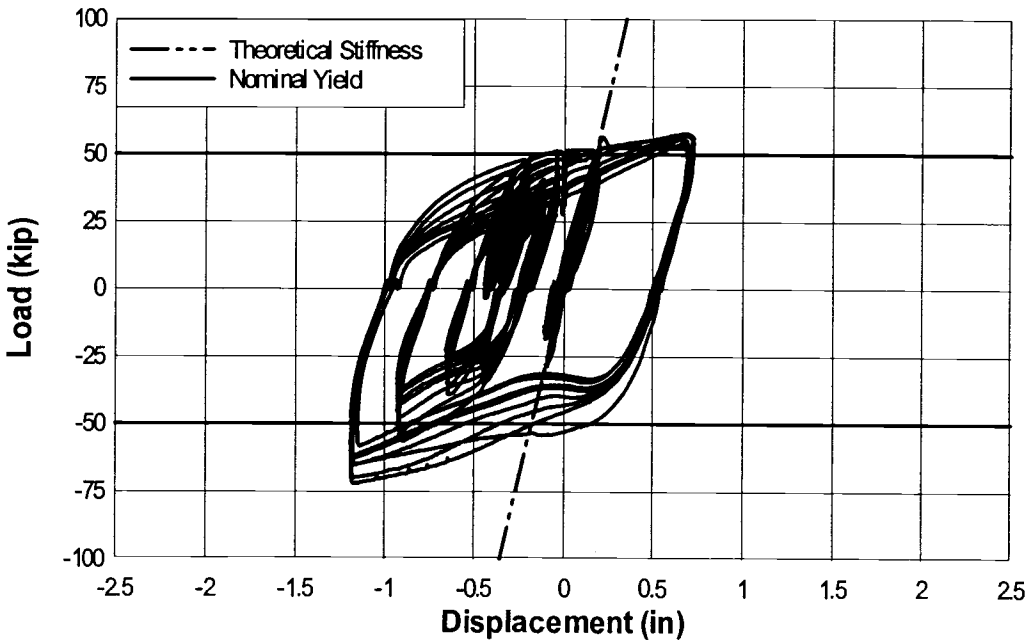

Figure 23: Specimen 50P-2 hysteresis.

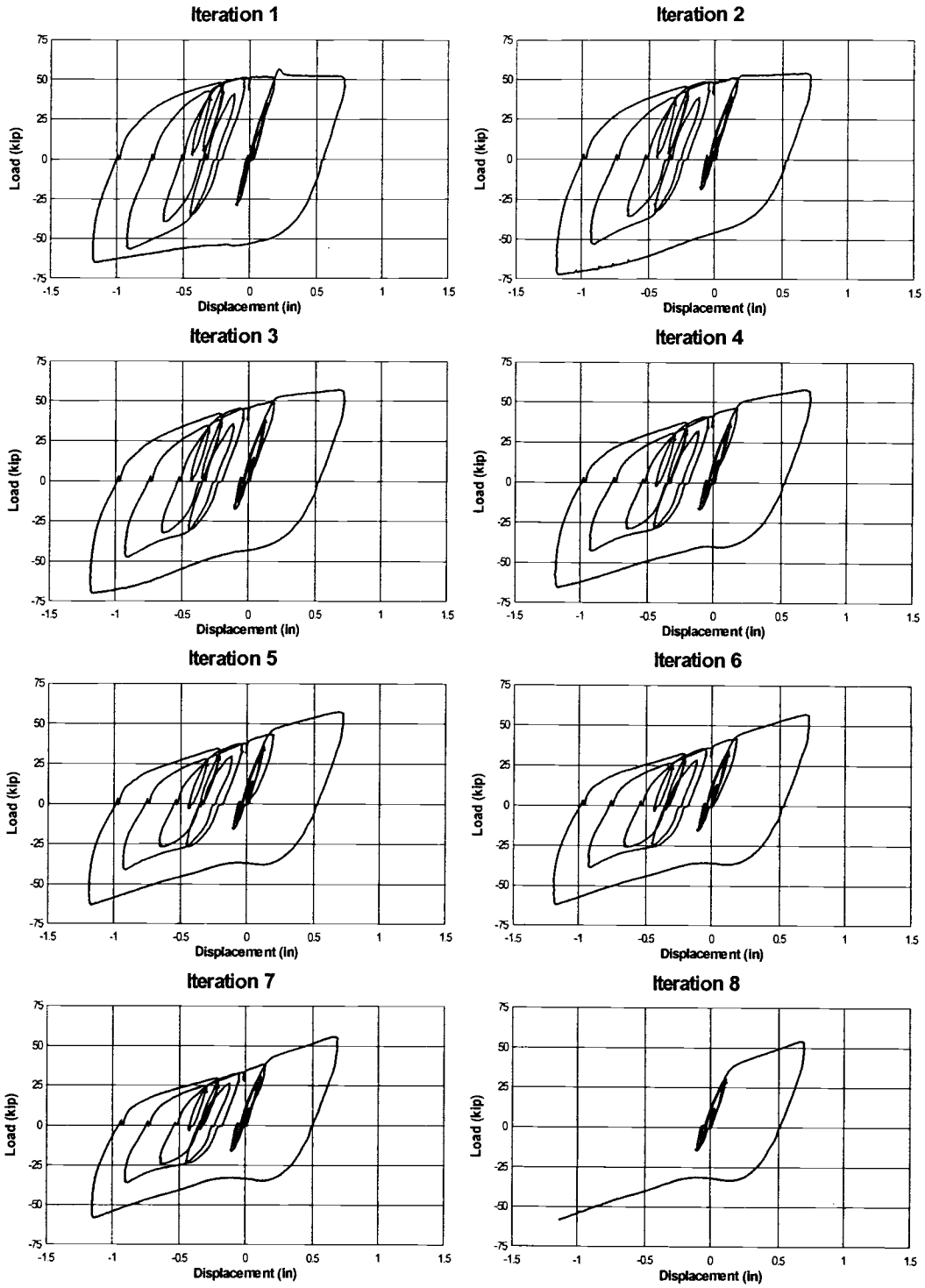

Figure 24: Specimen 50P-2 hysteresis for each iteration of imposed random displacement history.

Table 8: Random Displacement History Iteration Comparison

Iteration	Max. Tensile Force T		Max. Compressive Force C		C/T	Max. Tensile Displacement		Max. Compressive Displacement		Total Energy Dissipated		Cumulative Ductility
	(kip)	(kN)	(kip)	(kN)		(in)	(mm)	(in)	(mm)	(kip-in)	(kN-mm)	(Δ_{by})
(1)	(2)		(3)		(4)	(5)		(6)		(7)		(8)
1	56.4	250.8	65.1	289.4	1.15	0.718	18.24	1.176	29.87	230	26039	24.0
2	53.8	239.3	72.1	320.9	1.34	0.719	18.26	1.186	30.12	223	25186	24.6
3	56.9	253.1	70.0	311.5	1.23	0.724	18.39	1.185	30.10	211	23891	24.3
4	57.9	257.7	65.5	291.3	1.13	0.726	18.44	1.188	30.18	196	22134	24.3
5	57.6	256.1	63.0	280.3	1.09	0.727	18.47	1.183	30.05	186	20990	24.4
6	57.2	254.3	62.0	275.9	1.09	0.727	18.47	1.186	30.12	179	20233	24.5
7	55.8	248.0	58.4	259.7	1.05	0.692	17.58	1.149	29.18	159	18019	22.8
8	54.3	241.4	58.4	259.6	1.08	0.698	17.73	1.132	28.75	90	10167	11.5
									Total	1475	166660	180.4

energy dissipation or secant stiffness on subsequent cycles of similar amplitude.

The experimental results were then compared with a PC-ANSR time history response for a CYD subjected to the imposed random displacement history. The original properties for the inelastic truss element used to model the brace were a compressive yield strength equal to 1.1 times the tensile yield strength; an effective Young's Modulus calculated from brace stiffness, length, and cross-sectional area; and a strain hardening modulus of 7.5% of Young's Modulus. These are the same brace properties used in the three-story building model to generate the time history response. When compared to actual CYD performance it was determined that a compressive yield strength equal to the tensile yield strength more accurately reflected experimental results. Also an efficiency factor of 80% was applied to Young's Modulus to better represent elastic CYD stiffness. The strain hardening modulus was divided by this efficiency factor to maintain the same post yield slope. Experimental and analytical results are illustrated in Fig. 25. The energy dissipated by specimen 50P-2 iteration 2 was 223 kip-in (25186 kN-mm) while the analytical model dissipated 170 kip-in (19206 kN-mm). The analytical model therefore conservatively underestimates the energy dissipation capacity of the CYD.

The response of the model three-story building was then determined with the revised CYD properties to determine if the developed random

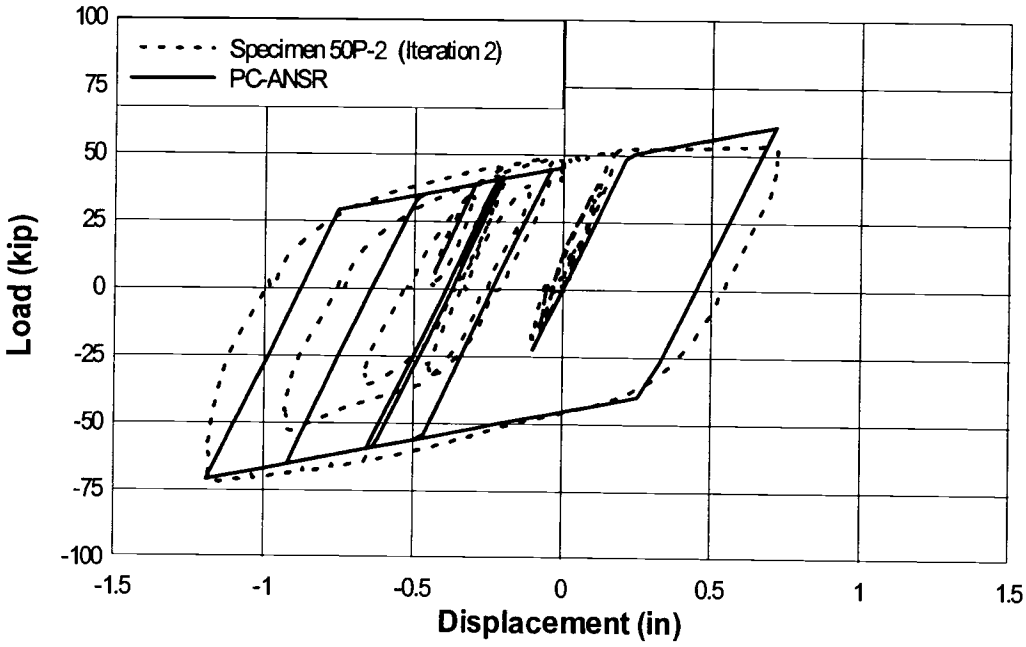

Figure 25: Experimental and analytical force-deformation response for specimen 50P-2 during second iteration of imposed random displacement history.

displacement history was still an accurate representation of expected BRB demand. First story BRB time history response (Fig. 26) for the initial and revised cases show a 16% increase in maximum brace axial displacement. Roof displacement increased by 14% for the revised BRB properties as shown in Fig. 27. Residual displacements also increased as given in Table 9. This increase in displacements would not significantly change overall BRB ductility demand during the event.

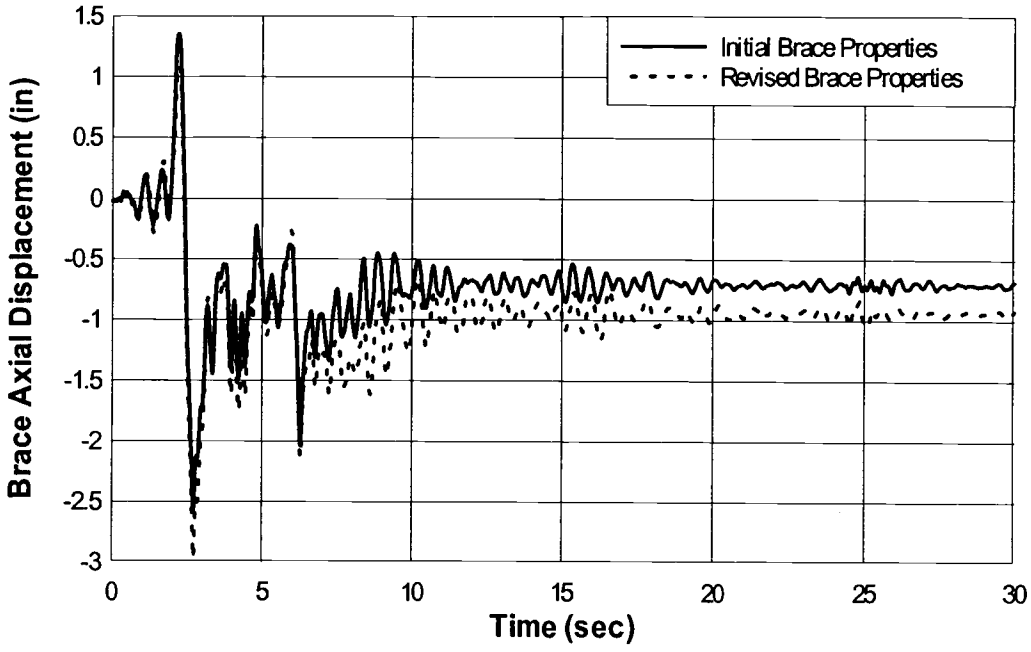

Figure 26: Analytically predicted BRB axial displacement in the first story time history using theoretical CYD response and modified based on experimental results.

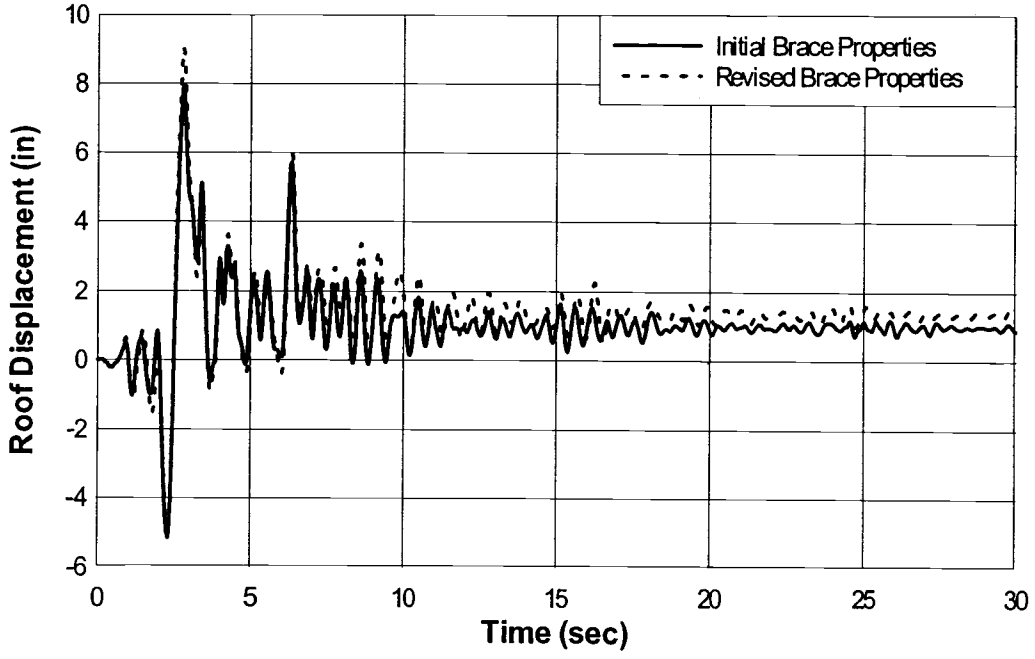

Figure 27: Analytically predicted roof displacement time history using theoretical CYD response and modified based on experimental results.

Table 9: Nonlinear Dynamic Time History Results

Element	Initial Brace Properties				Revised Brace Properties			
	Max. Displacement		Residual Displacement		Max. Displacement		Residual Displacement	
	(in)	(mm)	(in)	(mm)	(in)	(mm)	(in)	(mm)
(1)	(2)		(3)		(4)		(5)	
Local Brace	2.57	65.28	0.72	18.29	2.97	75.44	0.96	24.38
Horizontal Roof	7.94	201.68	0.99	25.15	9.03	229.36	1.34	34.04

CONCLUSIONS

A new type of tension-compression yielding brace or buckling-restrained brace to dissipate seismic induced forces has been investigated and tested. The Confined Yielding Damper consists of a steel yielding core element within a structural tube filled with non-cohesive media. This non-cohesive media is placed under a normal confining force to provide buckling resistance of the core, enabling the device to yield in compression without global buckling of the brace. The testing program examined the effects of different confining media, perforation blocking configurations, and random displacement histories. Based on Confined Yielding Dampers test results the following observations and conclusions are presented:

1. A properly designed, detailed, and constructed CYD device exhibits reasonably stable and symmetric hysteretic response of input fully reversed cyclic loading.
2. Bolt slip was avoided with slip-critical bolted connections, class A slip surfaces, and fully tensioned A490 high strength structural bolts.
3. Extending the unreduced length of steel yielding core further into the confining tube would help to reduce local buckling at the end of the yielding core by providing more rotational and translation resistance.

4. Confining media particle size and shape must be such that localized crushing of the confining media does not create a significant volume loss.
5. Confining media particle size and shape must be such that there is adequate particle interlock to limit yielding core translation through the confining media.
6. Reducing the perforation leg length would increase the perforation buckling capacity and limit the necessity for perforation blocking.
7. Gradual compressive degradation was observed when a CYD was subjected to multiple iterations of a random displacement history, although the performance as measured by cumulative ductility or energy dissipation was quite good even after the 6^{th} iteration.
8. CYDs can be uninstalled, inspected, reconstructed, and reinstalled after a seismic event while reusing major components of the device.
9. Cumulative ductility performance specifications should consider other quantitative measures to ensure reasonably stable and symmetric hysteretic response for all types of yielding dampers. Change in energy dissipation or secant stiffness on subsequent cycles of similar amplitude would provide an additional indication of device performance.
10. The cross-sectional area and mechanical properties of the yielding core can be tailored to provide a device with the desired strength,

stiffness, and yield surface properties. Use of the perforated configuration provides greater flexibility in design.

11. The CYD can provide performance similar to that of the UBB, but has the additional benefits of reduced cost, post event inspection, simplified design, detailing, and construction.

The Confined Yielding Damper may provide a cost effective passive energy dissipation option that builds upon the strengths of the UBB. Desired structural performance properties of the CYD can be achieved by varying the cross-sectional area and mechanical properties of the steel core. Strength, stiffness, and yield surface properties can be adjusted using different grades of steel and different geometry of the steel core element. Multiple plates, of the same or different material, combined in parallel would permit further refinement of the design performance of the CYD device facilitating achievement of performance based design objectives. Additional testing of configurations of perforations, confining tube geometry, and confinement would aid future development of this type of damper.

BIBLIOGRAPHY

American Institute of Steel Construction. (1993). "Load and Resistance Factor Design Specification for Structural Steel Buildings." Chicago, Illinois.

American Institute of Steel Construction / Structural Engineers Association of California. (2001). "Recommended Buckling-Restrained Braced Frame Code Provisions (Draft)."

Applied Technology Council. (1992). ATC-24. "Guidelines for Cyclic Seismic Testing of Components of Steel Structures." Redwood City, California.

Aiken, I., Clark, P., Tajirian, F., Kasai, K., Kimura, I., Ko, E. (2000). "Unbonded Braces in the United States-Design Studies, Large-Scale Testing and the First Building Application." *Proceedings of International Symposium on Passive Control*, Tokyo Institute of Technology, Tokyo, Japan. pp. 203-217.

Black, C., Makris, N., Aiken, I. (2002). "Component Testing, Stability Analysis and Characterization of Buckling Restrained Braces." *Final Report to Nippon Steel Corporation,* Tokyo, Japan.

Federal Emergency Management Agency (1997). "1997 Edition NEHRP Recommended Provisions for Seismic Regulation of New Buildings and Other Structures." Washington, D.C.

Higgins, C. and Newell, J., "Development of Two New Hysteretic Dampers," *Proceedings of the Seventh U.S. National Conference on Earthquake Engineering*, Boston, Massachusetts, July 2002.

Higgins, C. and Newell, J., "Development of Economical Hysteretic Dampers," *Proceedings of the International Symposium on Passive Control*, Tokyo Institute of Technology, Tokyo, Japan, December, 2001.

International Conference of Building Officials. (1997). "Uniform Building Code." Whittier, California.

BIBLIOGRAPHY (Continued)

Maison, B. (1992). "PC-ANSR A Computer Program for Nonlinear Structural Analysis." University of California, Berkley, California.

Research Council on Structural Connections. (1994). "Specification for Structural Joints Using ASTM A325 or A490 Bolts." Chicago, Illinois.

Sabelli, R. (2000). "Research of Improving the Design and Analysis of Earthquake-Resistant Steel-Braced Frames." *2000 NEHRP Professional Fellowship Report,* EERI, Oakland, California.

Watanabe, A. (1992). "Development of Composite Brace with a Large Ductility." *US-Japan Workshop on Composite and Hybrid Structures*, San Francisco, California.

Watanabe, A., Hitomi, Y., Saeki, E., Wada, A., Fujimoto, M. (1988). "Properties of Brace Encased in Buckling-Restraining Concrete and Steel Tube." *Proceedings of Ninth World Conference on Earthquake Engineering*, Tokyo-Kyoto, Japan. Paper No. 6-7-4. Vol. IV, pp. 719-724.

Woodward-Clyde Federal Services. (1997). "Draft Report: Develop Suites of Time Histories." *Report to SAC Joint Venture Steel Project.* Pasadena, California.

APPENDIX

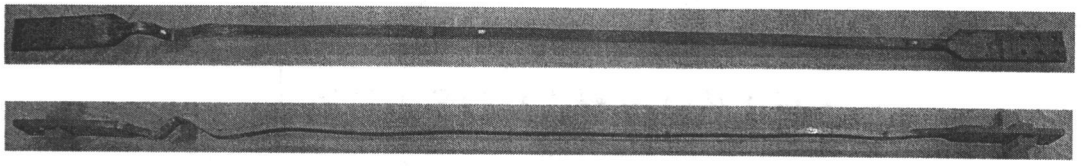

Figure A1: Specimen 125DB-1 Buckled Shape

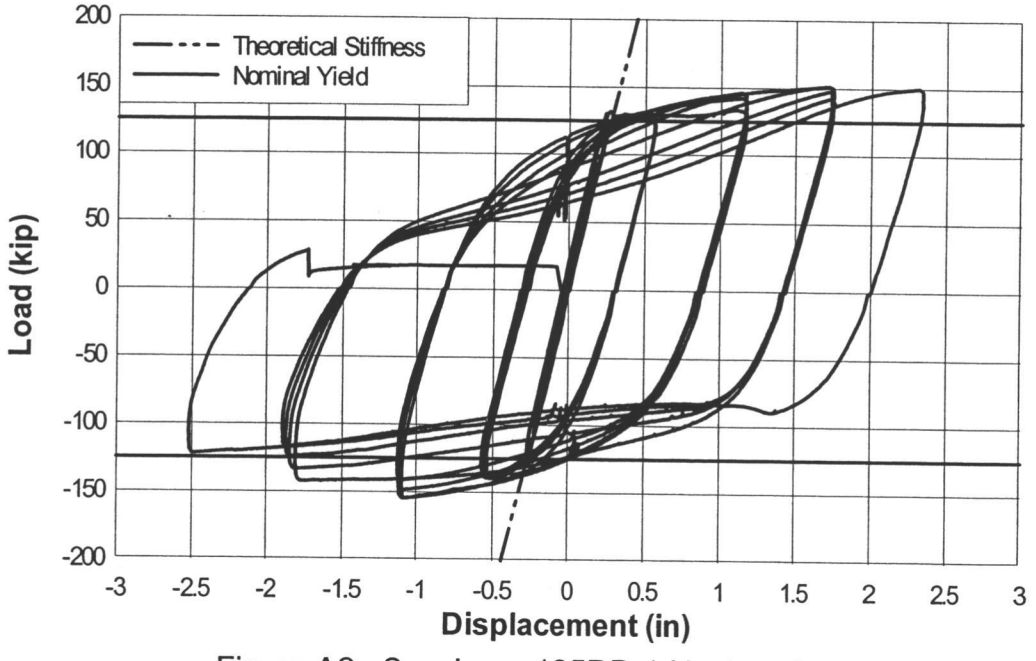

Figure A2: Specimen 125DB-1 Hysteresis

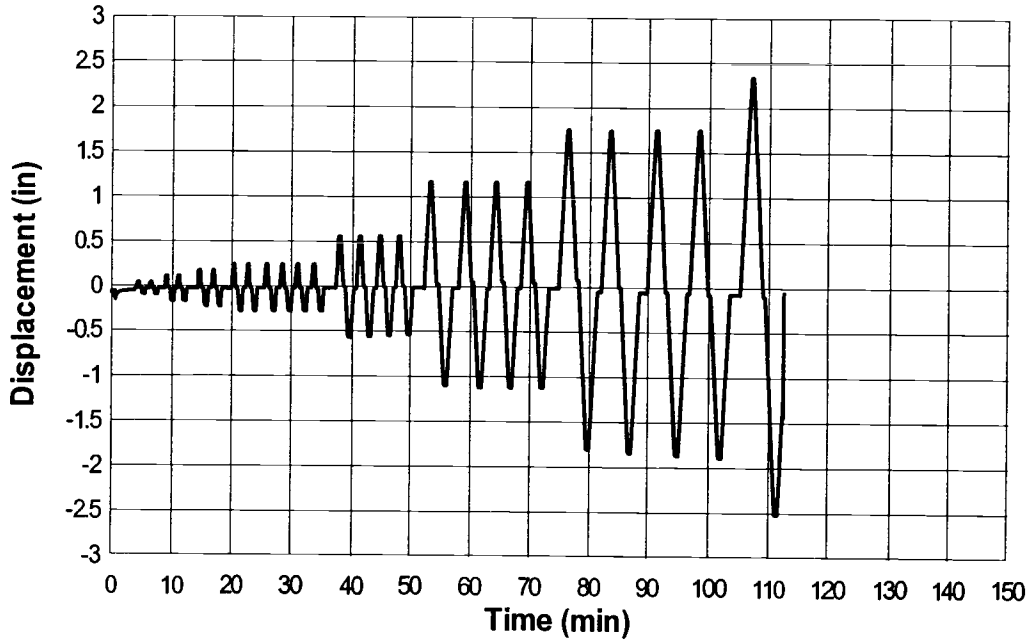

Figure A3: Specimen 125DB-1 Displacement

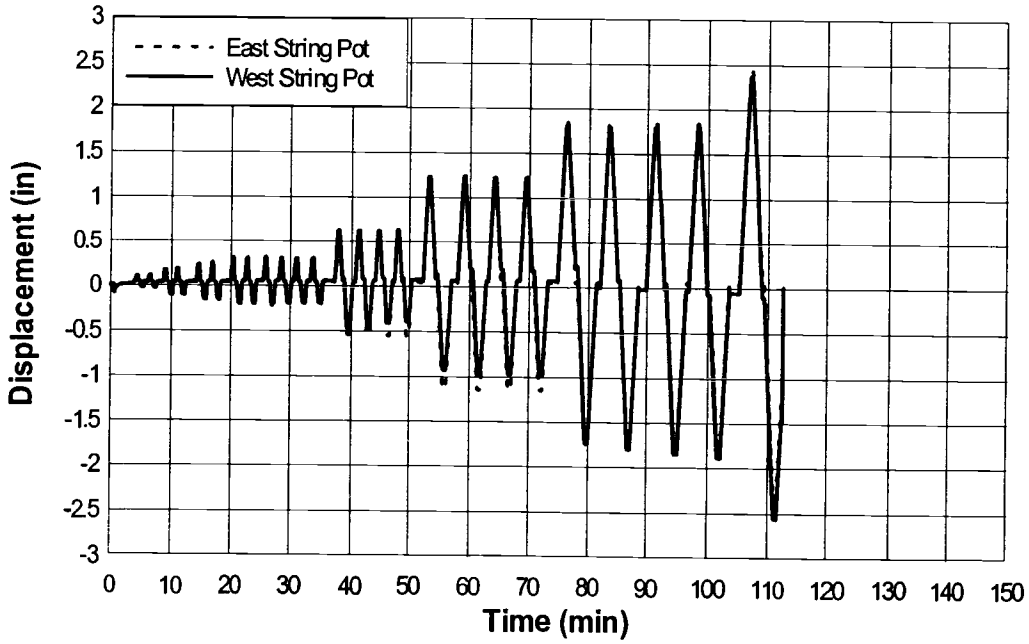

Figure A4: Specimen 125DB-1 String Pot Displacement

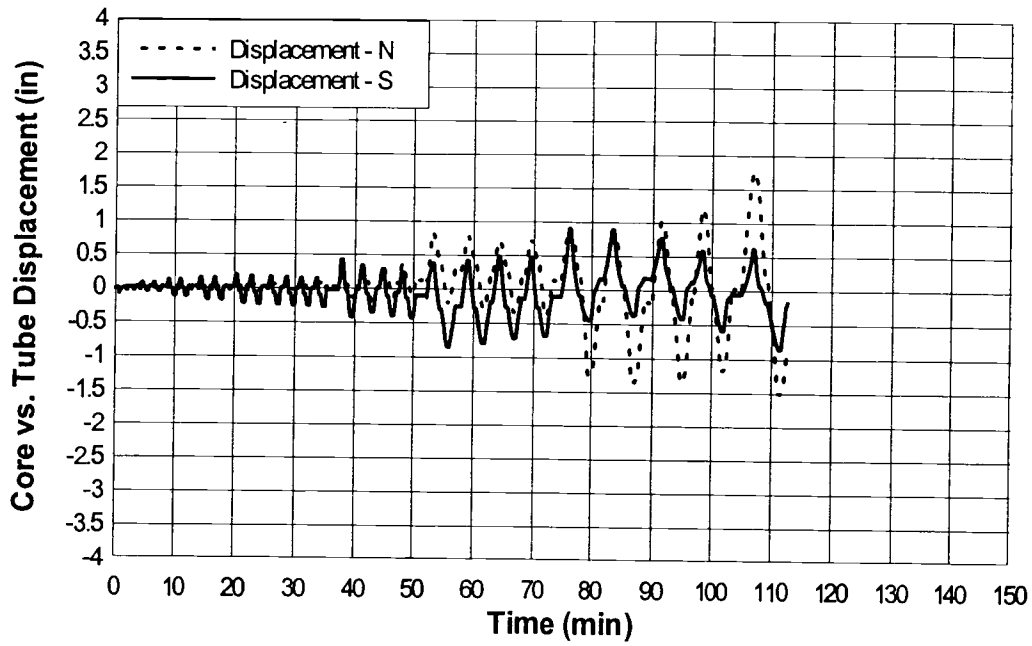

Figure A5: Specimen 125DB-1
Yielding Core/Confining Tube Relative Displacement

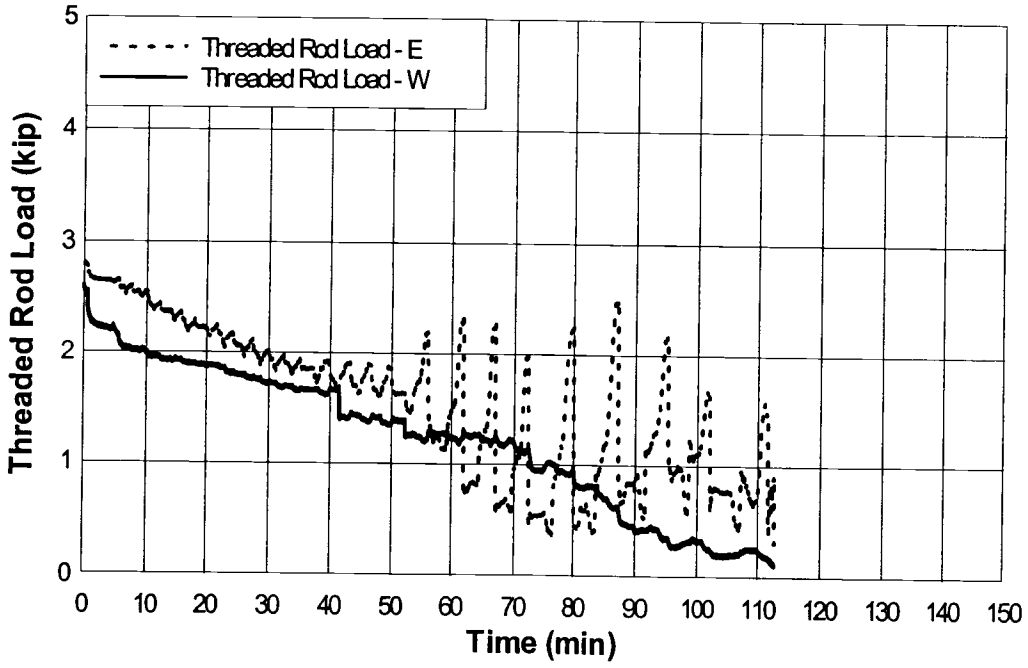

Figure A6: Specimen 125DB-1 Threaded Rod Load

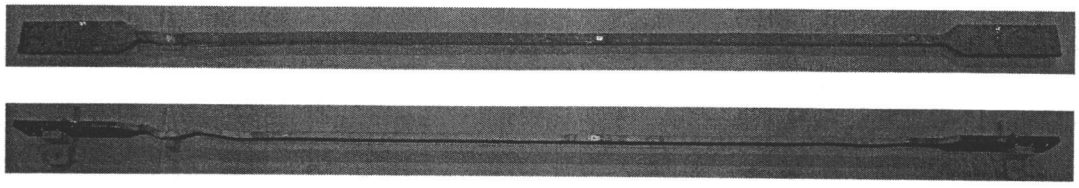

Figure A7: Specimen 125DB-2 Buckled Shape

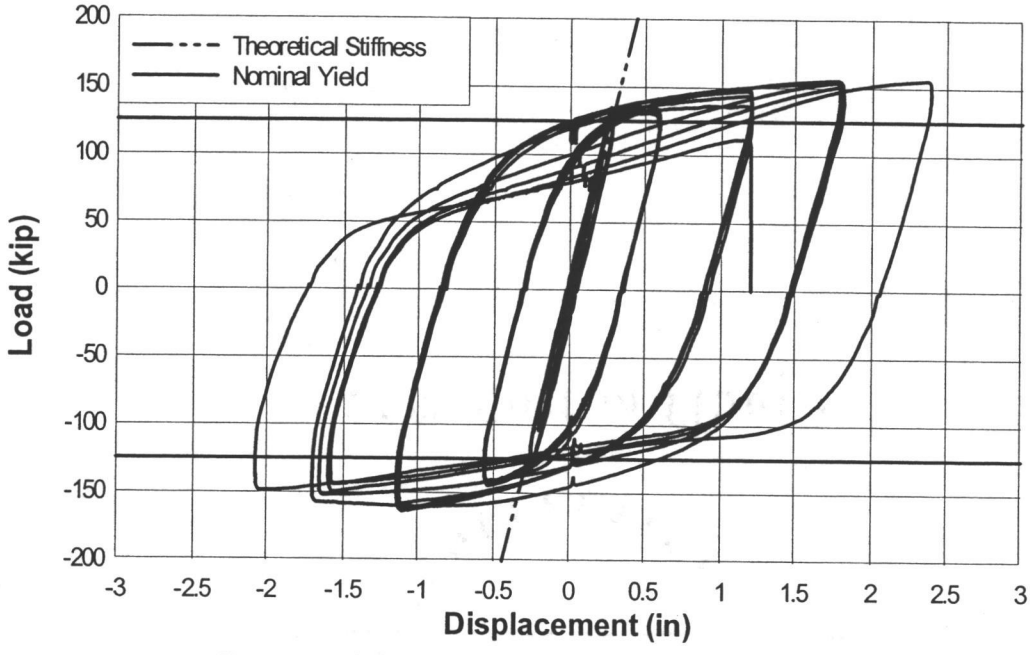

Figure A8: Specimen 125DB-2 Hysteresis

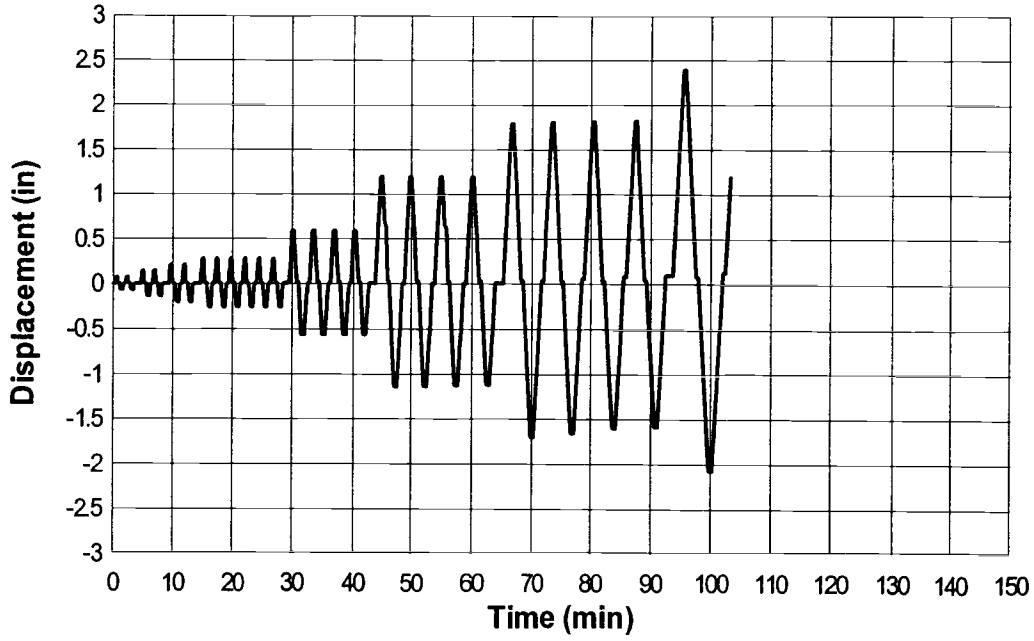

Figure A9: Specimen 125DB-2 Displacement

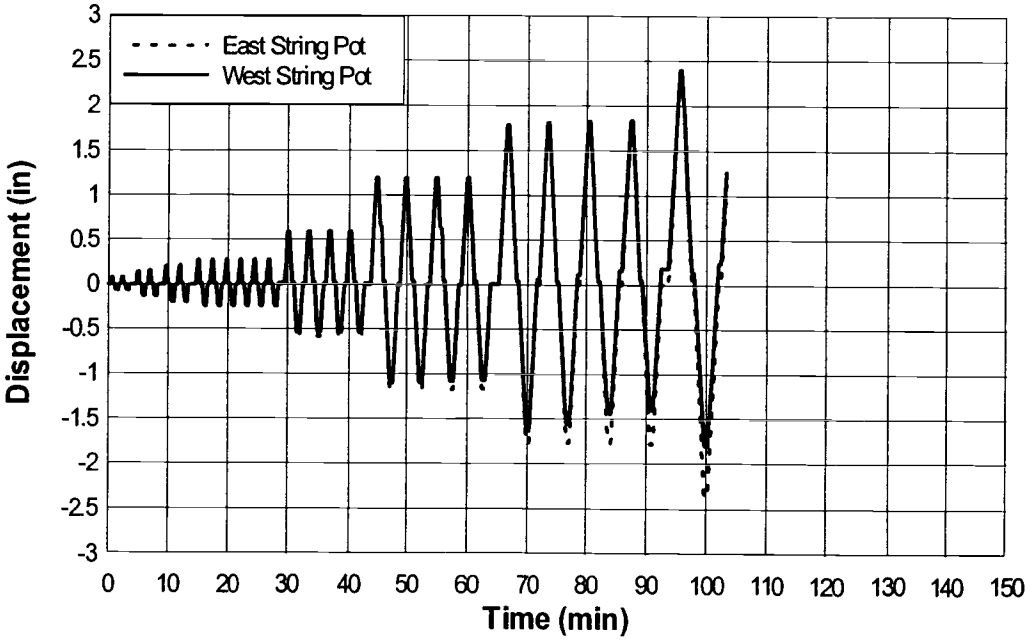

Figure A10: Specimen 125DB-2 String Pot Displacement

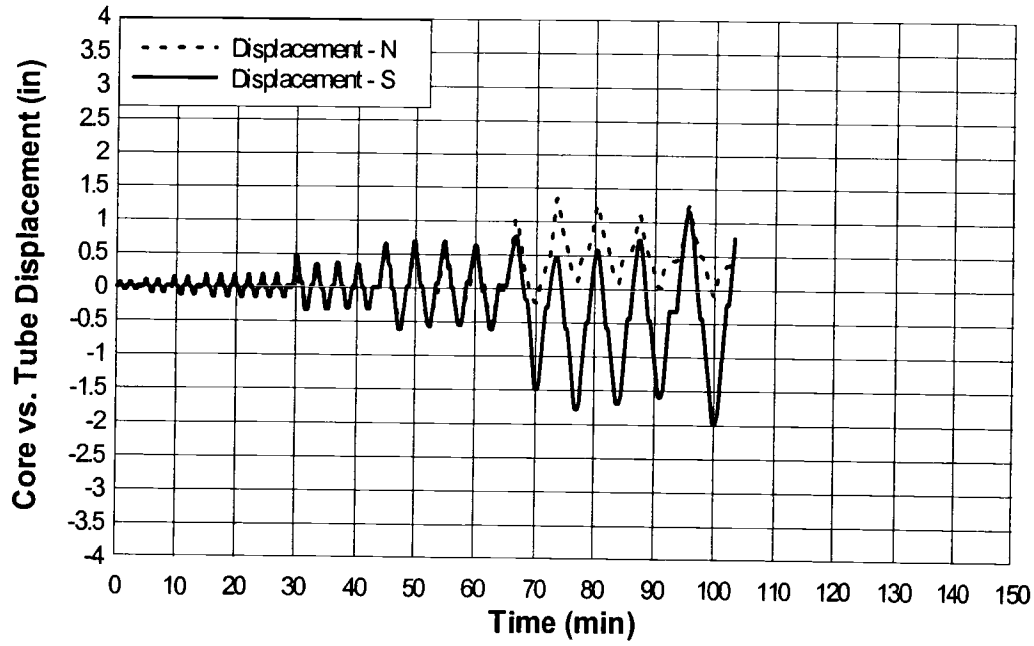

Figure A11: Specimen 125DB-2
Yielding Core/Confining Tube Relative Displacement

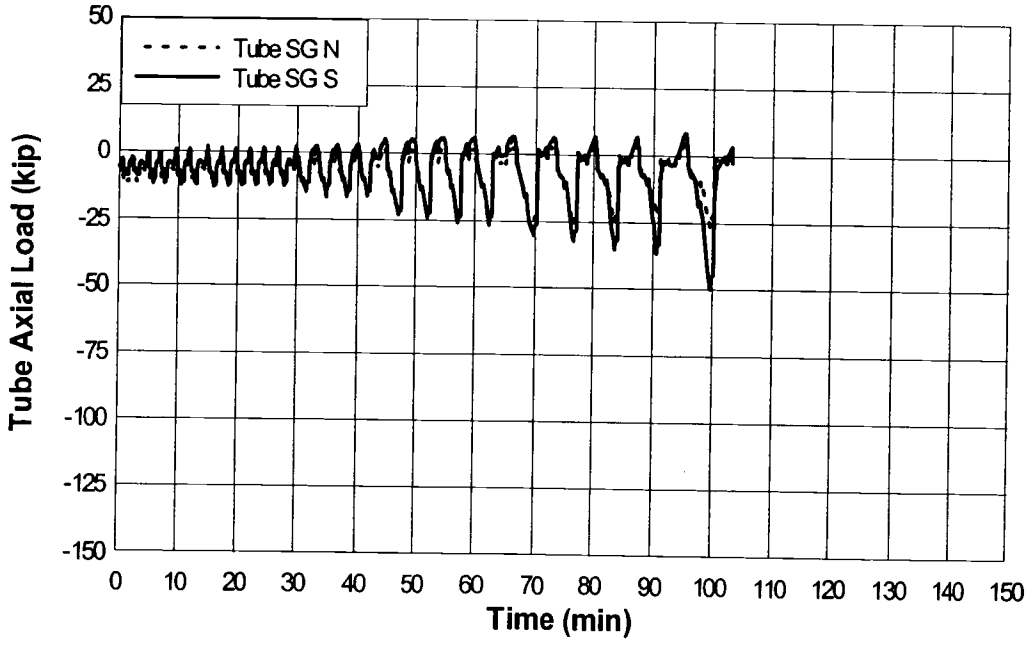

Figure A12: Specimen 125DB-2 Confining Tube Axial Load

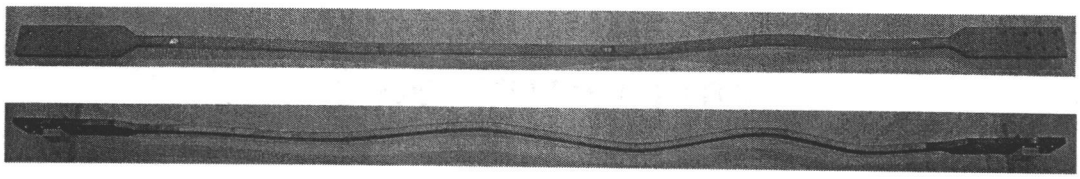

Figure A13: Specimen 125DB-3 Buckled Shape

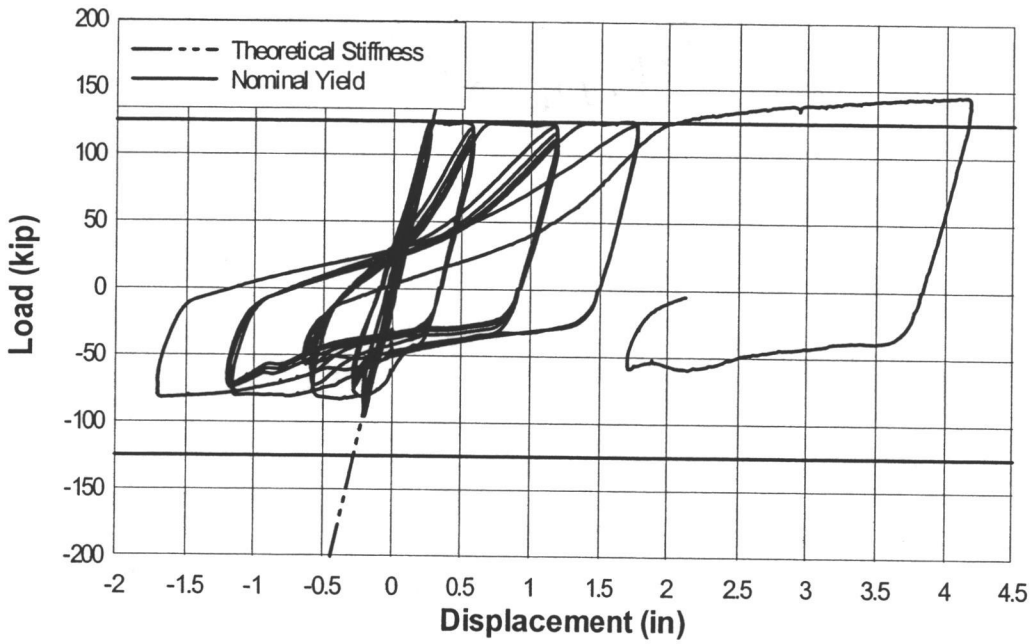

Figure A14: Specimen 125DB-3 Hysteresis

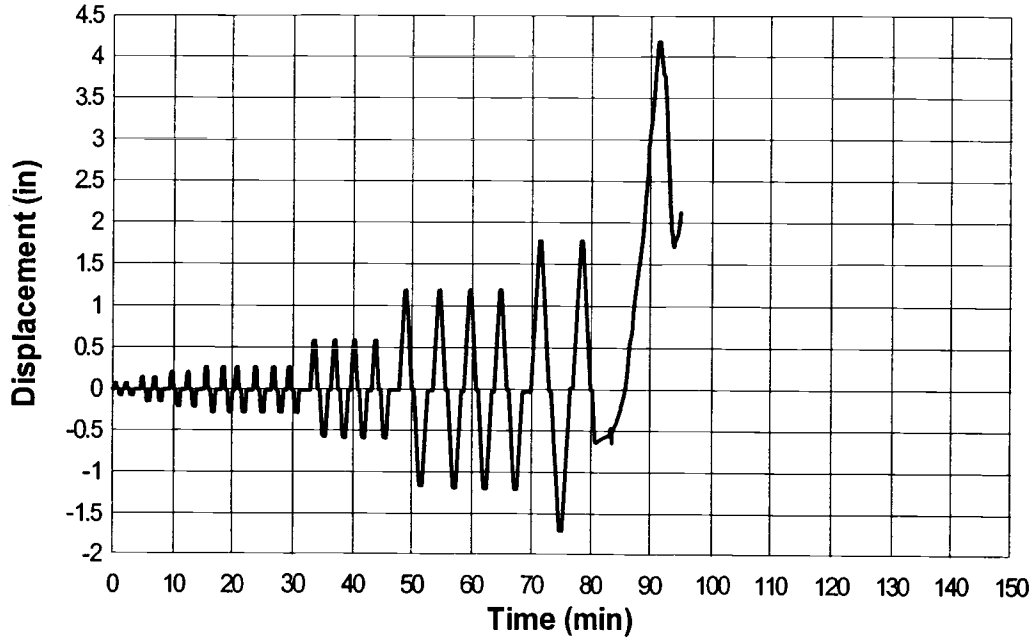

Figure A15: Specimen 125DB-3 Displacement

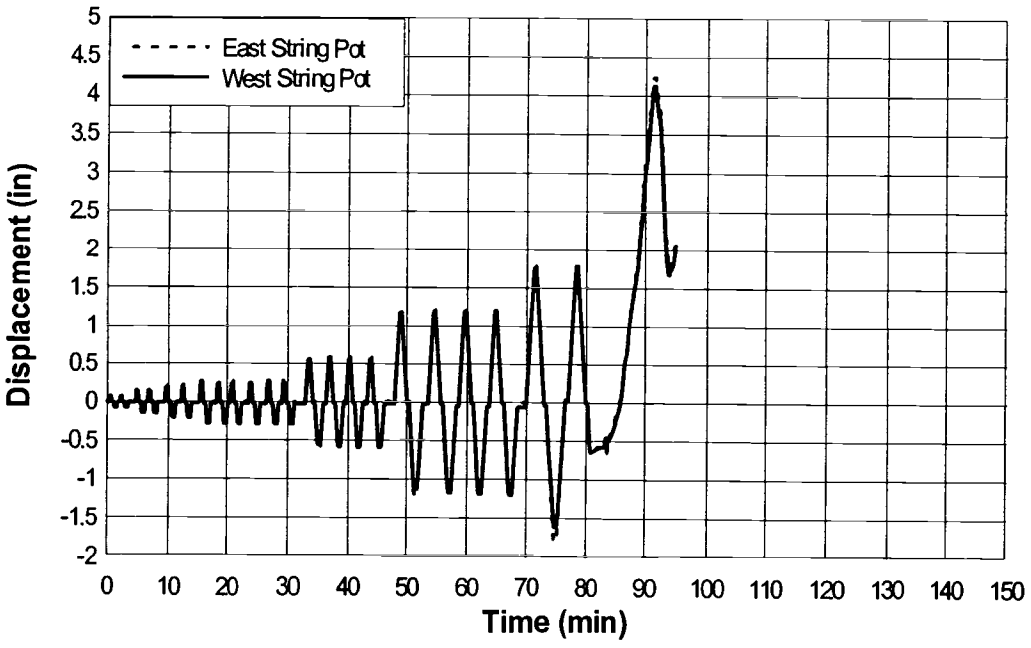

Figure A16: Specimen 125DB-3 String Pot Displacement

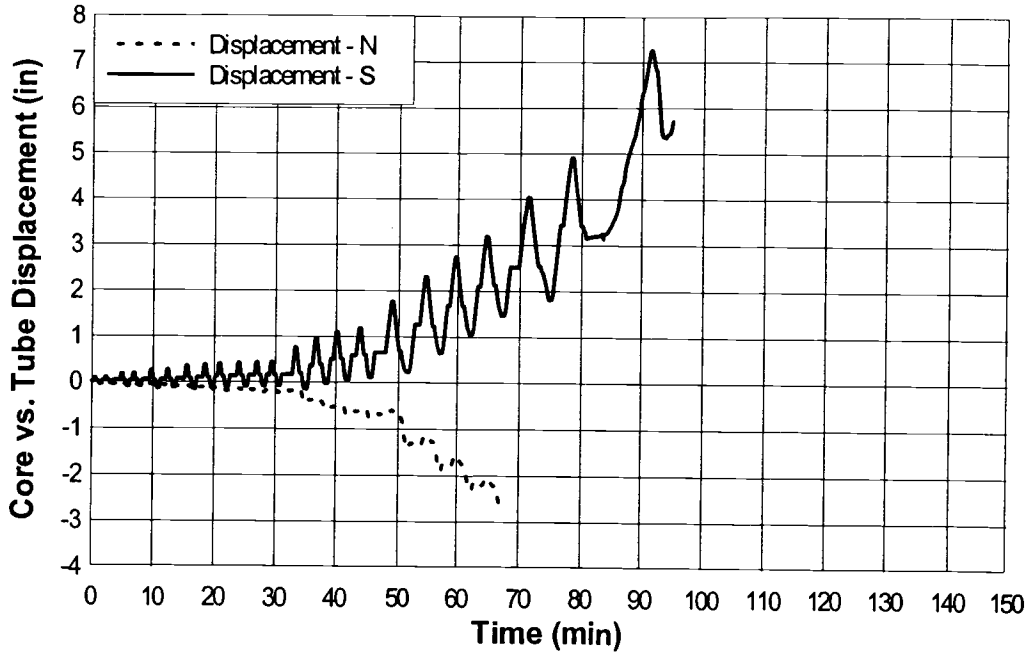

Figure A17: Specimen 125DB-3
Yielding Core/Confining Tube Relative Displacement

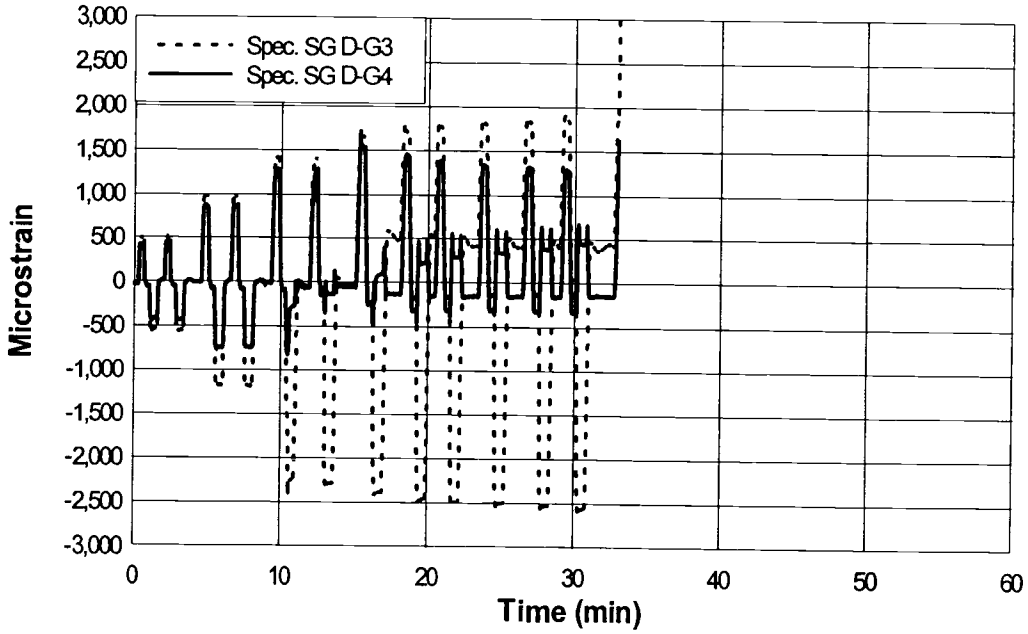

Figure A18: Specimen 125DB-3 Yielding Core Strain Gages D-G3, 4

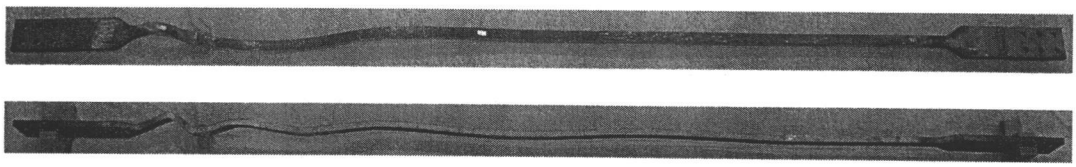

Figure A19: Specimen 125DB-4 Buckled Shape

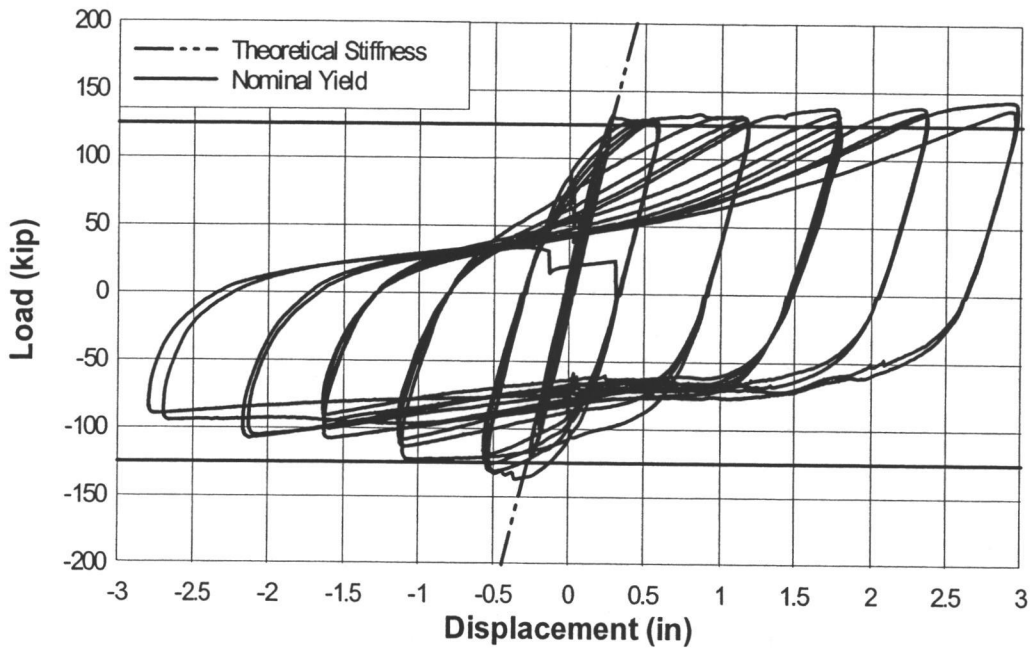

Figure A20: Specimen 125DB-4 Hysteresis

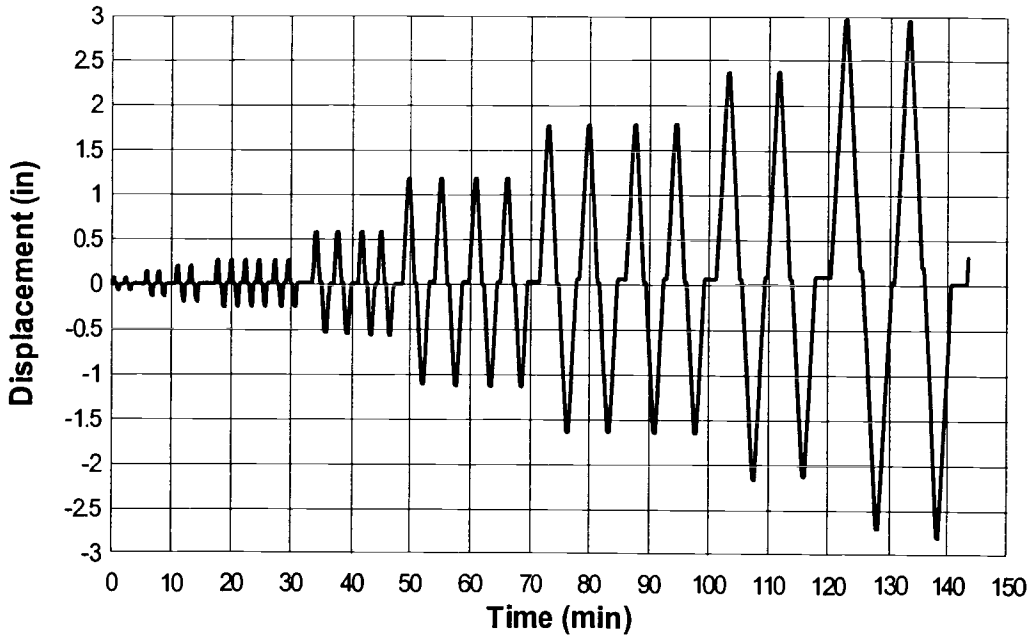

Figure A21: Specimen 125DB-4 Displacement

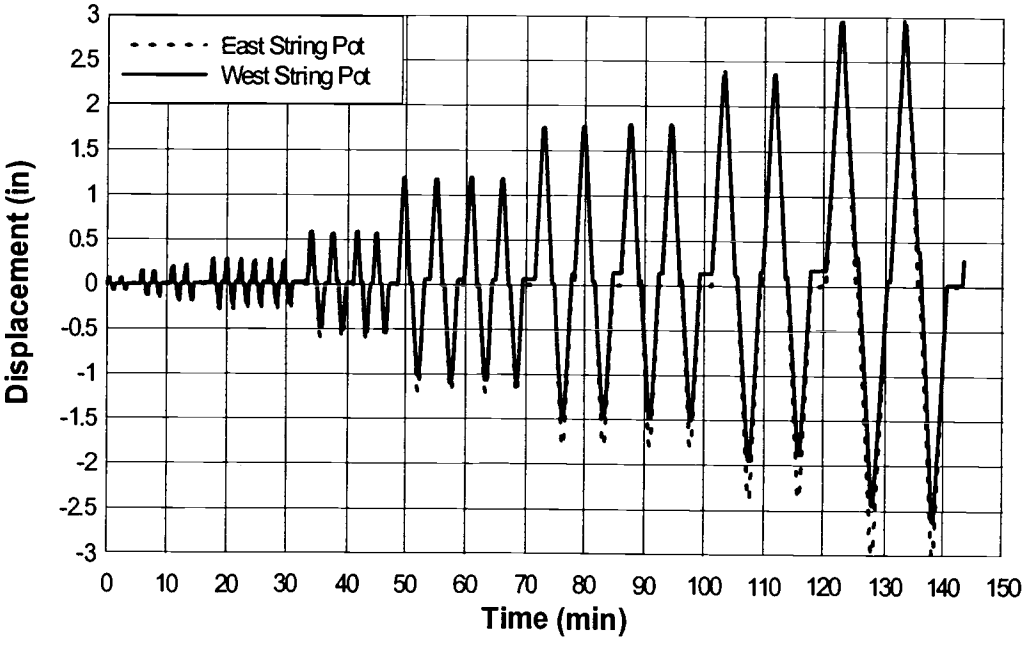

Figure A22: Specimen 125DB-4 String Pot Displacement

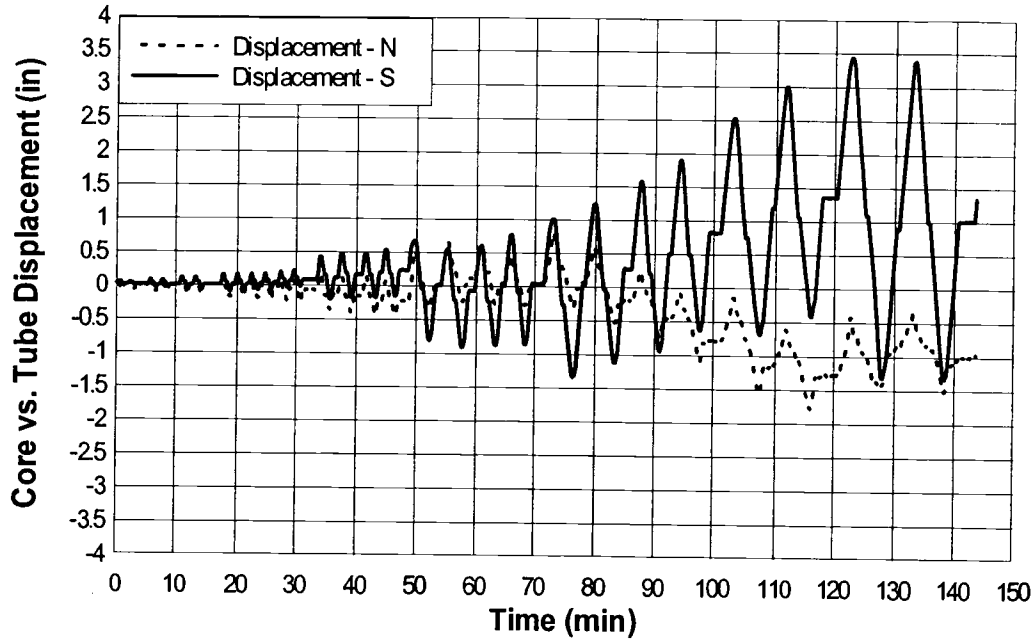

Figure A23: Specimen 125DB-4
Yielding Core/Confining Tube Relative Displacement

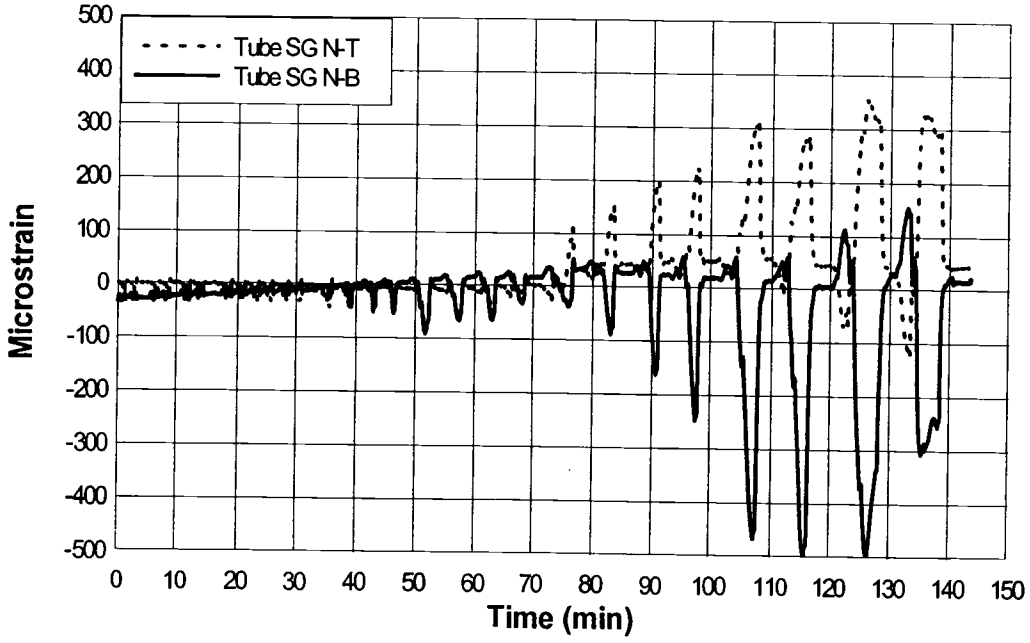

Figure A24: Specimen 125DB-4 Confining Tube Strain Gages N-T, B

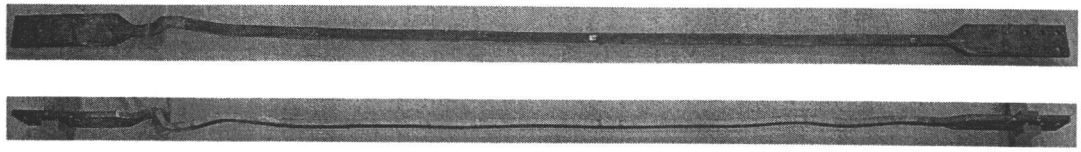

Figure A25: Specimen 125DB-5 Buckled Shape

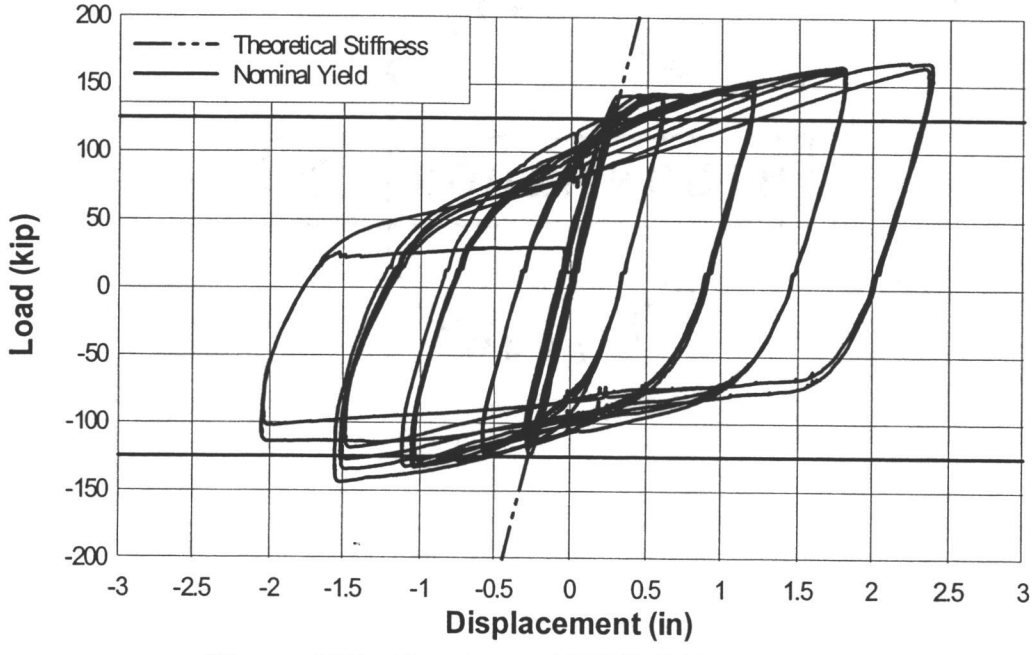

Figure A26: Specimen 125DB-5 Hysteresis

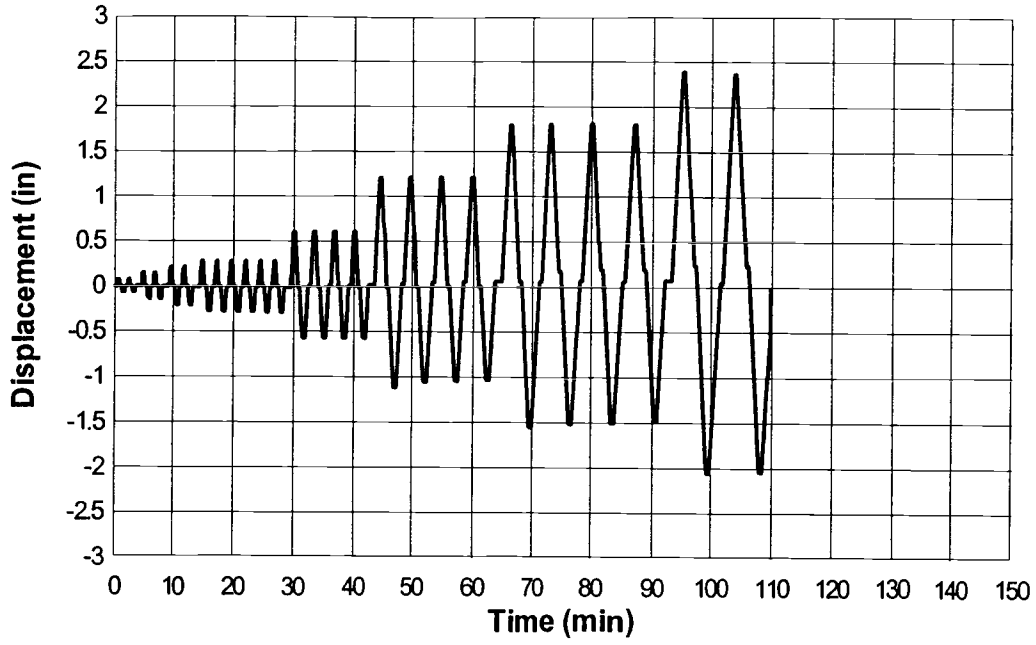

Figure A27: Specimen 125DB-5 Displacement

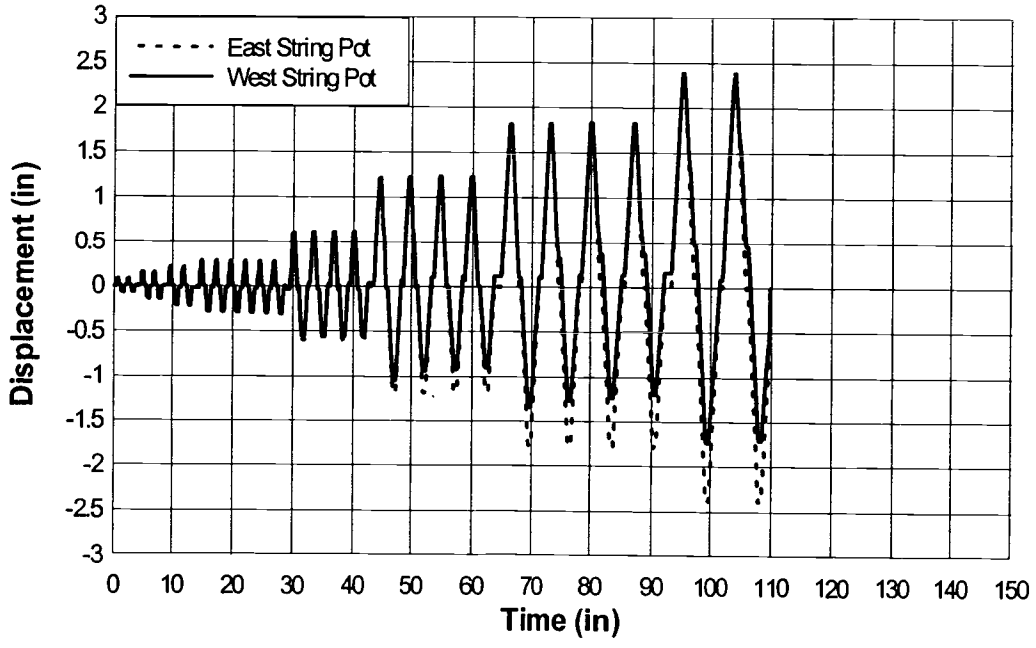

Figure A28: Specimen 125DB-5 String Pot Displacement

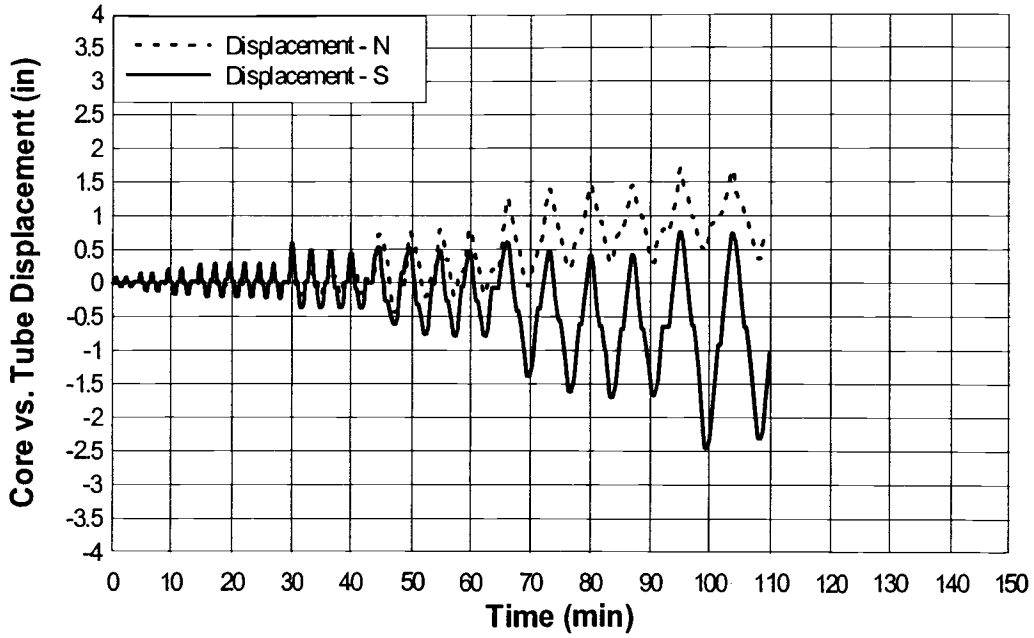

Figure A29: Specimen 125DB-5
Yielding Core/Confining Tube Relative Displacement

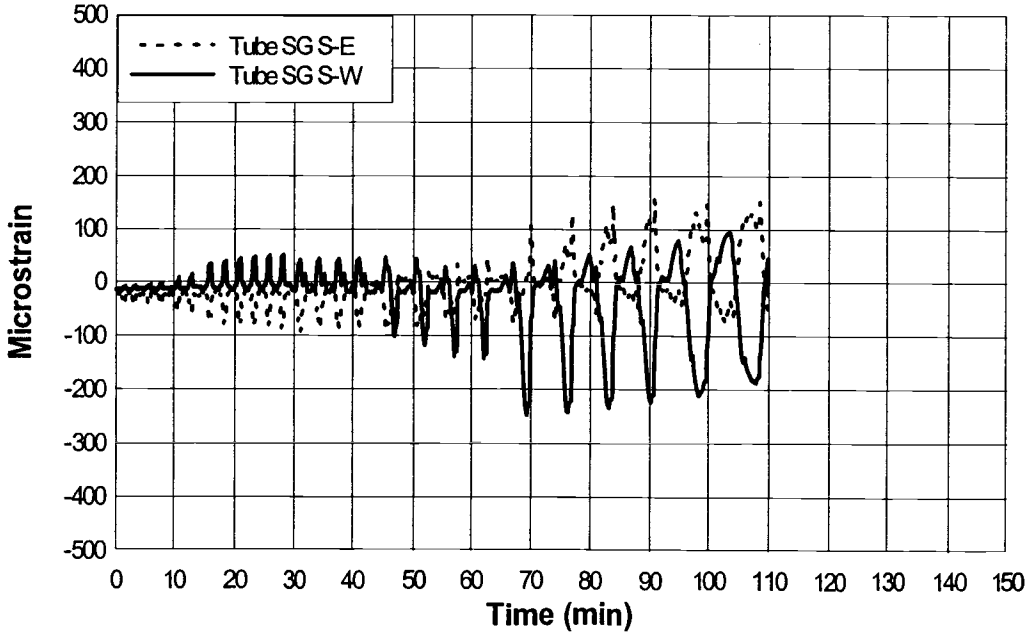

Figure A30: Specimen 125DB-5 Confining Tube Strain Gages S-E, W

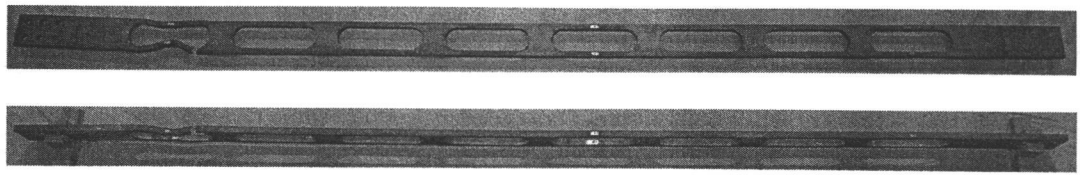

Figure A31: Specimen 125P-1 Buckled Shape

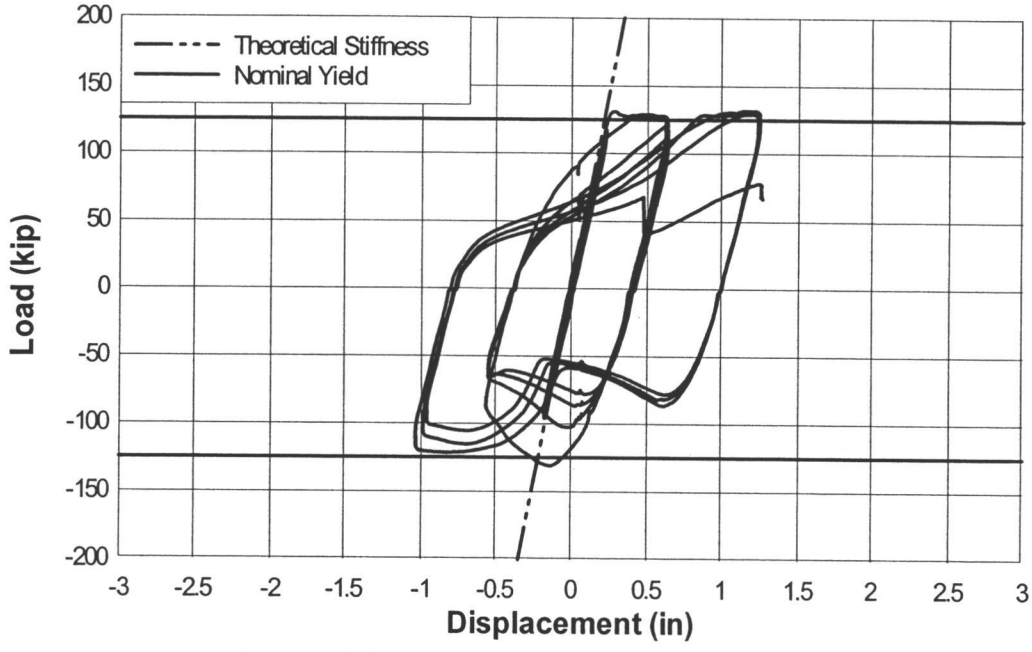

Figure A32: Specimen 125P-1 Hysteresis

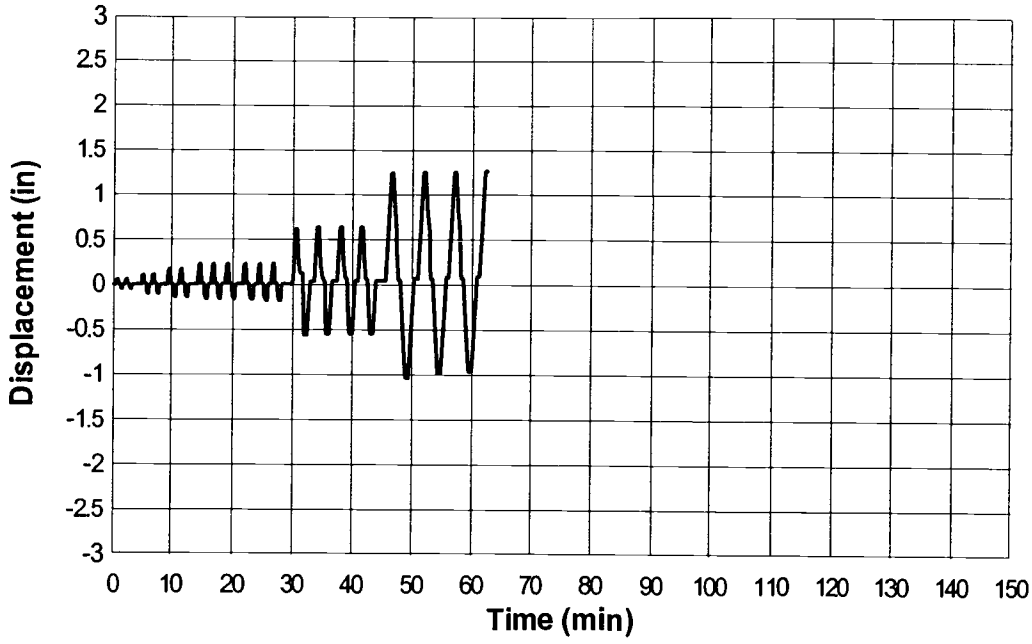

Figure A33: Specimen 125P-1 Displacement

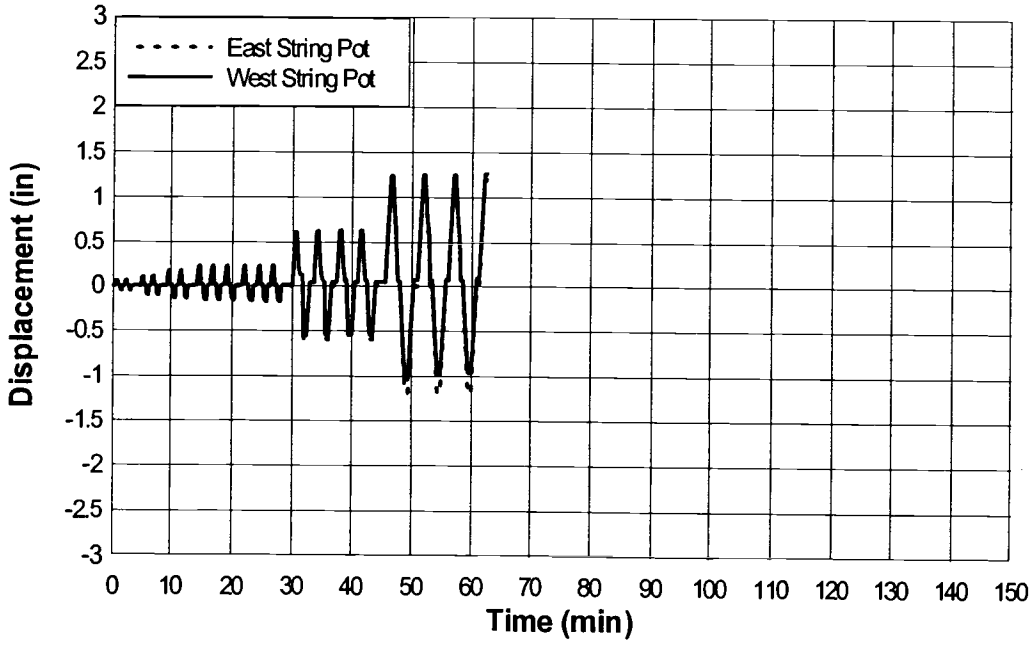

Figure A34: Specimen 125P-1 String Pot Displacement

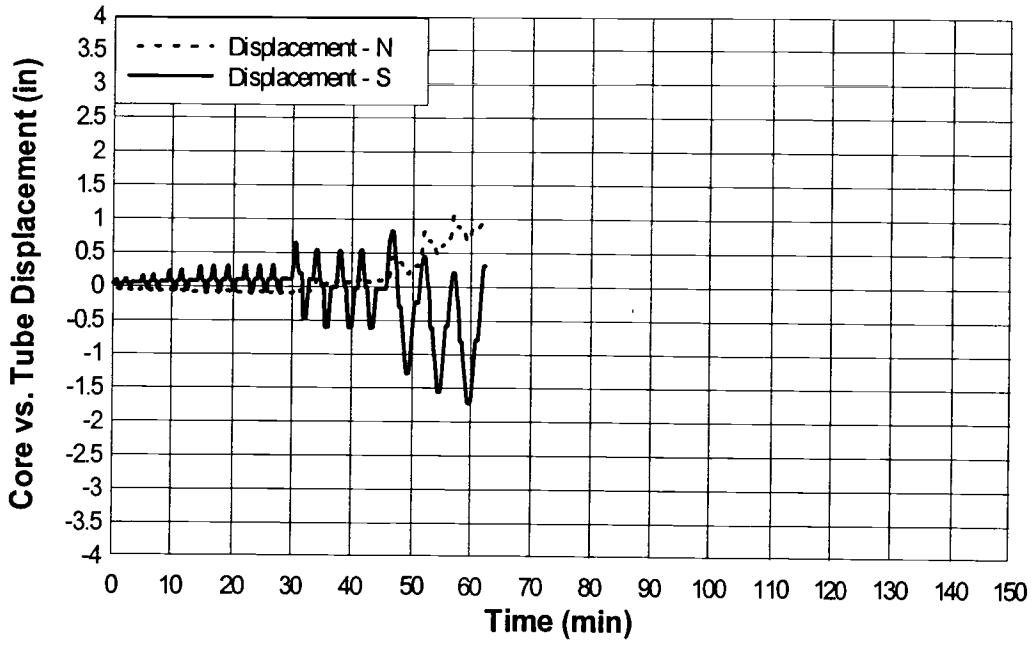

Figure A35: Specimen 125P-1
Yielding Core/Confining Tube Relative Displacement

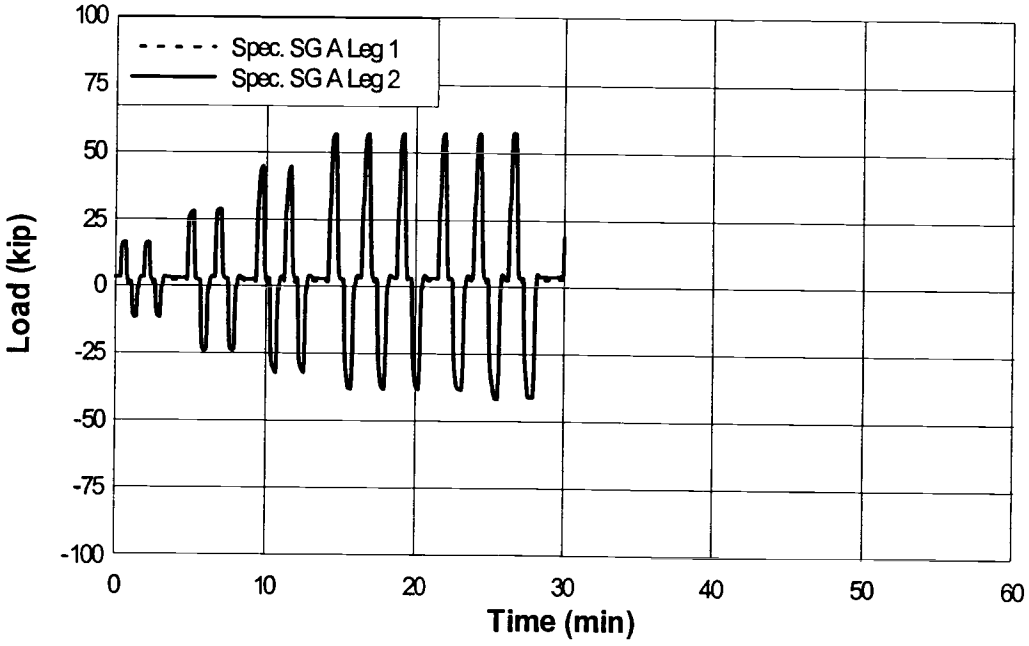

Figure A36: Specimen 125P-1 Yielding Core Load, Location A-Leg 1, 2

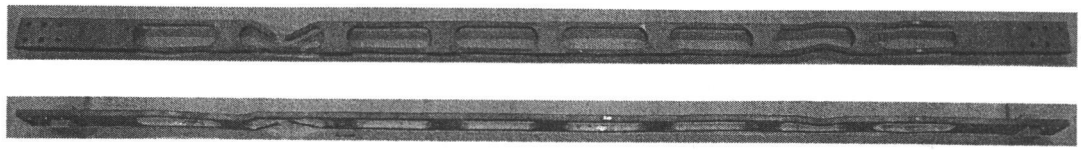

Figure A37: Specimen 125P-2 Buckled Shape

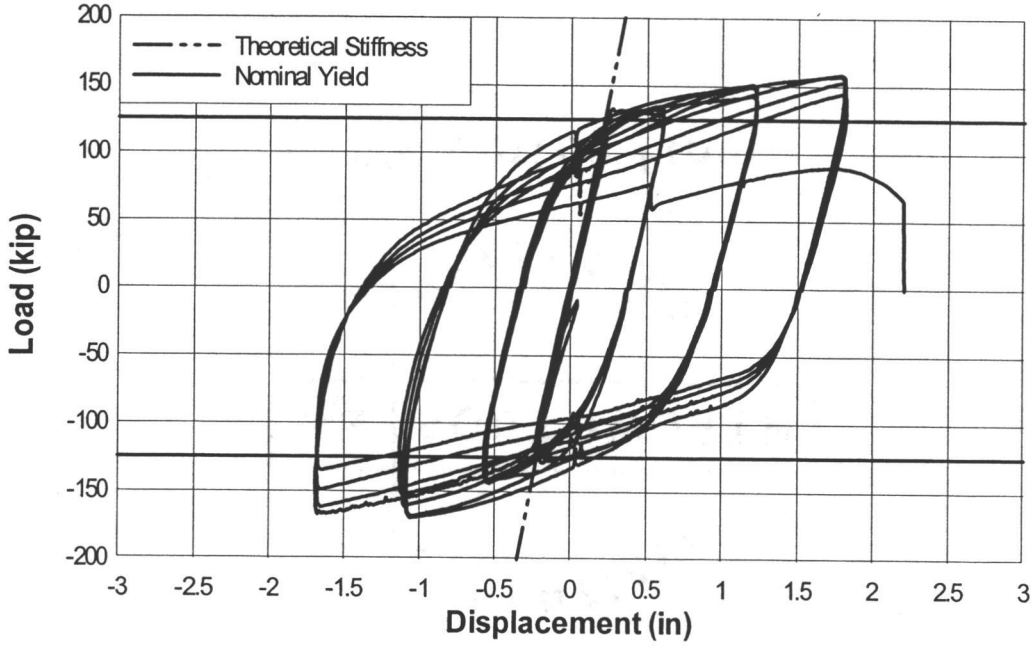

Figure A38: Specimen 125P-2 Hysteresis

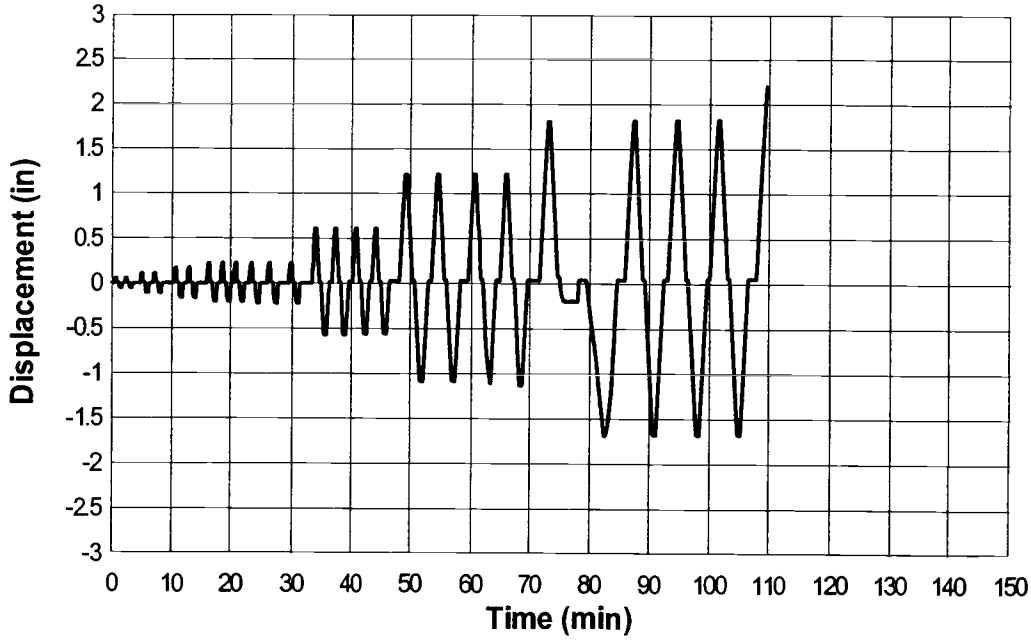

Figure A39: Specimen 125P-2 Displacement

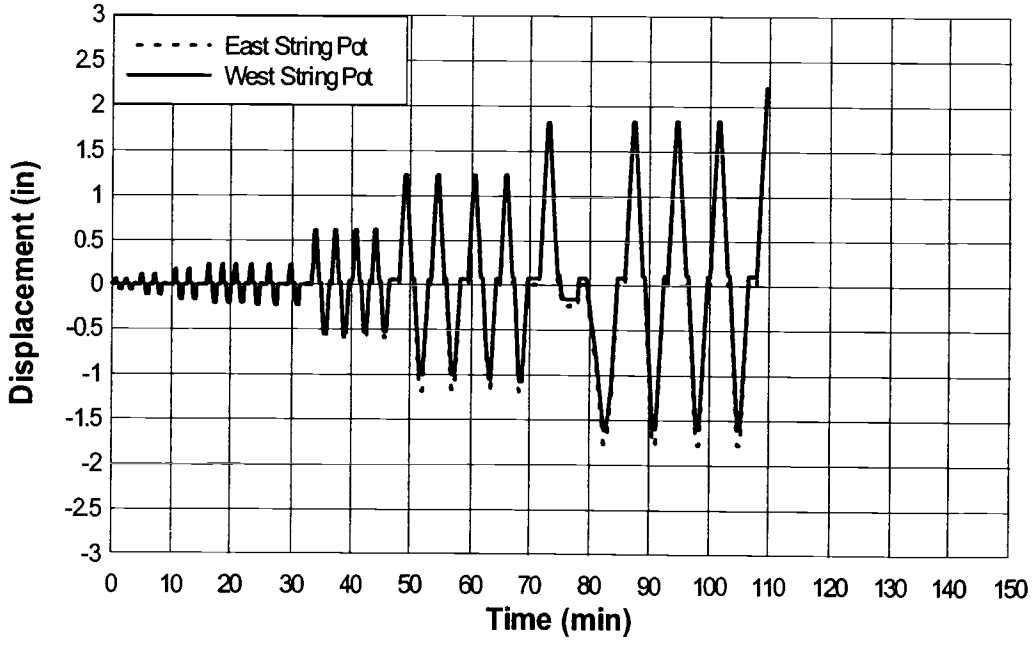

Figure A40: Specimen 125P-2 String Pot Displacement

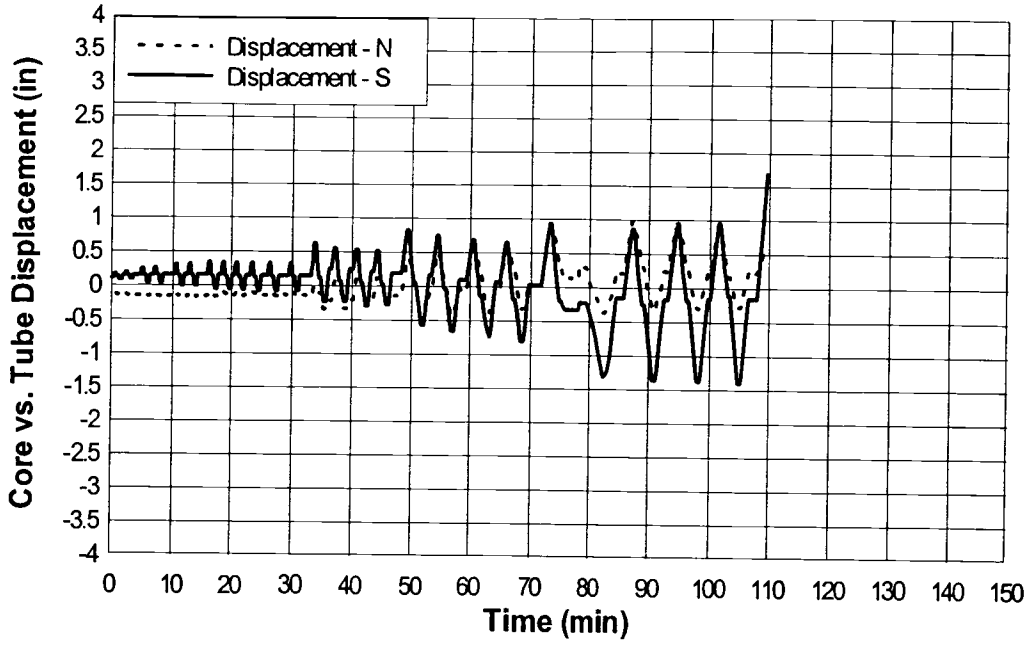

Figure A41: Specimen 125P-2
Yielding Core/Confining Tube Relative Displacement

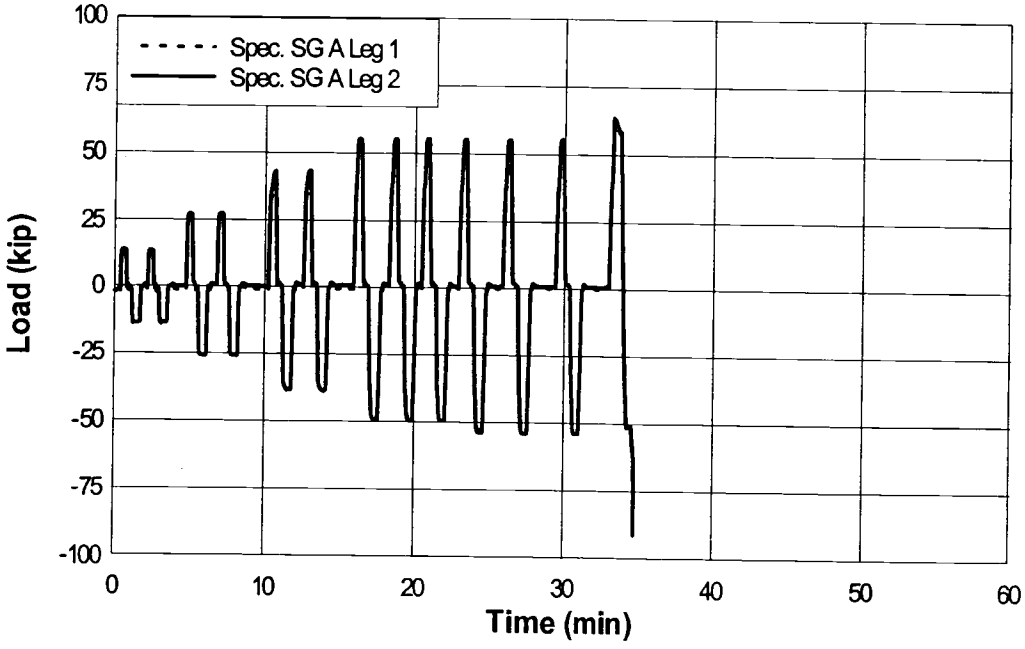

Figure A42: Specimen 125P-2 Yielding Core Load, Location A-Leg 1, 2

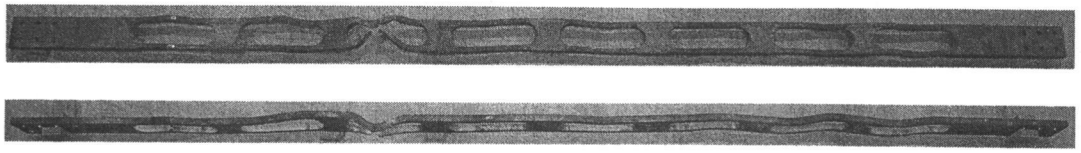

Figure A43: Specimen 125P-3 Buckled Shape

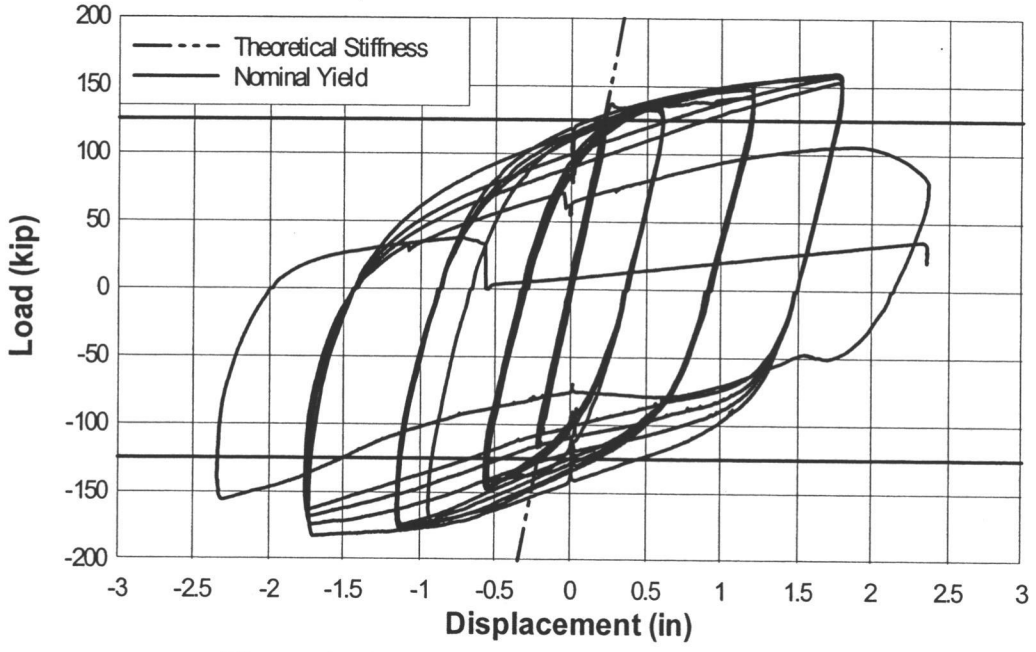

Figure A44: Specimen 125P-3 Hysteresis

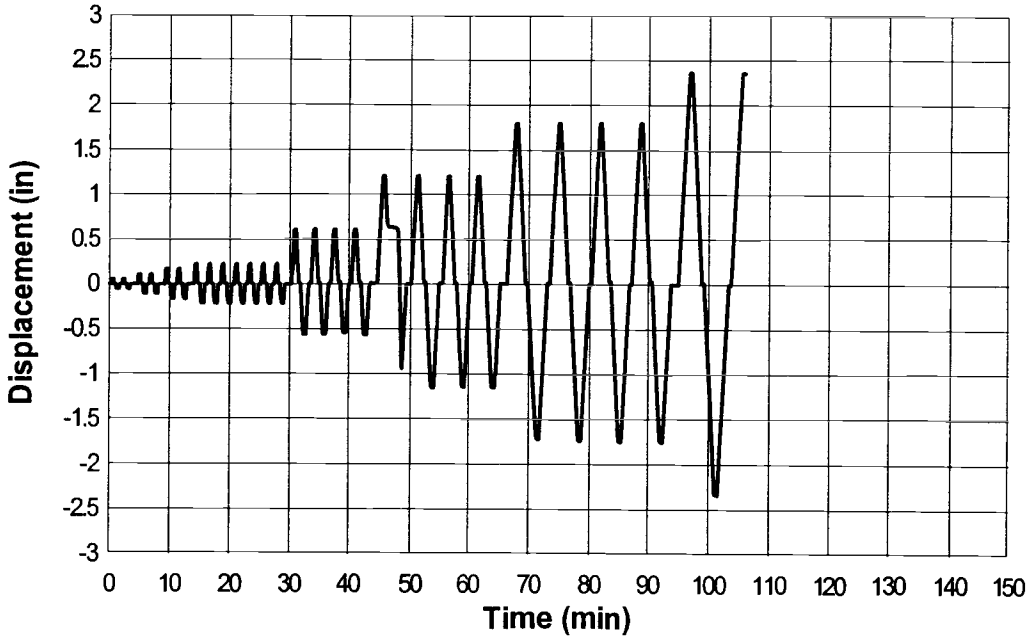

Figure A45: Specimen 125P-3 Displacement

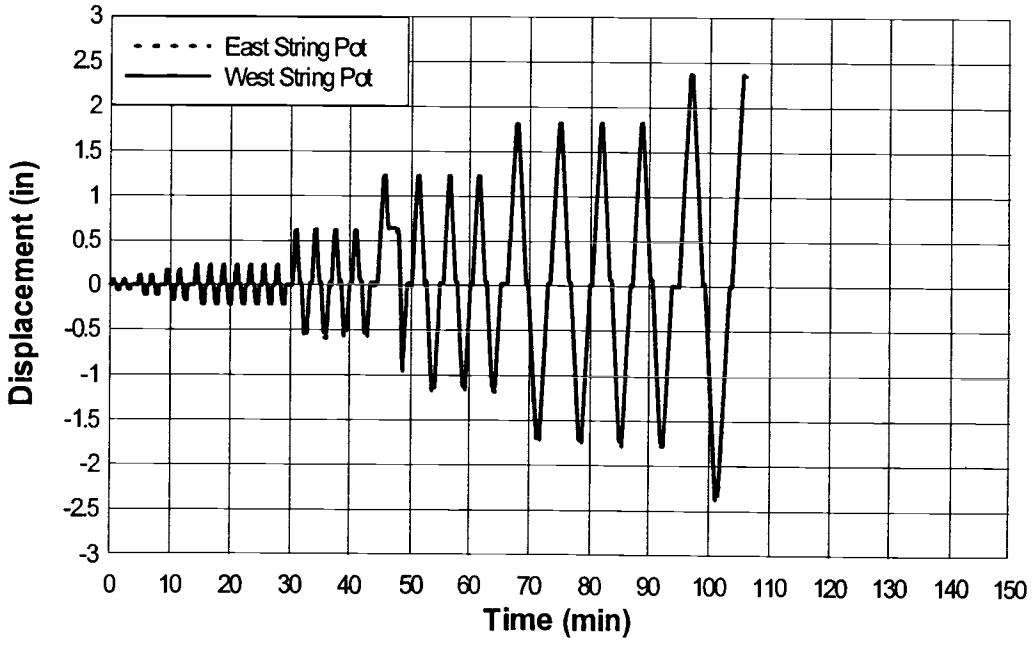

Figure A46: Specimen 125P-3 String Pot Displacement

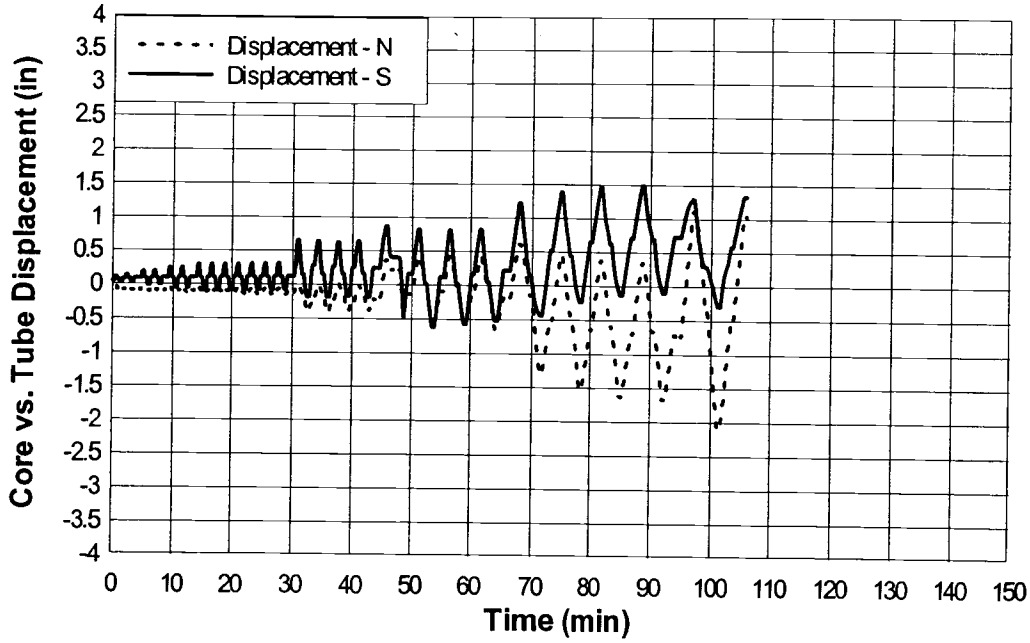

Figure A47: Specimen 125P-3
Yielding Core/Confining Tube Relative Displacement

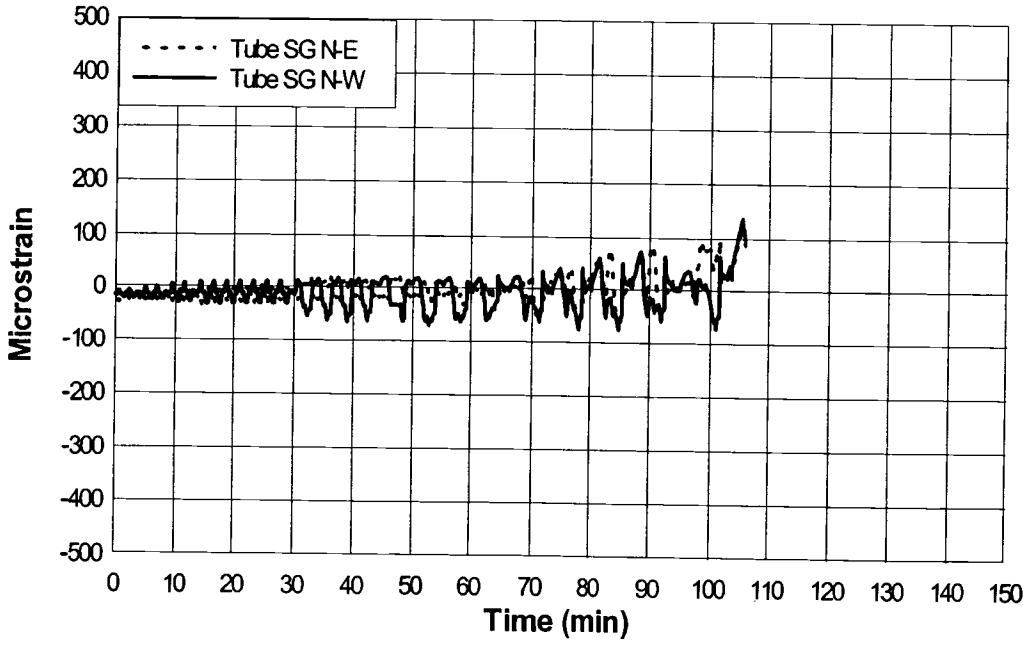

Figure A48: Specimen 125P-3 Confining Tube Strain Gages N-E, W

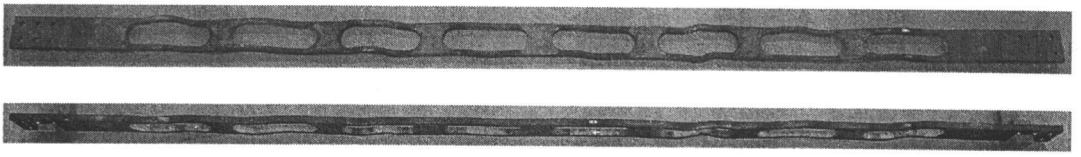

Figure A49: Specimen 125P-4 Buckled Shape

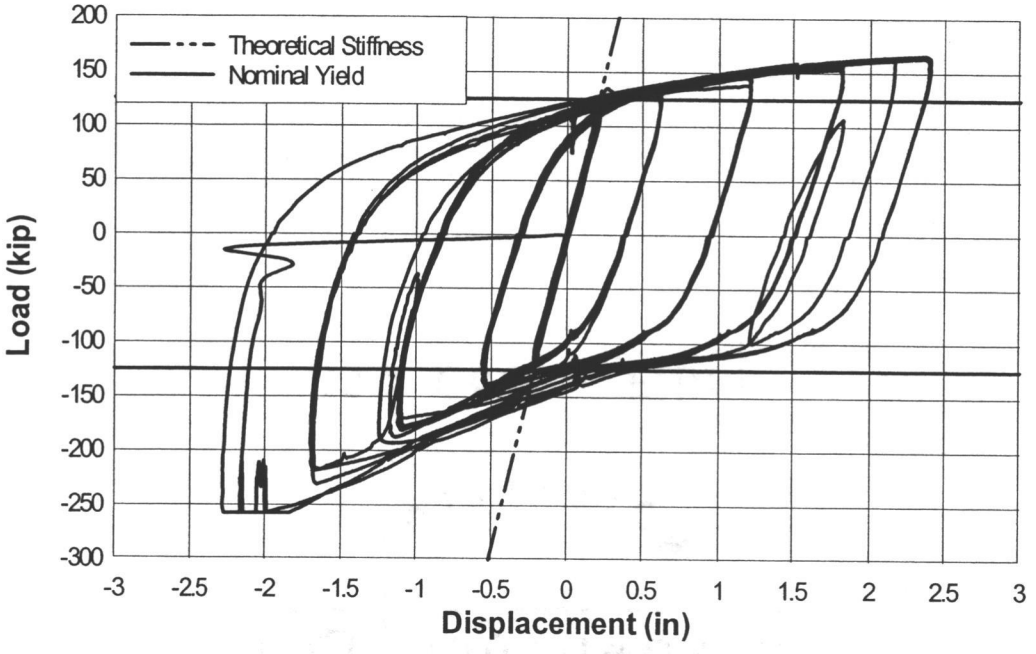

Figure A50: Specimen 125P-4 Hysteresis

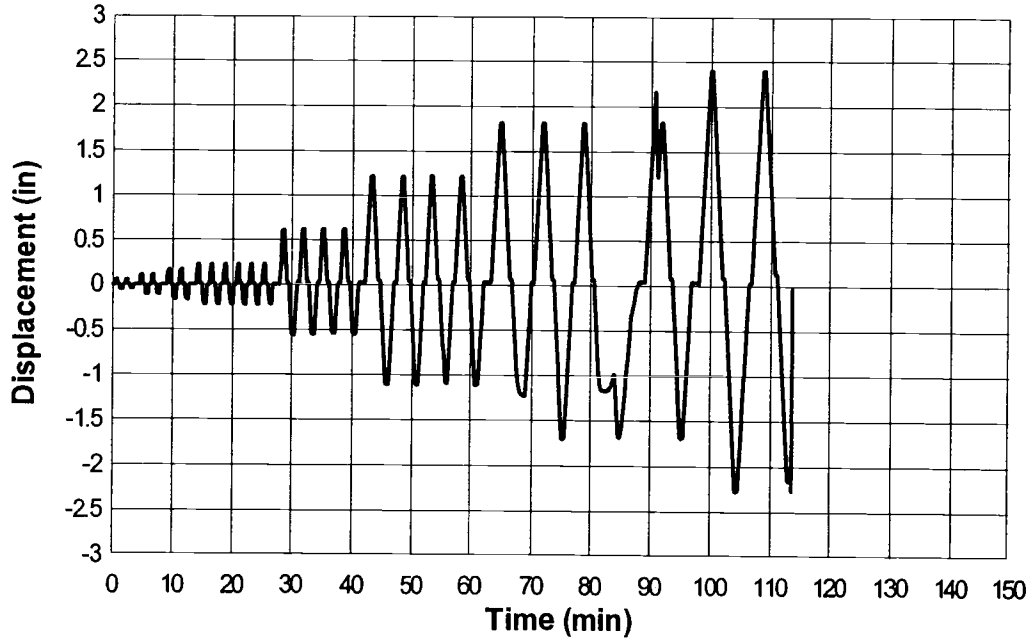

Figure A51: Specimen 125P-4 Displacement

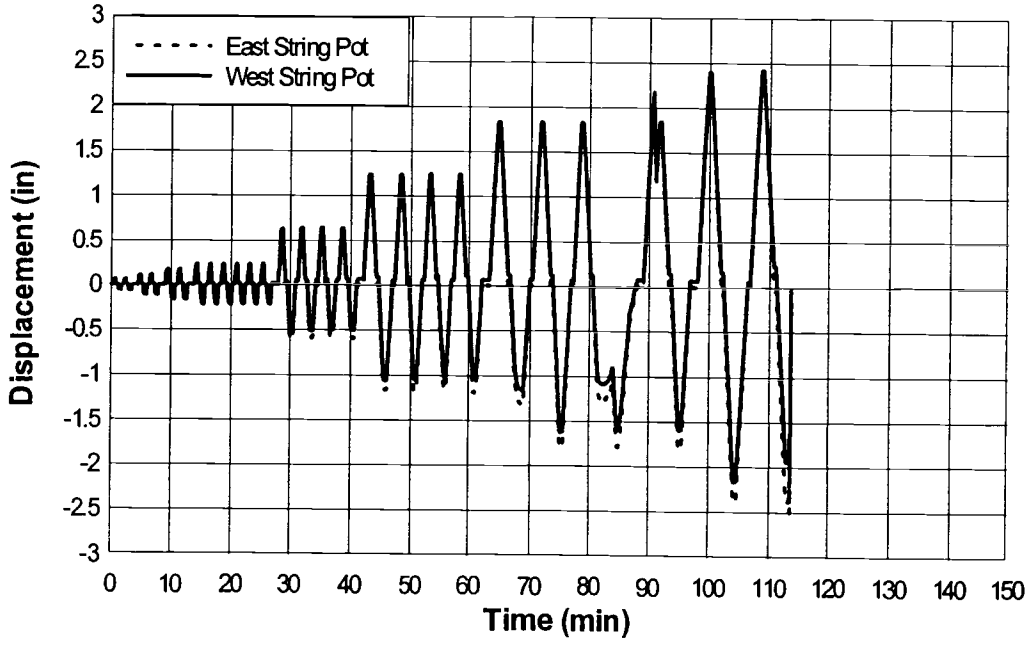

Figure A52: Specimen 125P-4 String Pot Displacement

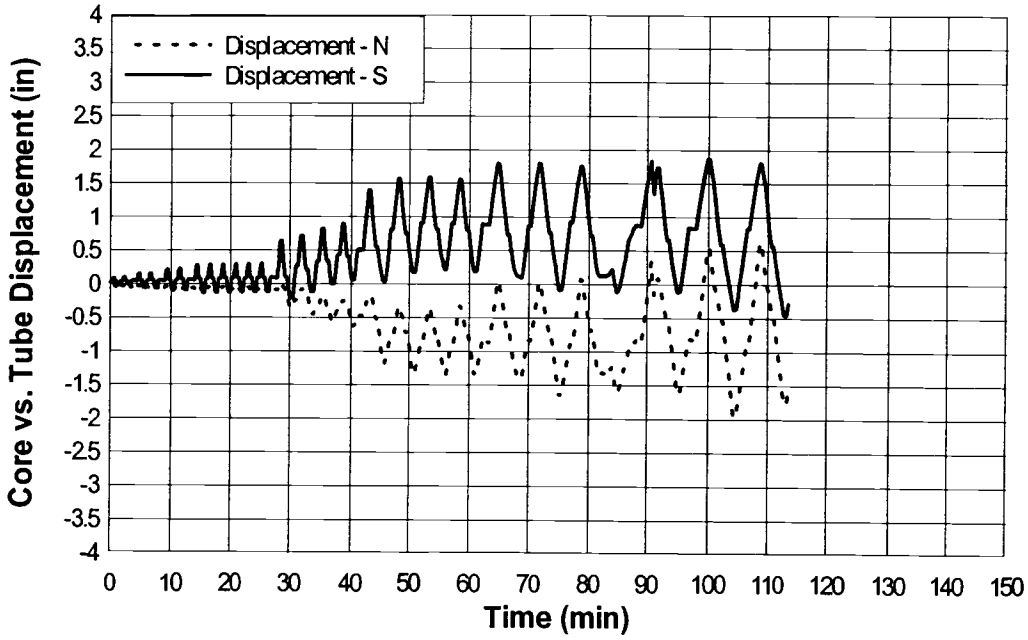

Figure A53: Specimen 125P-4
Yielding Core/Confining Tube Relative Displacement

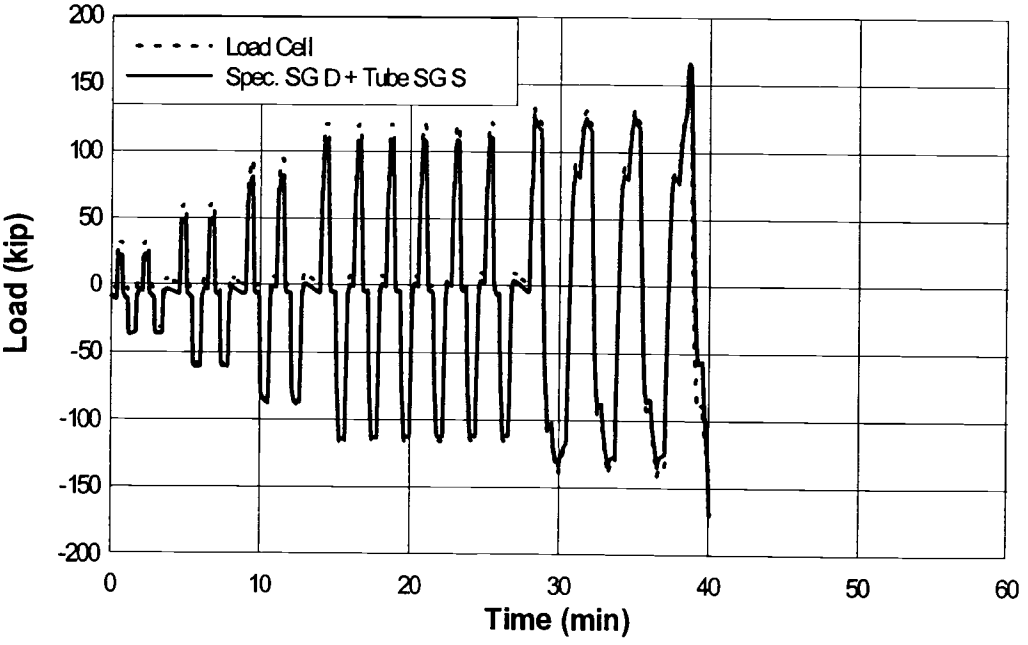

Specimen A54: Specimen 125P-4 Load Cell, Yielding Core Strain Gages Location D + Confining Tube Strain Gages Location S

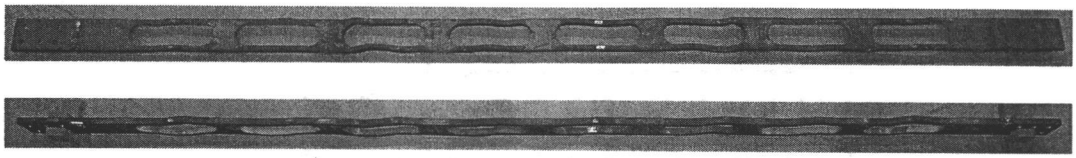

Figure A55: Specimen 125P-5 Buckled Shape

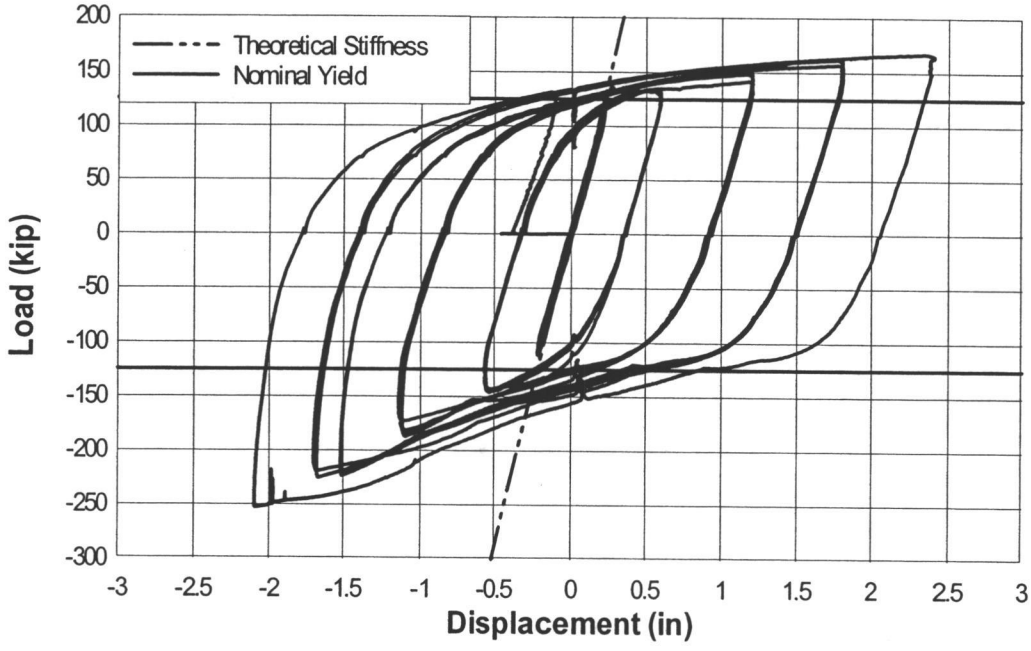

Figure A56: Specimen 125P-5 Hysteresis

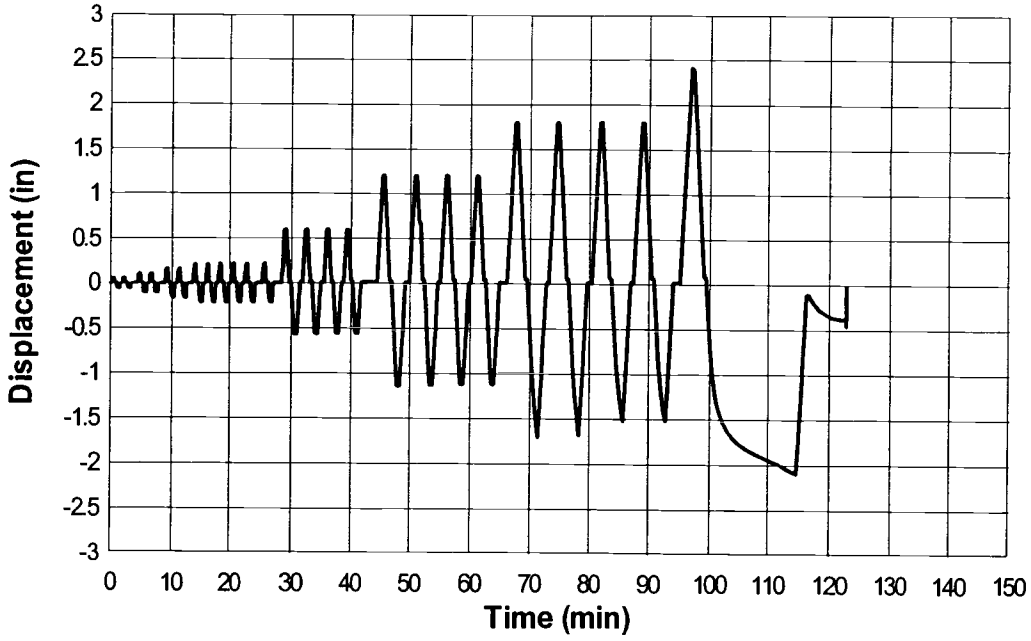

Figure A57: Specimen 125P-5 Displacement

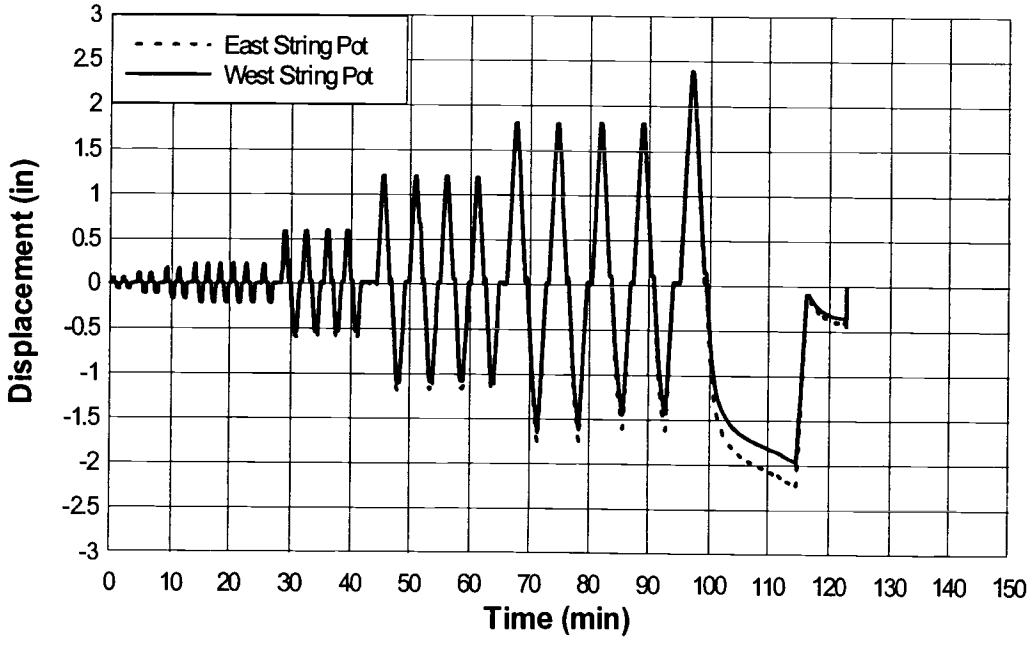

Figure A58: Specimen 125P-5 String Pot Displacement

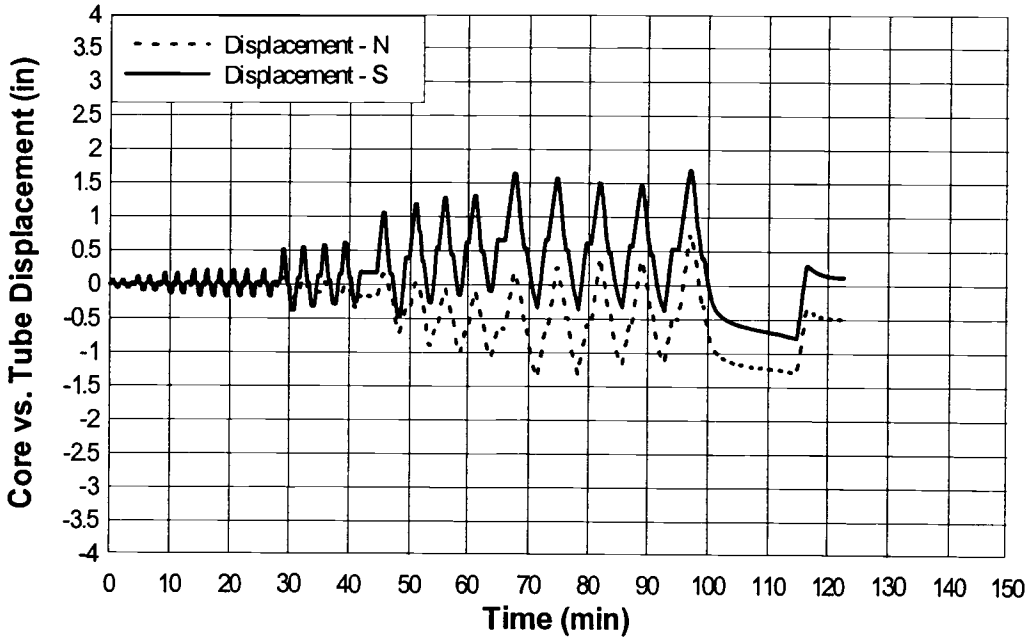

Figure A59: Specimen 125P-5
Yielding Core/Confining Tube Relative Displacement

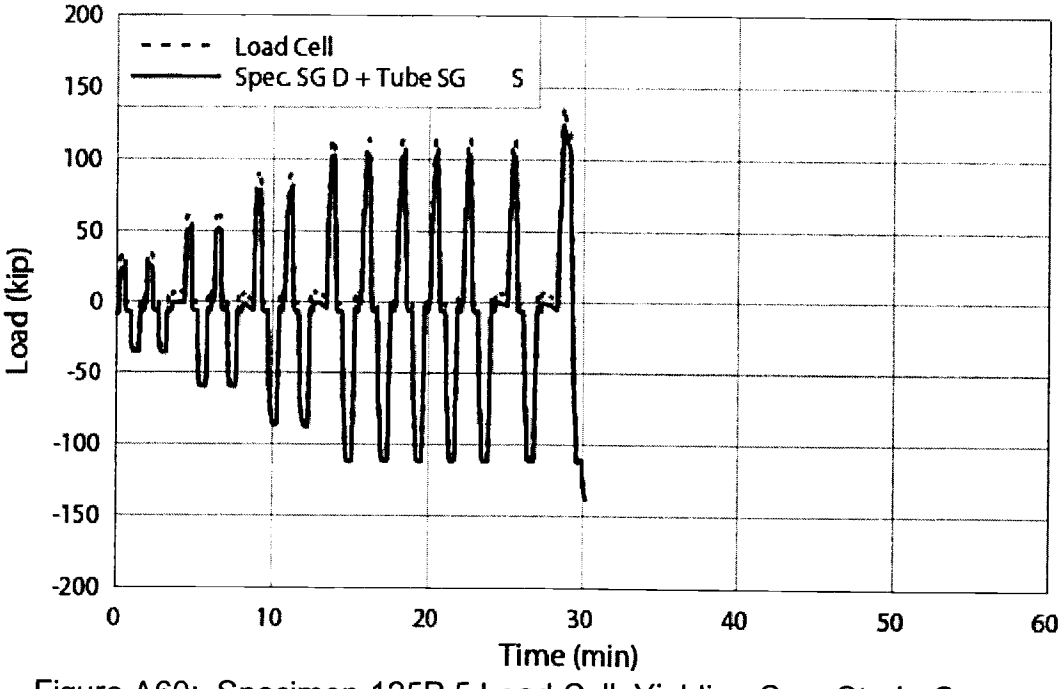

Figure A60: Specimen 125P-5 Load Cell, Yielding Core Strain Gages Location D + Confining Tube Strain Gages Location S

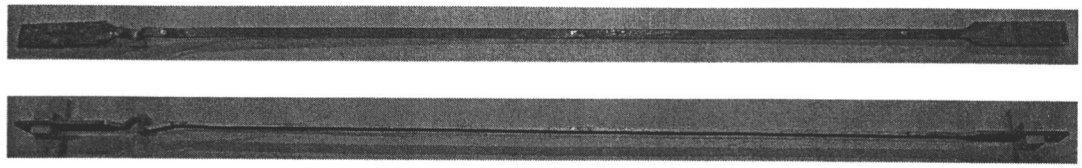

Figure A61: Specimen 50DB-1 Buckled Shape

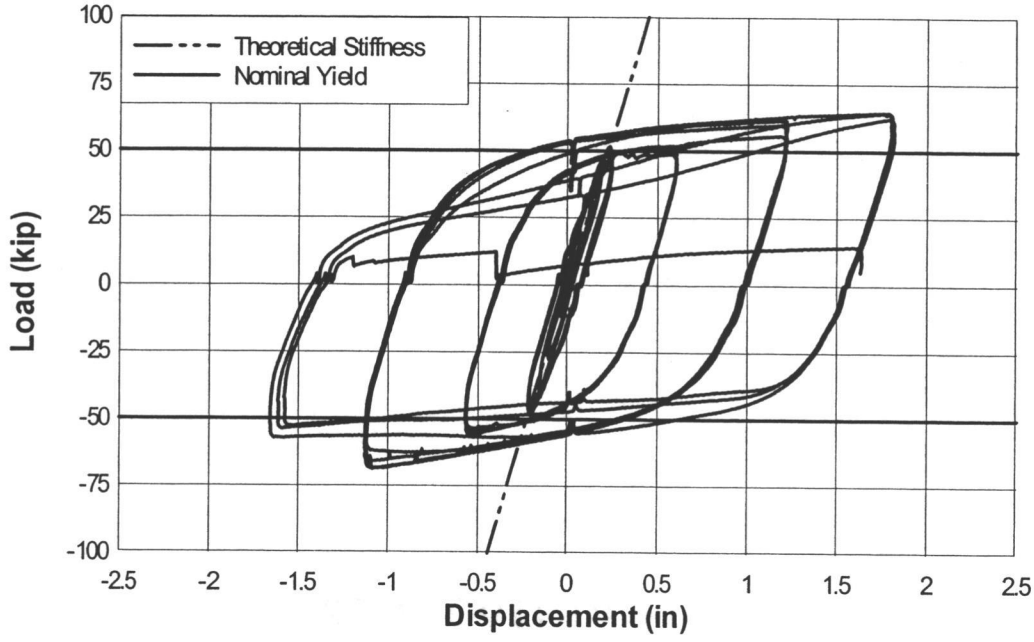

Figure A62: Specimen 50DB-1 Hysteresis

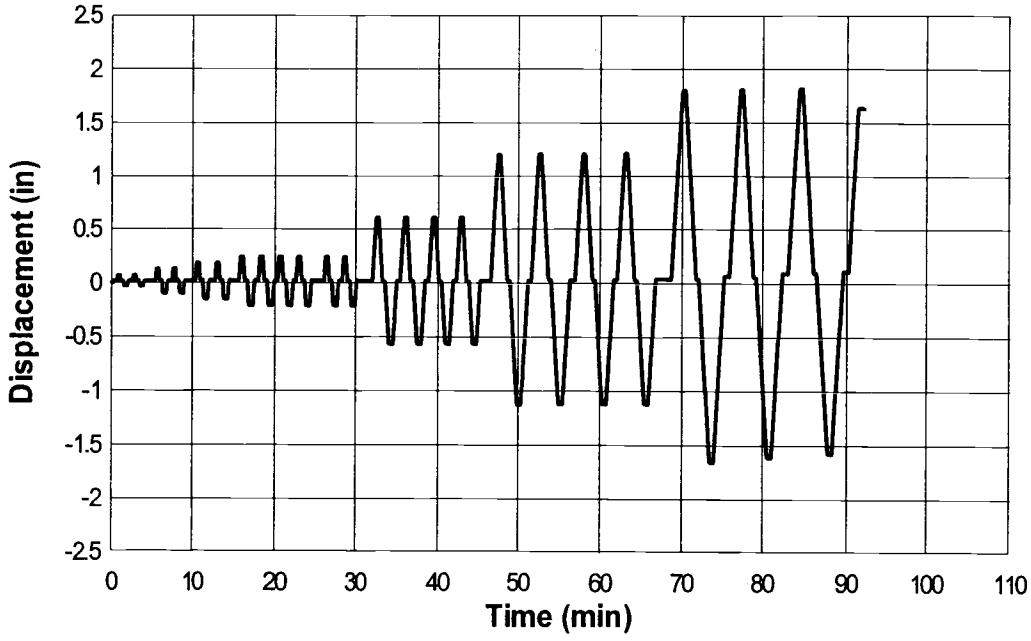

Figure A63: Specimen 50DB-1 Displacement

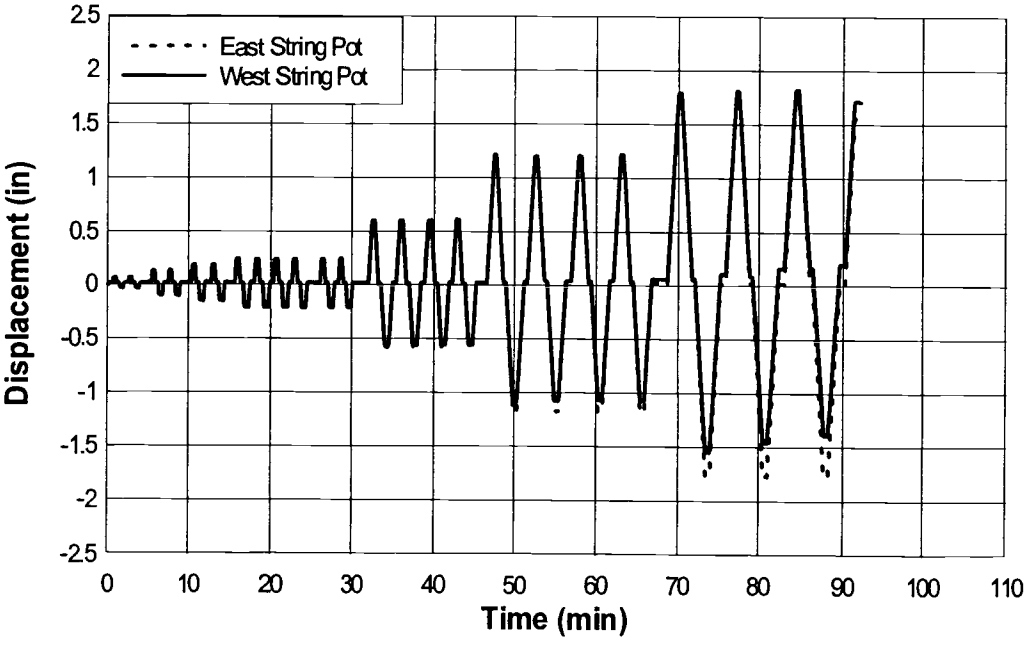

Figure A64: Specimen 50DB-1 String Pot Displacement

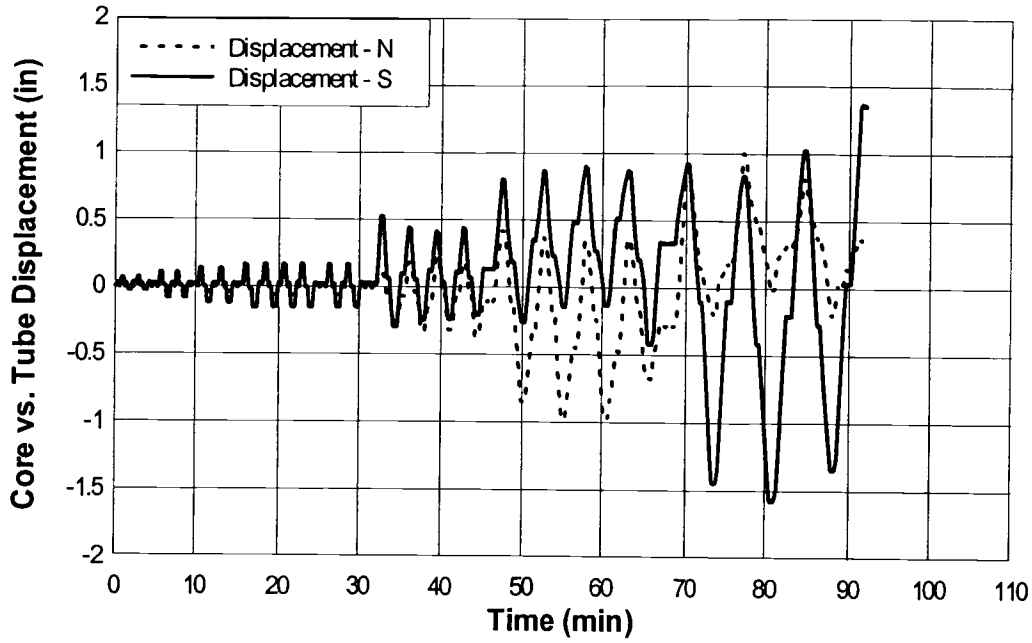

Figure A65: Specimen 50DB-1
Yielding Core/Confining Tube Relative Displacement

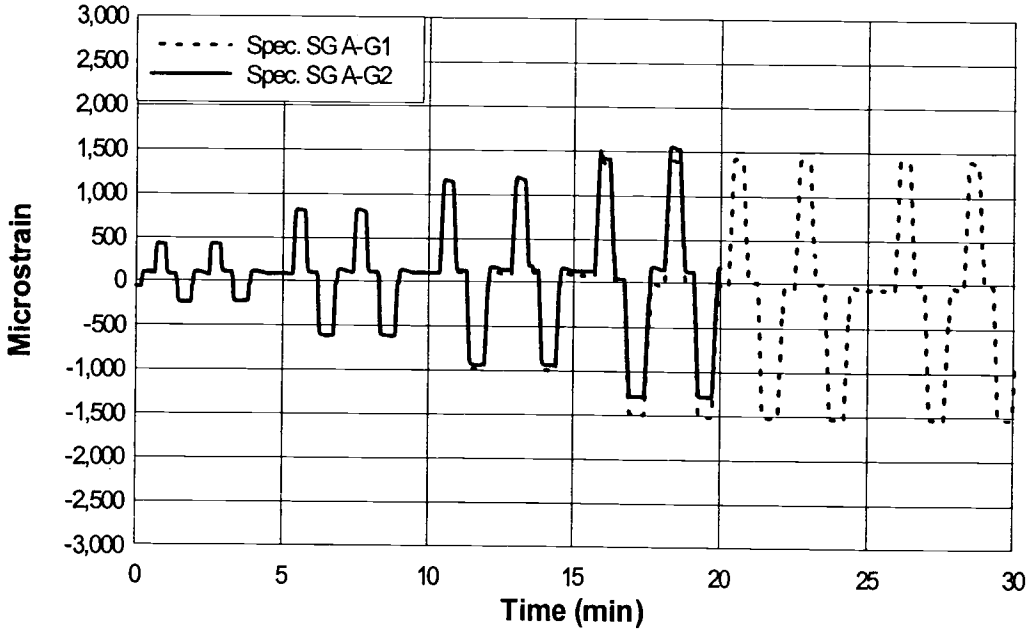

Figure A66: Specimen 50DB-1 Yielding Core Strain Gages A-G1, 2

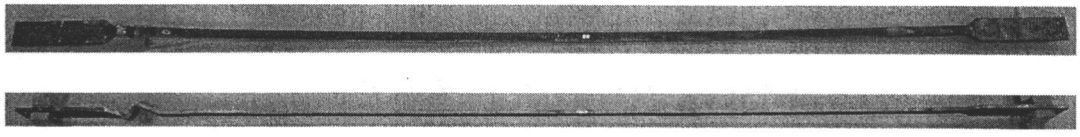

Figure A67: Specimen 50DB-2 Buckled Shape

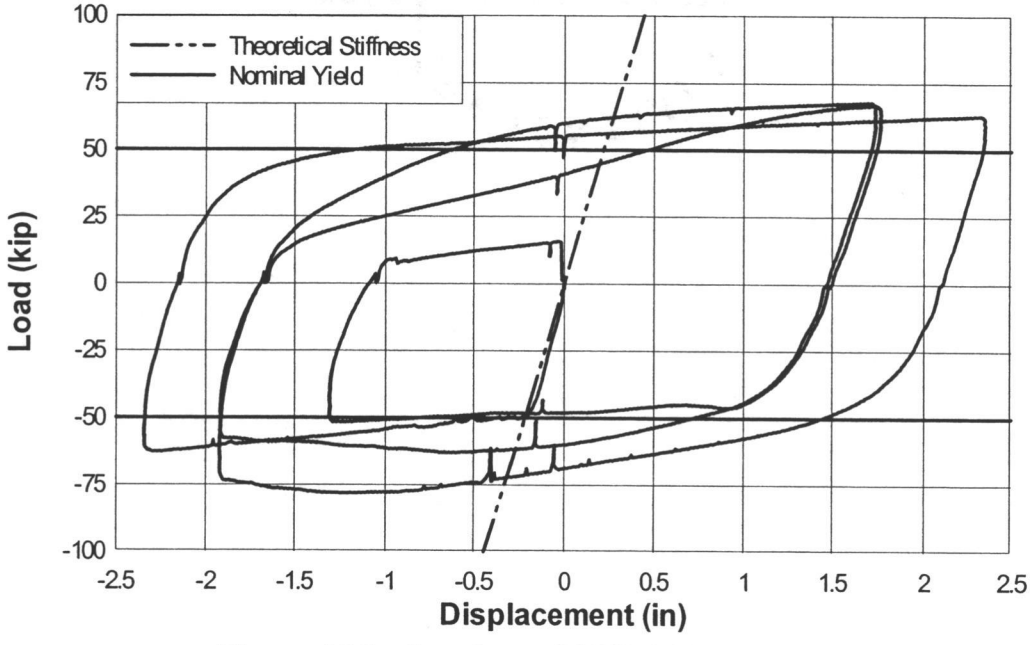

Figure A68: Specimen 50DB-2 Hysteresis

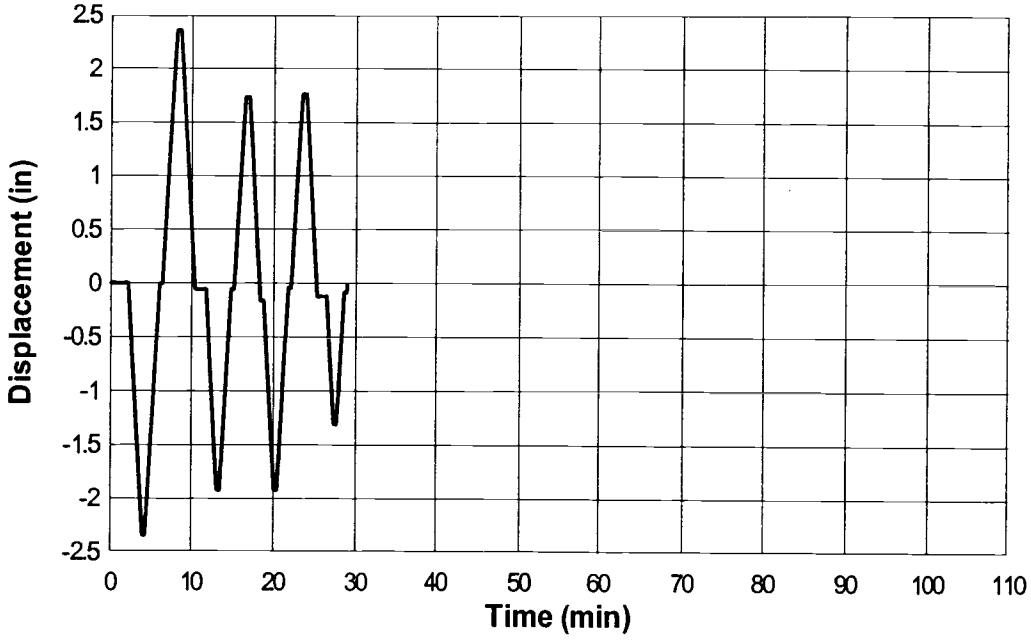

Figure A69: Specimen 50DB-2 Displacement

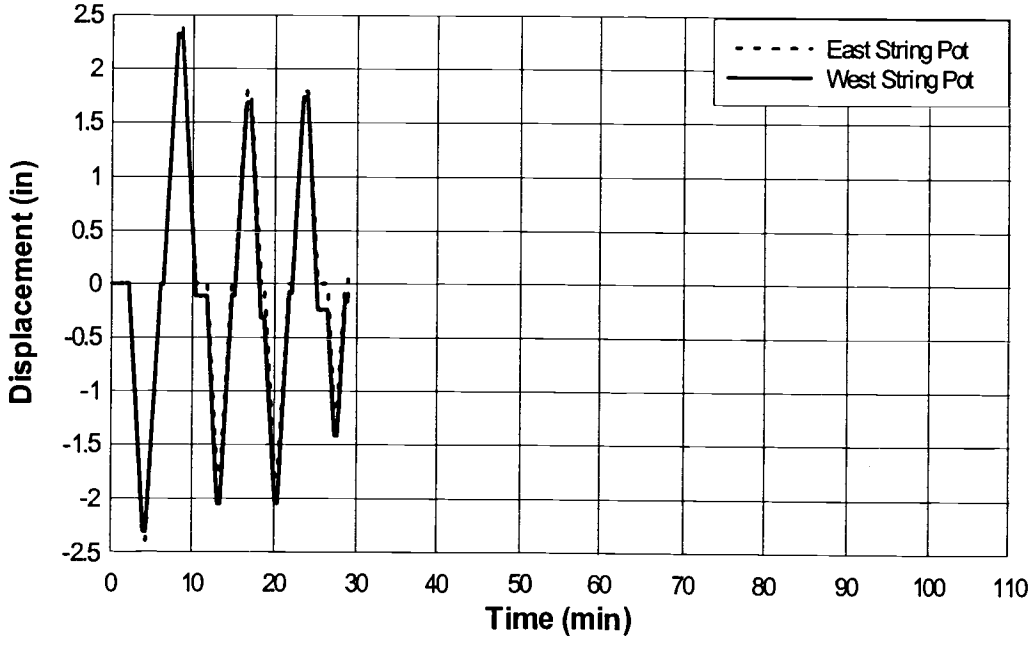

Figure A70: Specimen 50DB-2 String Pot Displacement

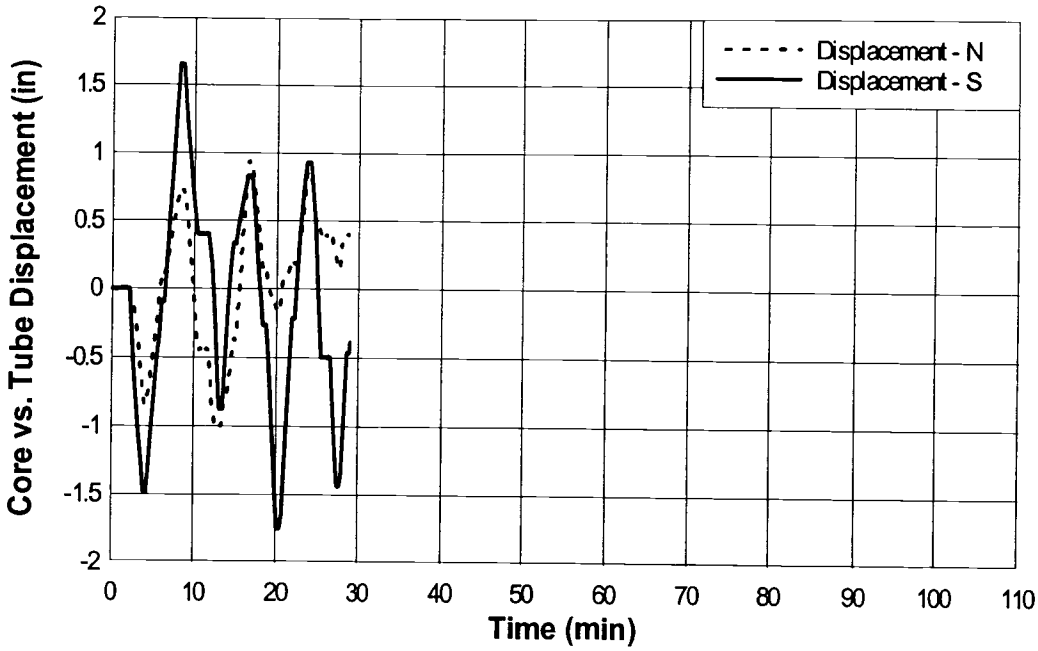

Figure A71: Specimen 50DB-2
Yielding Core/Confining Tube Relative Displacement

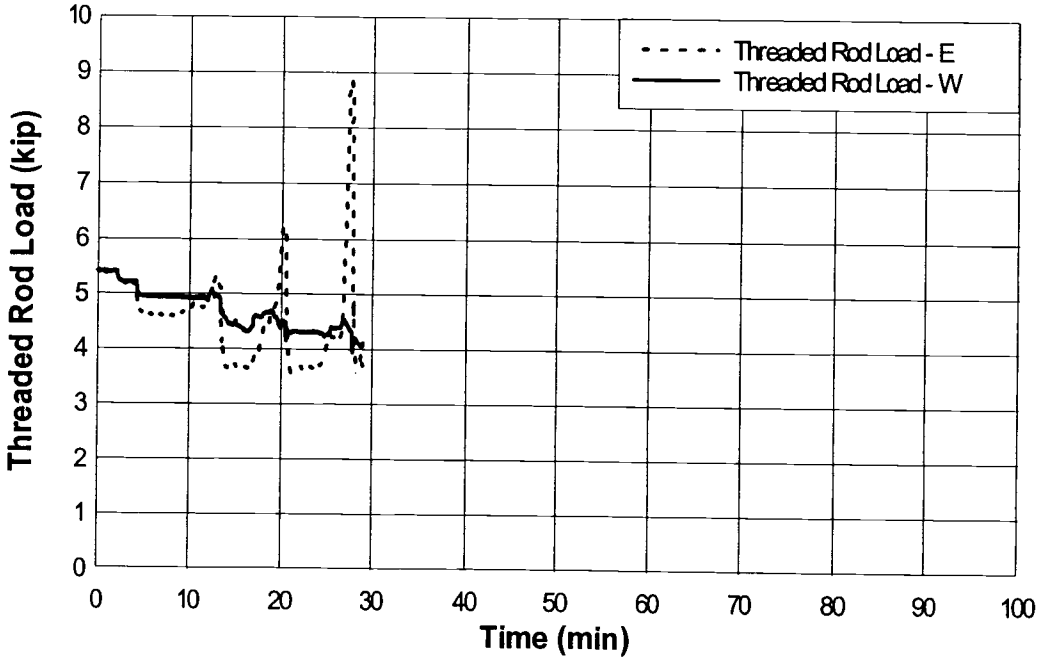

Figure A72: Specimen 50DB-2 Threaded Rod Load

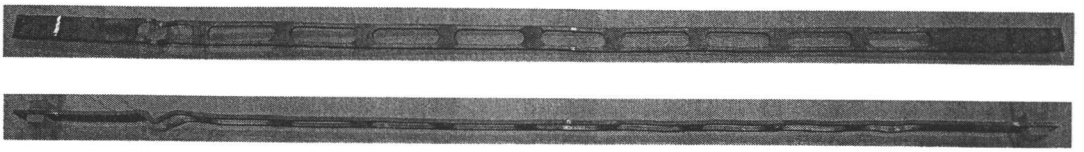

Figure A73: Specimen 50P-1 Buckled Shape

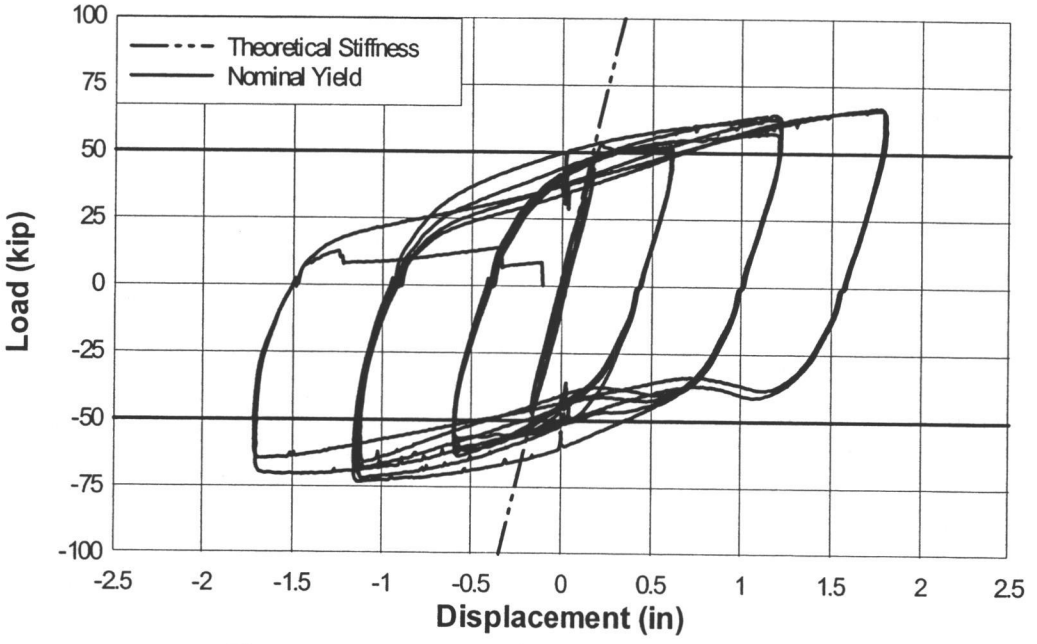

Figure A74: Specimen 50P-1 Hysteresis

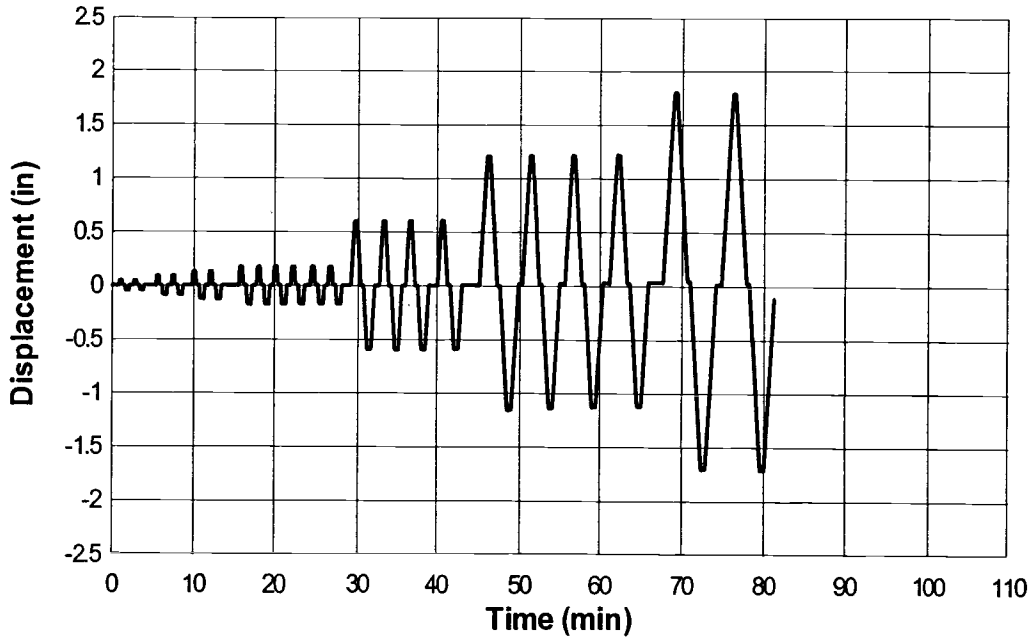

Figure A75: Specimen 50P-1 Displacement

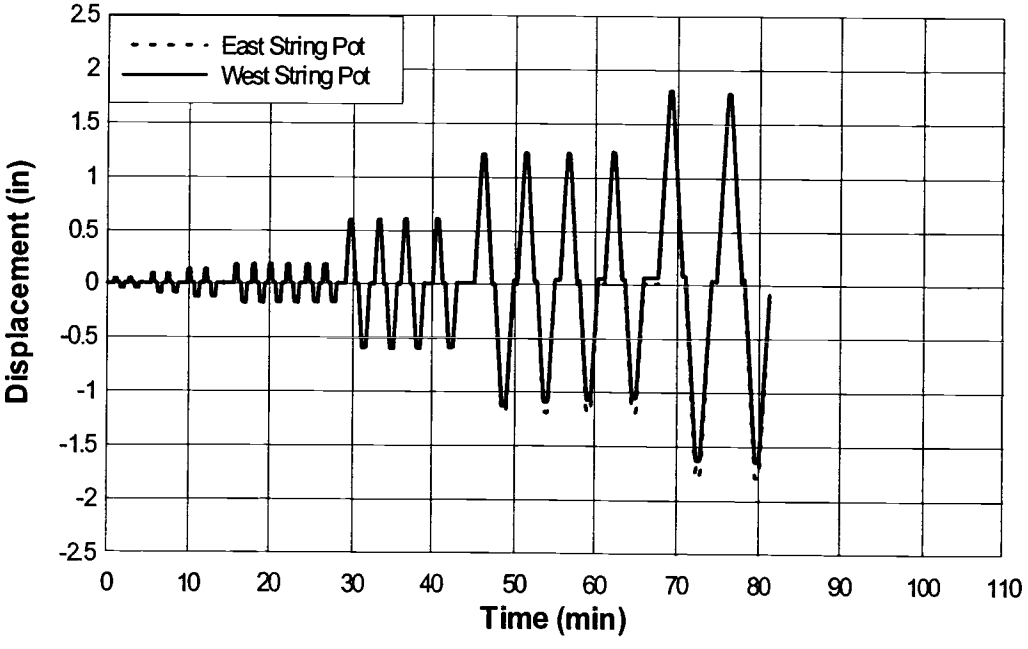

Figure A76: Specimen 50P-1 String Pot Displacement

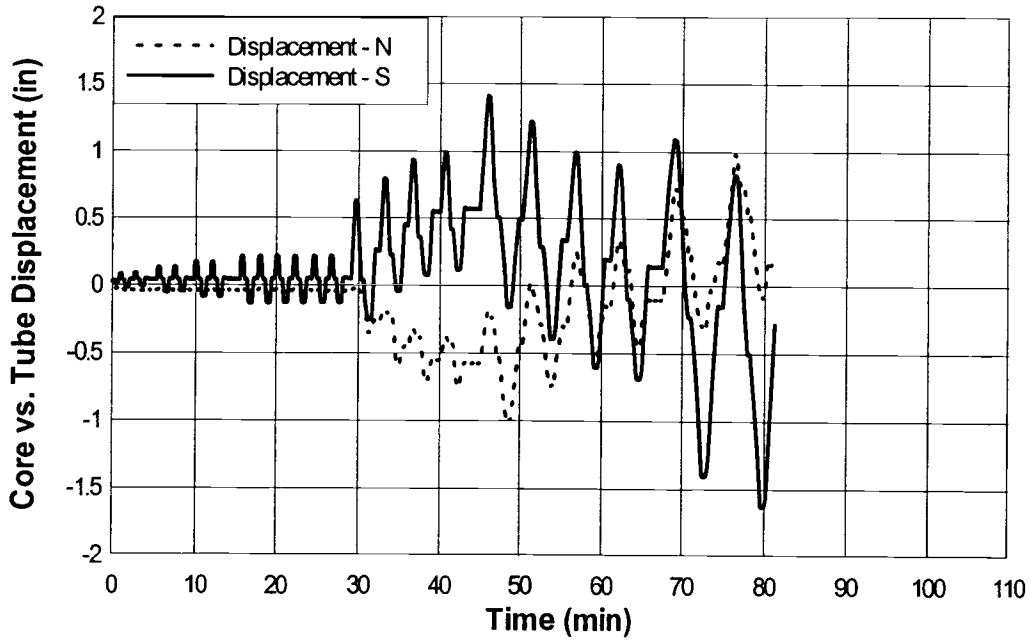

Figure A77: Specimen 50P-1
Yielding Core/Confining Tube Relative Displacement

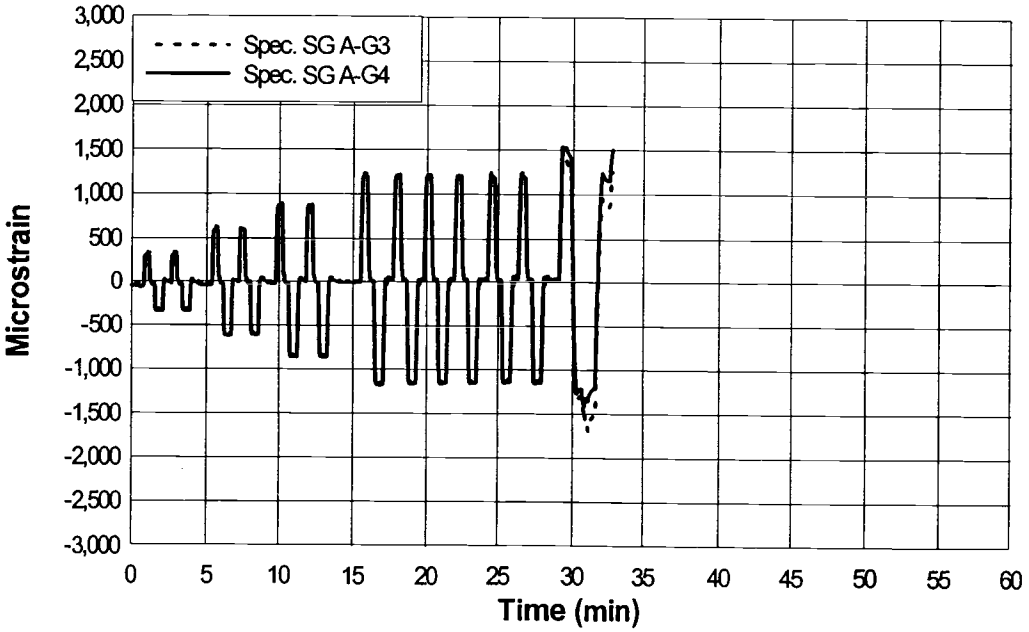

Figure A78: Specimen 50P-1 Yielding Core Strain Gages A-G3, 4

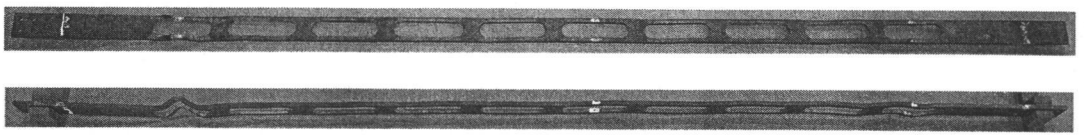

Figure A79: Specimen 50P-2 Buckled Shape

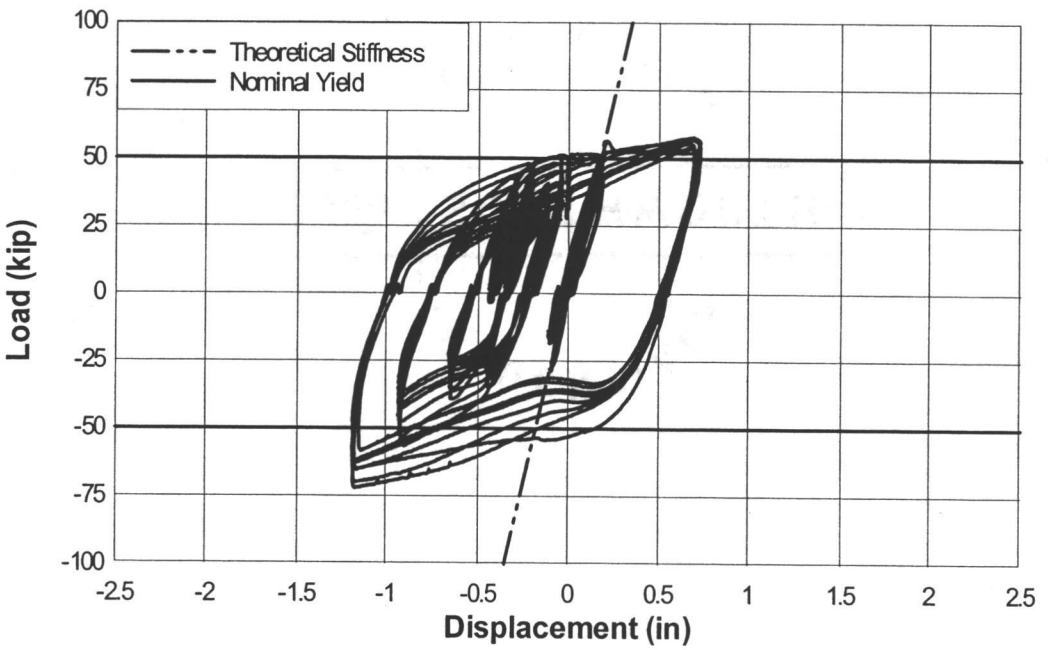

Figure A80: Specimen 50P-2 Hysteresis

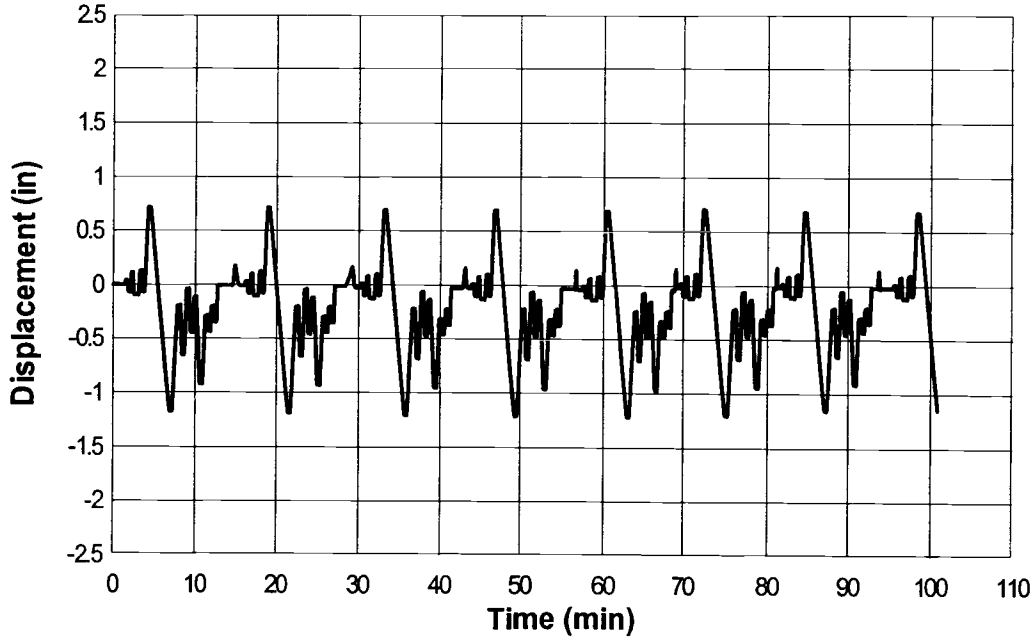

Figure A81: Specimen 50P-2 Displacement

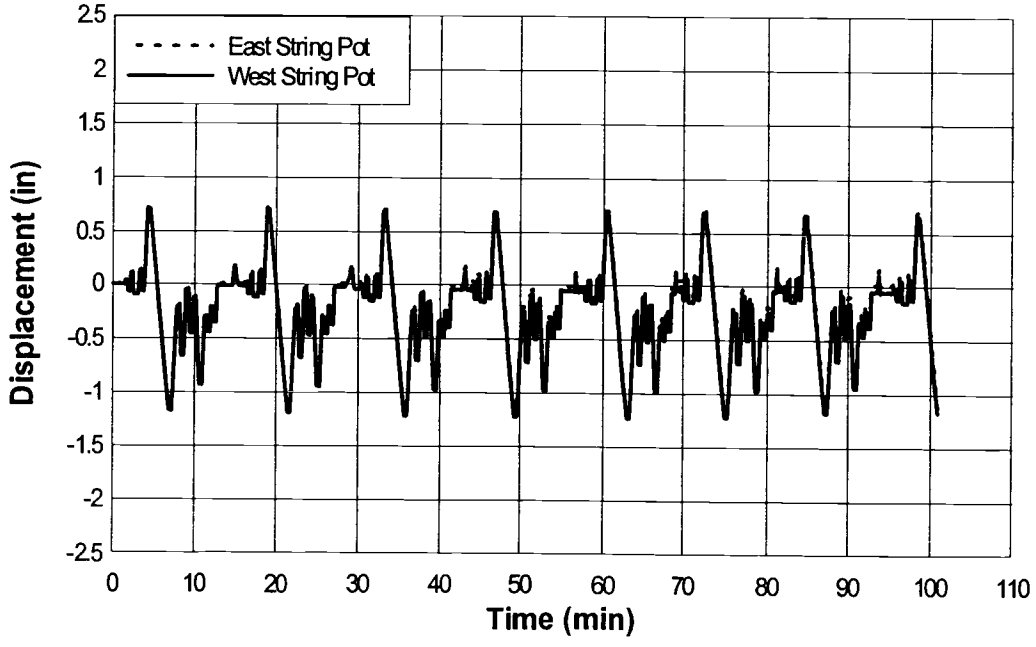

Figure A82: Specimen 50P-2 String Pot Displacement

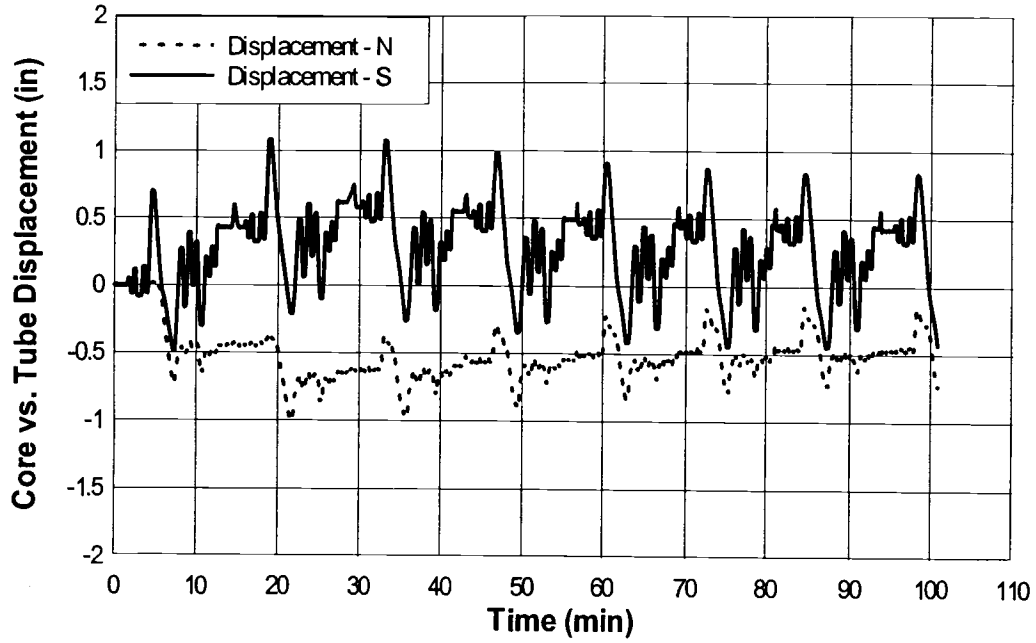

Figure A83: Specimen 50P-2
Yielding Core/Confining Tube Relative Displacement

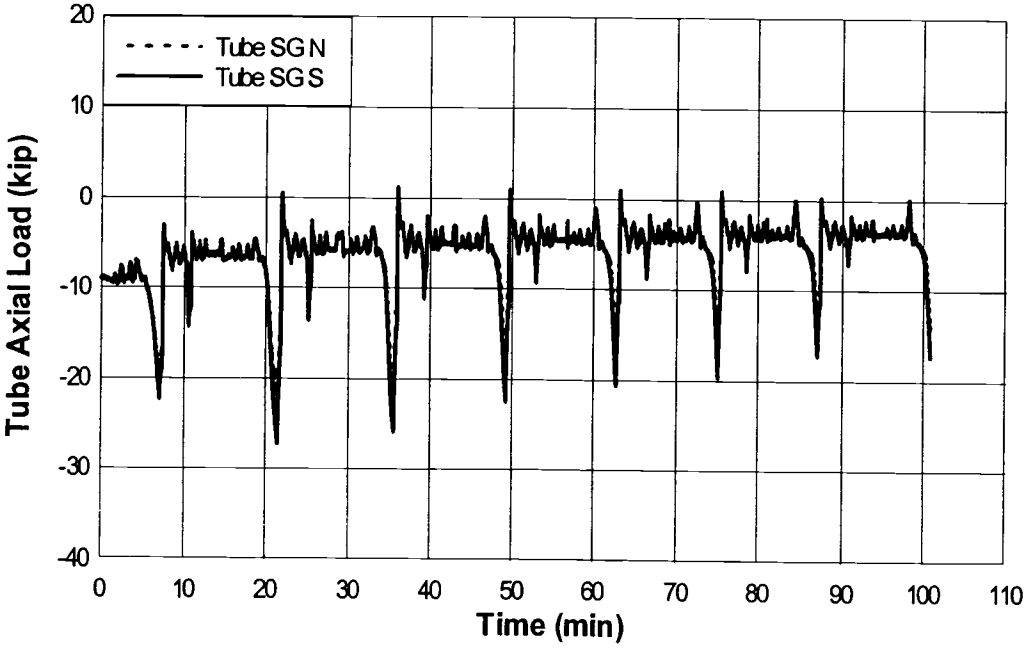

Figure A84: Specimen 50P-2 Confining Tube Axial Load